EVALUATION OF EROSION RATES AND THEIR IMPACT ON RIVERBANK STABILITY

By

ARJAN JIANFAR

A Thesis
Submitted to the Faculty of Graduate Studies
in Partial Fulfillment of the Requirements for the Degree of

Master of Science

Department of Civil Engineering
University of Manitoba
Winnipeg, Manitoba

July, 2014

THE UNIVERSITY OF MANITOBA

FACULTY OF GRADUATE STUDIES

✶✶✶✶✶

COPYRIGHT PERMISSION

EVALUATION OF EROSION RATES AND THEIR IMPACT ON RIVERBANK
STABILITY

A Thesis submitted to the Faculty of Graduate Studies of The University of Manitoba in
partial fulfillment of the requirement of the degree of

Master of Science

ARJAN JIANFAR © 2014

ABSTRACT

A research program was undertaken to quantify the effect of flow induced erosion on the stability of natural river banks along the Red River in Manitoba. The study was conducted on nine sites along the Red River within the Province of Manitoba. Soil samples from the sites were characterized and their erosion rate profiles approximated using laboratory testing measurements. Two simulations of a natural flood event and one of the same flood with the operation of the Floodway were then used to determine the difference in the lower toe erosion and the slopes reduction of the global factor of safety.

It was observed that samples from the outside bends of the river had lower erosion rates and higher threshold shear stresses than inside bend samples. This was expected due to the nature of the deposition of the sediments. The inside bends are mostly composed of alluvial sediments which are larger in size and less cohesive juxtaposed to outside bends which are mostly glacial sediments consisting of finer particles (i.e. more cohesive) and they are also much older deposits allowing for more consolidation. Laboratory observations also showed roots to have a large influence on reducing erosion rates.

It was hypothesised that the operation of the Floodway would have a negative impact on the stability of the river banks upstream of the Floodway inlet.

Two models were calibrated using provided hydrograph and piezometric data. A natural flood and one with the operation of the Floodway were simulated. The models showed an approximate reduction in factor of safety of 13% and 9% for the natural state simulation and the simulation with the Floodgate in operation, respectively. These results indicate that the operation of the Floodway does not have negative impact on the stability of river banks upstream of the Floodway inlet.

ACKNOWLEDGEMENTS

TABLE OF CONTENT

LIST OF FIGURES

LIST OF TABLES

CHAPTER 1: INTRODUCTION

The Province of Manitoba built the Red River Floodway in 1968 to protect the City of Winnipeg after the record 1950 flood. The floodway has operated over 20 times since its construction resulting in savings of billions of dollars in potential infrastructure damage. Operating the floodway causes backwater effects that result in river levels upstream of the inlet structure exceeding what would naturally occur without the floodway. The controlled change in river level can also impact the water velocity profile and as a result can impact erosion along the riverbanks. Long-term erosion can ultimately lead to over steepening of the riverbanks and subsequent failure resulting in loss of property for landowners. Given the impacts that operations may have on properties upstream of the inlet structure, any changes to the operating rules for the floodway (as defined in Provincial Legislation) could potentially have an impact on the properties within the affected backwater curve region.

An integral part of examining the impact of floodway operation on riverbank stability is to determine the erodability of typical soils that comprise the riverbanks. This is a difficult exercise as there are no generally accepted methods to measure the erodability of river sediments in-situ. The relationship between near bed shear stress and erosion rate must be determined in order to predict the transient erosion taking place due to varying river levels. After establishing this relationship, the erosion of specific riverbank geometries can be estimated using erosion rate functions and water velocity profiles acting on a riverbank cross-section over time.

1.1 Importance of Riverbank Research

Natural riverbanks are sites of many of Manitoba's infrastructure, private property, and invaluable natural assets. Due to the high cost associated with remediating failed riverbanks, there is a need to gain a better understanding of the causes of riverbank failure. Several factors contribute towards destabilization of riverbanks, in particular erosion, which has been recognized to have a significant contribution towards instability. The purpose of this research is to quantify how flow-induced erosion affects overall riverbank stability at sites along the Red River representing inside, outside, transition and straight sections of the river's bends. The research will test the hypothesis:

"The operation of the Red River Floodway has a negative impact on Red River riverbanks' stability upstream of the Floodway inlet."

1.2 Objectives of Thesis

Objectives of the research include the following:

1. Design and build a device to measure erosion of soils.

2. Collect laboratory measurements of samples' grain size distribution, index properties, erosion rate curves, and hydraulic conductivity.

3. Assess the impact of sediment load of the eroding water on erosion rate.

4. Determine the relationship between erosion rate and soil properties.

5. Numerically model erosion impact on the river bank cross sections and determine reduction in factor of safety after a selected flood event with and without the operation of the Floodway.

1.3 Past Research

Since the 1960s there has been ongoing research on slope stability. Baracos (1960) concentrated on the relationship between actual and theoretical factor of safety of slopes greater than 1.0 for slopes that had previous failure(s). The concern was that the undrained shear strengths of clay measured in the laboratory were higher than the actual shear strengths of the clay at failure. Modified shear strengths along parts of the failure plane using total stress analysis were used to formulate a method for analyzing the stability of the slopes. Natural riverbanks were surveyed by Mishtak (1962) to examine the slope at which they were stable, at which they failed, and at which they became stable following failure. The goal of Mishtak's research was to recommend a stable slope at which the Winnipeg Floodway was to be designed and constructed. Of the 141 riverbanks surveyed only six were determined to be stable. It was found that outside banks of river bends had previous slides and were actively moving or had required stabilizing of the slopes. Mishtak found that the few riverbanks that were stable were at a slope of 6:1 or flatter. Sutherland followed this investigation in 1966 focusing on conventional methods of slope stability, i.e. undrained shear strengths measured in laboratory. Sutherland concluded that these shear strengths overestimate stability of the slopes when end of construction and long term stability conditions are analysed and observed. Sutherland for design suggested a slope of 6:1 for banks that did not have previous sliding and 9:1 for banks where previous sliding was observed.

In 1971 Baracos initiated the first full scale study that continuously monitored in-situ pore water pressures and slope movements over a long term period of two sites along the Red River. The study showed that there was virtually no movement of the slopes during the high river levels of spring and summer, and rapid movements after the river level was lowered in the fall and

continued at a lower rate through the winter. Spring snow melt, precipitation and possibly the leaking of water mains and sewers were also found to be factors influencing the riverbanks' stability.

Freeman and Sutherland (1974) followed by studying the mechanisms of slope failure, in particular non-circular arcs, in anisotropic clays. Their conclusion was that using residual shear strengths for the entire length of the slip surface would underestimate the factor of safety.

The preceding studies showed that neither undrained shear strengths nor effective stress strengths could successfully predict slope stability in clay. The parameters required are residual shear strengths of c' = 0 and phi' = 8 - 13 degrees with the worst combination of pore water pressures and river elevation.

The effects of seasonal variations of the river and upper aquifer elevations on the riverbank stability were researched by Tutkaluk (Tutkaluk 2000, Tutkaluk *et al*. 2002). The slope stability over a 97-day time period with consideration of the most critical period of stability when the river level decreases and bedrock aquifer levels increase was modeled using a finite element modeling software. The factor of safety showed a decrease of 13% to 17% at the end of the period. In 2001 a report of the studies conducted in the prior ten years on Red River and Assiniboine River riverbank stability was submitted to the Government of Canada. One of the major conclusions was that a primary cause of deep-seeded riverbank sliding was due to the erosion of the lower banks and river bottom during flood conditions.

Baracos and Lew (2003) qualitatively assessed riverbank slides. One of the primary causes identified was erosion due to high river flows. Tutkaluk (2000) quantified the effect of seasonal variations of bedrock aquifer and river levels on slope stability. This research will consider the

4

combination of these two effects to quantify the resulting effect on slope instability along the

Red River.

CHAPTER 2: LITERATURE REVIEW

2.1 Introduction

The background theory of river systems, riverbank erosion and instability, and characteristics of the Red River are provided in the following sections.

2.2 River Systems

The two primary purposes (Morisawa 1968) rivers serve are:

1. Transport of the water that drains from land surfaces back to seas and oceans.

2. Transport of sediment suspended in the water by the shear force applied to the channel beds and banks.

The primary factors that determine the characteristics of flow and sediment load are climate and geology of a region (Morisawa 1968). The climate determines the amount of precipitation and consequently the river's discharge. The composition of the channels' beds and banks, sediment load concentration and grain size are determined by the geology of the region. Morphology of a river is influenced by discharge and sediment load, which are secondary factors. River morphology is the time-dependent evolution of the longitudinal profile and transverse cross-section of the channel and its associated pattern (Morisawa 1968). The first-order independent variables are climate and geology. They determine discharge and sediment load which are second-order variables. The third-order morphologic configuration of the river determined via the collective interaction of these variables as presented in Figure 2.1. A change in any one of these variables results in the alteration of the river morphology to counteract the effect. This is a

process/response system, meaning that a change in any part of the system results in a response that can occur at the location of the disturbance or be transferred downstream to another location in the system (Morisawa 1985). The processes that change the morphology of a river are erosion, transportation and deposition (Richards 1982).
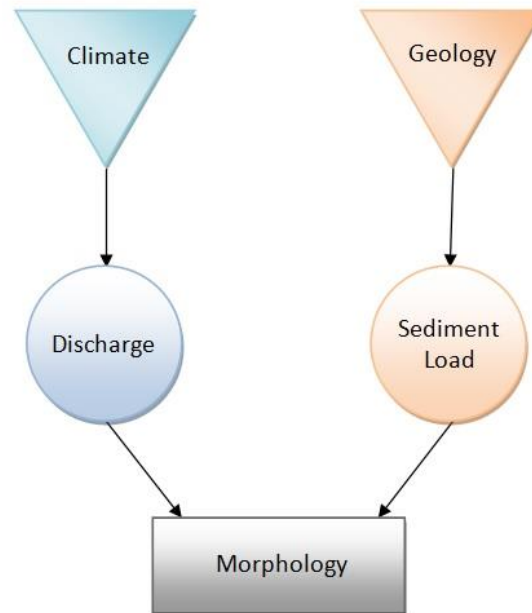
Figure 2.1: Variables affecting the morphology of a river (based on ideas from Morisawa 1985)

2.2.1 Hydraulics of Flow

Erosion of bed and banks of a channel is the result of the shear stress of water acting over the cross-section of the channel. Shear stress is directly related to the velocity gradient and viscosity of the eroding fluid as defined by Equation 2.1 (Knighton 1998). An increase in velocity gradient results in an increased shear stress.

$$\tau = \upsilon \frac{dy}{dv}$$ Equation 2.1

7

where,
τ = shear stress
dv/dy = velocity gradient
υ = viscosity

In Figure 2.2 the velocity distribution of laminar flow in a symmetrical river channel cross-section is shown to have a parabolic shape along the channel depth with the velocity decreasing to zero at the channel bed due to frictional resistance between the fluid and channel bed (Knighton 1998). The maximum velocity gradient is found in the bed and lower bank region, which experience the greatest amount of erosion due to the highest shear stress acting on them. Flow is described as laminar or turbulent. Laminar flow is the smooth flow of layers of fluid, moving together without mixing and crossing each other. Turbulent flow is the chaotic movement of fluid, which causes greater erosion (Morisawa, 1968). The configuration of the cross section can further change the velocity distribution.
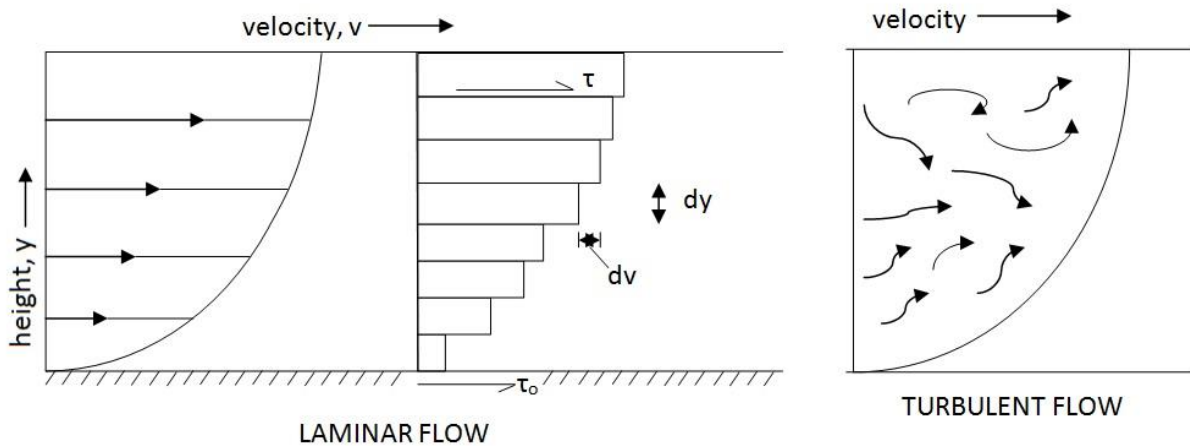
Figure 2.2: Average velocity distribution at the center of a channel under laminar and turbulent flow conditions

8

The mean velocity distributions (lines of equal velocity) for different symmetrical and asymmetrical channel cross-sections are shown in Figure 2.3 and Figure 2.4. Generally the isovels are closer together near the boundaries. The maximum velocity observed is at the center of the channel due to the decline in frictional effects from the channel banks (Knighton 1998). Velocity gradient and therefore shear stresses are highest where the isovels are closer together. The shear stress is greatest at the bed in wide shallow sections and greatest on the banks in narrow deep sections, which produce greater bank erosion (Knighton 1998). The velocity distribution becomes skewed when compared to asymmetrical cross-sections. As shown in Figure 2.4, the maximum velocity shifts from the center to the outer edge of the channel (Morisawa, 1985).
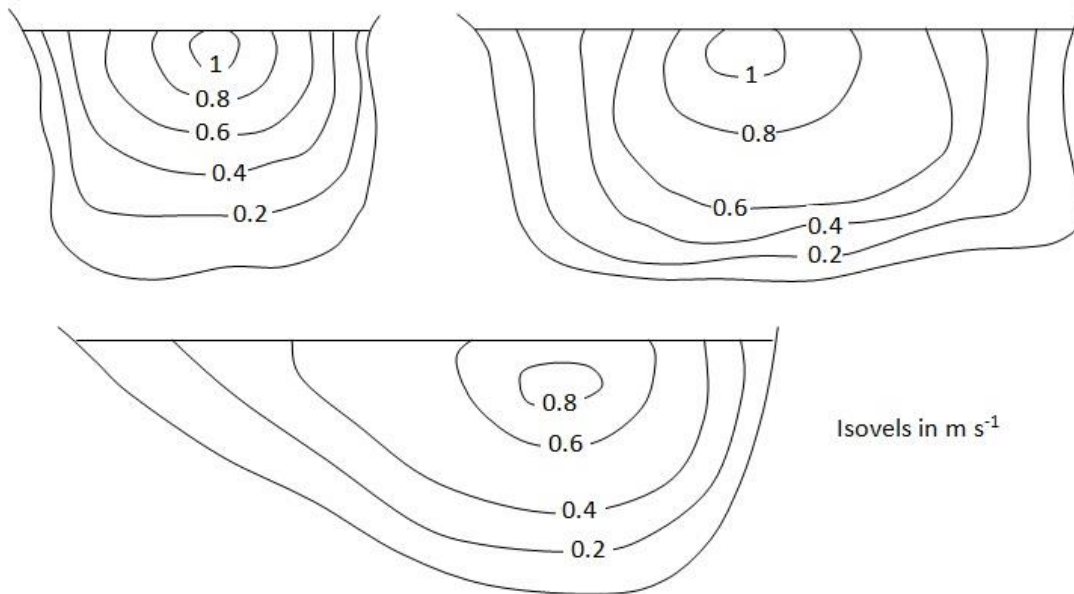
Figure 2.3: Velocity isovels in different channel cross-sections

9
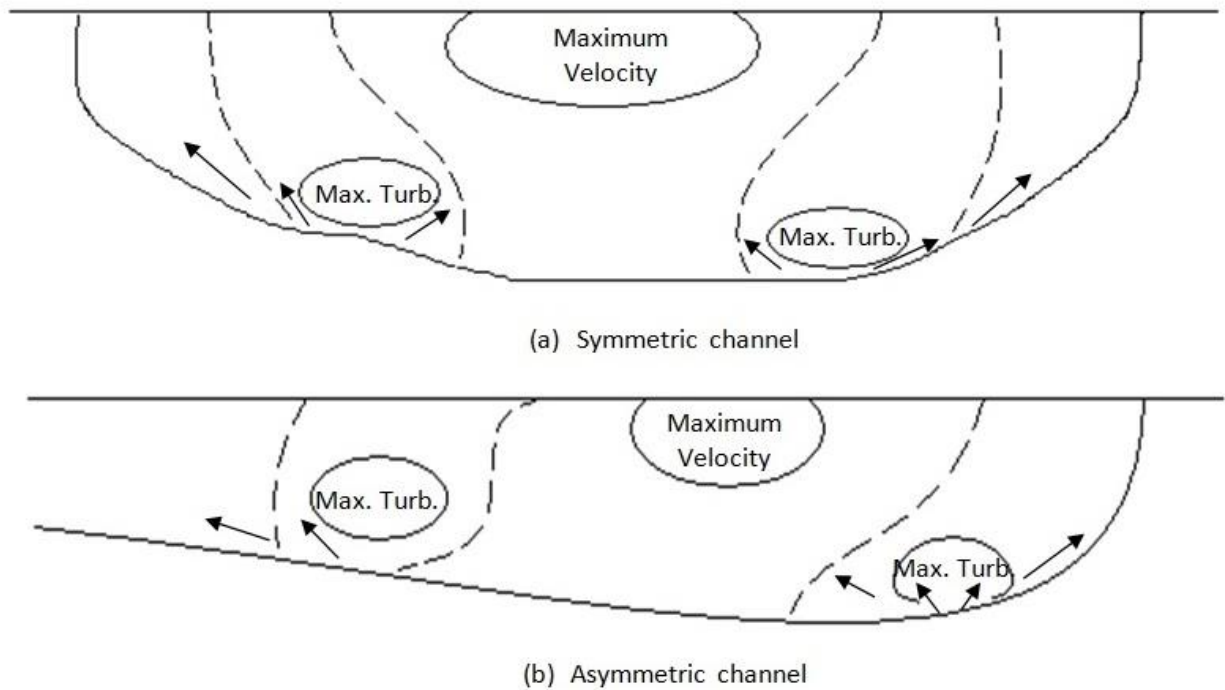
Figure 2.4: Velocity and turbulence distribution in (a) symmetrical channel and (b) asymmetrical channel

The Reynolds number expressed by Equation 2.2, represents the ratio of inertial to viscous forces and is defined by the density (ρ), mean velocity (V), hydraulic radius (R) and the viscosity (υ). The flow is laminar if the Reynolds number is less than 500 and turbulent or chaotic if it is greater than 2500. Values between these two limits are classified as transitional (Knighton 1998). Roughness of the channel surface due to particles that protrude from the bed surface generates turbulence which increases the dissipation of energy in the stream (Morisawa, 1968). Turbulence increases with increasing velocity and bed roughness.

$$Re = \rho \frac{VR}{\upsilon} \hspace{5cm} \text{Equation 2.2}$$

2.2.2 Sediment Load

There are two main classifications of transported sediment load by a river: bed load and suspended load. Coarse-grained material greater than 0.062 mm in diameter (classified as coarse sand and gravel) is known as the bed load, which characteristically rolls and slides intermittently along the bed of the channel due to the weight of the material being too heavy to be transported in suspension (Knighton 1998). Conversely, suspended load is composed of finer particles such as silts and clays, which require little or no energy to be transported. In contrast, greater amount of energy is required to keep the bed load particles in motion. Suspended load increases the efficiency of a river by decreasing its inner turbulence and therefore reducing frictional energy losses (Knighton 1998).

Load transportation depends on the energy of the river, which is a function of its velocity. To entrain and transport grains of a given size, the velocity must exceed a minimum value. If the velocity is lower than this critical value, sediment will drop out of suspension (Knighton 1998). The relationship between entrainment, transportation and deposition in terms of velocity and grain size is explained through the Hjulstrom Curve shown in Figure 2.5. This conceptual curve shows four distinct regions: erosion, entrainment, transport and deposition. The band designated by entrainment indicates the velocity required to initiate erosion as a function of sediment size in millimetres; this is also referred to as the critical velocity. Due to inter-particle attractions, clays and silts require higher velocities to start eroding than do larger-sized particles of approximately 0.4 mm and higher, as shown on the curve in Figure 2.5. The critical velocity increases linearly for grains larger than 0.5 mm in diameter, due to the higher weight of the sediment (related to the increasing grain size) which requires greater energy to initiate movement. Grains smaller than 0.5 mm are typically classified as cohesive and also show a linear increase in critical velocity.

11

Greater velocities are required to mobilize cohesive materials due to the strong inter-particle bonds, referred to as electrochemical bonds. Once the fluid velocity increases past the erosion velocity, the soils will actively erode in the designated "erosion" region. The curve further shows that once silts and clays are entrained, they are easily maintained in suspension at a lower velocity than the one initially required to entrain the grains, as designated by the transport region of the graph (Richards 1982). The deposition region of the graph shows the opposite to be true for coarse-grained sediment, where deposition occurs if the velocity drops below the erosion velocity.

Deposition also occurs when river flows overtop the riverbanks. Flow velocity decreases as water spreads across the plain, reducing its ability to transport the sediments. Coarser sediments are typically deposited near the edge of the channel, whereas finer materials are transported farther from the channel. Floodplains are formed by this action (Morisawa 1968).
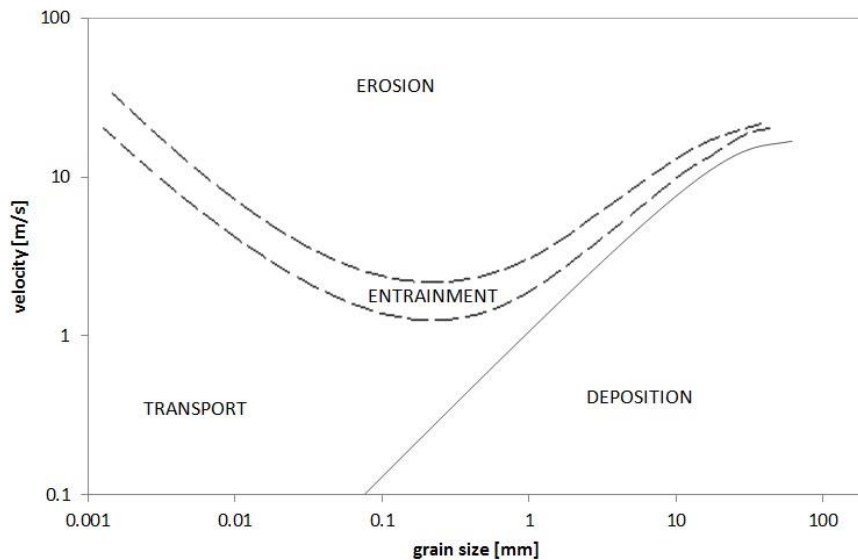
Figure 2.5: Hjulstrom Graph for erosion, transportation and deposition of sediment as a function of grain size

12

2.2.3 Channel Morphology

Channel morphology is the time-dependent adjustment of a river's longitudinal and transverse cross-section to allow the river to transport most efficiently the discharge and sediment load supplied to it (Morisawa, 1968). The hydrology and geology of the site are the secondary factors that directly affect the discharge and type of sediment in a channel (Morisawa 1968). The hydrology determines the amount of precipitation and therefore the discharge of a river, and the geology determines the soils that make up the bed and banks of a channel. The processes that transform the shape and pattern of rivers are erosion, deposition, and transportation of sediment load (Richards 1982).

Heavy precipitation, for example, increases both the discharge and velocity of the flow in a river. The shear stress on the bed and banks will increase as the velocity increases, causing erosion of the bed and banks. The river responds to the increase in discharge by widening the cross-sectional area available to transport the flow.

The geology of the bed and banks, where different sediment types respond differently to erosion, determines the resulting cross-section of the river (Richards 1982). Sandy banks are easily eroded and typically produce wide channels with shallow beds. In contrast, clayey and silty banks are more resistant to erosion and typically produce channels that are deep and narrow, with steep side slopes (Richards 1982). If a river bed is bedrock-controlled, the banks are eroded regardless of the sediment type. Flooding occurs when a river overtops its banks when the discharge increases too quickly for the channel. As the water flows across the land surface, sediment is deposited and the flow's velocity decreases. Deposited sediments are referred to as alluvial deposits; these deposits make up the banks and surface of the floodplain. Coarser and

heavier sediments are typically deposited near the edge of the channel and finer and lighter ones are deposited further (Simons and Senturk 1992).

As rivers gain flow along their channel due to the accumulation of run-off they grow headward with respect to their cross-sectional area (Morisawa 1968).

Rivers originate in regions of high altitude and flow towards lower altitude and flatter regions, finally exiting into the ocean (Morisawa 1968). The cross-section and sediment load of a river changes as it progresses from one type of topography to another.

The sediment load also has a direct impact on the channel morphology, depending on the concentration and grain size of the sediments carried by the flow. When the increase in concentration of sediment load is higher than the increase in discharge, deposition on the bed may occur due to the rivers insufficient energy to transport the load. As deposition continues, the channel's cross-sectional area is reduced, which in turn increases the velocity of the river to pass the discharge and sediment load (Morisawa1968). The same applies for an increase in the grain size of the load.

2.2.4 River Meanders

A river with a distinct pattern of irregular bends along its length is defined as a meandering river (Simons and Senturk 1992). Meandering rivers typically have asymmetrical channel cross-sections along their lengths. This is due to deep pools of scoured bank on the outer bends and deposited sediment on the inner bends (Knighton 1998). As a result, the thalweg (defined as the deepest points in a channel joined by a line) of a meandering river is close to the outer edge of each bend and crosses over on the straight sections between bends (Morisawa 1968). Similarly streamlines of maximum velocity move downstream, crossing over from one bank to the other.

They converge at the outer edge of the bends and diverge at the inner sides. The converging streamlines result in acceleration of flow which also increases the ability to erode the banks and transport particles. Conversely, velocity decreases when streamlines diverge, resulting in deposition (Morisawa 1968).

Erosion and deposition in meanders can also be explained in terms of maximum and minimum turbulence. Erosion takes place where turbulence is maximized, and deposition results where turbulence is minimized (Morisawa 1968). Turbulence is expressed by the Reynolds number. As the velocity increases, so does turbulence and vice versa. As explained previously, the convergence and divergence of streamlines explain the increase and decrease in velocity.

Many researchers have studied and explained the meander behaviour of rivers; however none of the explanations have been accepted officially. Shulit's (1941) proposal was that rivers meander to decrease channel gradient by lengthening their course. He suggested that a river will adjust its slope to transport the material it must carry, which would mean the channel gradient is a function of grain size comprising the bed. As the grain size of load increases, so must the gradient in order to have enough energy to transport the load. Therefore a coarse-grained load requires a higher gradient than a fine-grained load. If the slope exceeds the energy required to transport the load, the river will meander to lengthen its course and decrease its gradient and total energy.

Schumm (1960) related rivers with higher concentrations of silts and clays in their bed and banks to rivers with higher meandering. This author also observed that meandering sections of a river tended to have deep, narrow cross-sections, whereas sections that were straighter and contained greater bed load were wide and shallow. He concluded that meandering was the result of the removal of a large proportion of load, such as suspended sediments.

15

Friedkin (1945) conducted flume experiments to gain a better understanding of the initiation of meandering in a channel. The experiment started with an initially straight channel that was subject to constant discharge with no additional sediment load. It was observed that the stream naturally developed meanders. Local erosion of the channel banks initiated the meandering pattern. Once the initial bend was formed, the meandering was transmitted downstream creating more bends. A variety of materials was used for the channels. It was found that fine-grained materials were more resistant to erosion, resulting in deeper channels with gentler gradients. In contrast, coarse-grained materials were more easily eroded, producing wide and shallow channels with steeper gradients.

2.2.5 Equilibrium

Due to the dynamic factors that control the morphology of rivers, it is unlikely that a river will attain a state of equilibrium where neither erosion nor deposition occurs. When any of these factors change, the river will respond with a change to its morphology. Some researchers have proposed the idea of dynamic equilibrium, i.e., a fluctuating or changing balance, in which parts of the river are continuously adjusting to maintain equilibrium (Richards 1982).

2.3 Erosion

Erosion is the process by which soil particles are removed from the banks and bed of a river channel and entrained into the flow of the river (Richards 1982). Numerous factors govern erosion, including the intensity of flow (river elevation), the bed and banks' soil characteristics, the channel's geometry, ice effects and the characteristics of the fluid. In order to quantify the amount of soil that can be eroded from the bed and banks under a given flow, the following three variables are required:

- Fluid shear stress

- Critical shear stress

- Erosion rate

The following sections provide an overview of a few select methods (among the various proposed by researchers) for calculating the above variables.

2.3.1 Fluid Shear Stress

Fluid shear stress is defined as the force per unit area in the direction of flow (Chang 1988). Figure 2.6 explains the shear stress distribution in a steady and uniform two-dimensional flow in a channel. All of the forces are acting on a unit volume of water described by ABCD within the channel. The direction of flow along the slope of the channel is defined by S on the x-axis and the z-axis perpendicular to the flow (Chang 1988). The forces and stresses include the hydrostatic forces on AB and CD, shear stress τ acting on BC, and the x-component of the fluid weight W_x. All forces act in the x-direction. When flow is uniform, the hydrostatic forces are equal and opposite, and the remaining force W_x (= WS) must be counterbalanced by the shear force.

$$WS = \tau\, Pdx$$
$$\gamma\forall S = \tau\, Pdx$$
$$\gamma AdxS = \tau\, Pdx$$
$$R = A/P$$

where,
τ = fluid shear stress
P = wetted perimeter
A = Area
$\forall$ = Volume
R = hydraulic radius of the channel
γ = unit weight of the soil

17

τ can be isolated from the above equations to produce Equation 2.3, which is the average shear stress exerted on the bed of the channel.

$$\tau = \gamma RS \hspace{8cm} \text{Equation 2.3}$$

Olsen and Florey (1952) expanded this equation further to describe the shear distribution along the bed and banks of straight trapezoidal channels in a finite difference analysis. Figure 2.7 (a) shows the graphical distribution where shear stresses are at a maximum along the bed and a minimum at the top of the bank. The maximum shear on the bed is 1.37γRS and 1.08γRS on the bank, approximately one third from the bed for this particular cross-section of side slope 2:1. Highway Research Board (1970) adjusted the coefficients of maximum γRS for the bed and bank as a function of the ratio of channel width (b) to water depth (D). Channels of different side slopes' values for the coefficient of maximum shear stress were also provided. Figure 2.7 (b) and (c) show the graphs for a channel of side slope 2:1. As the b/D decreases the coefficient for γRS approaches 1.0 and as b/D increases the coefficient can be as high as 1.4.
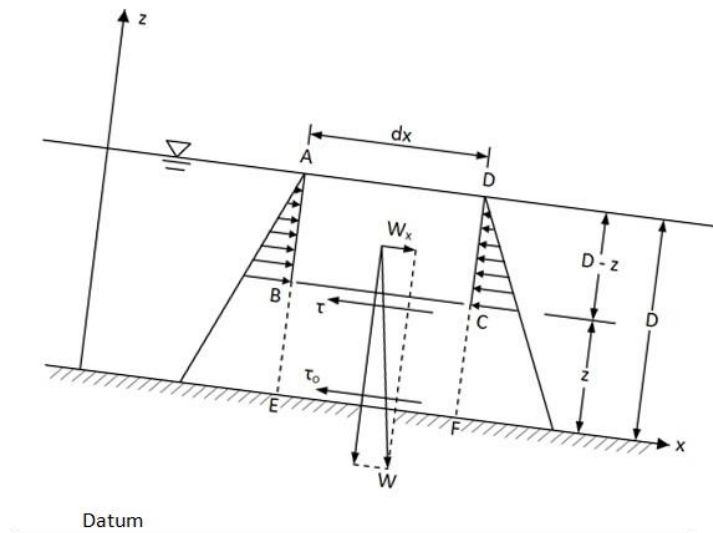
Figure 2.6: Schematic of forces acting on a unit volume of flow (used with permission from Dr. Chang April 9th 2013, reproduced from Chang 1998)
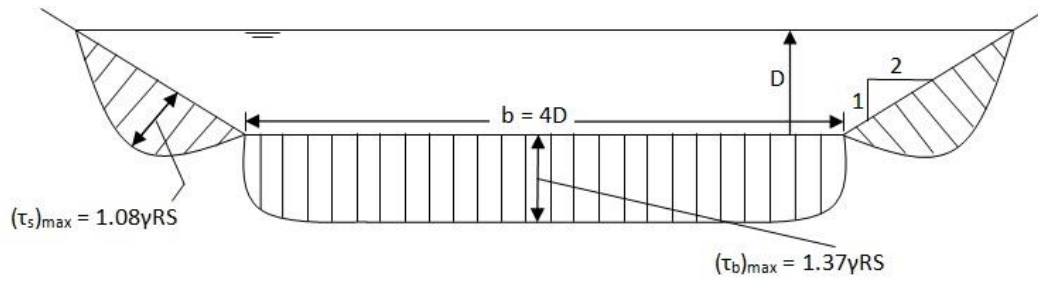
Figure 2.7 a
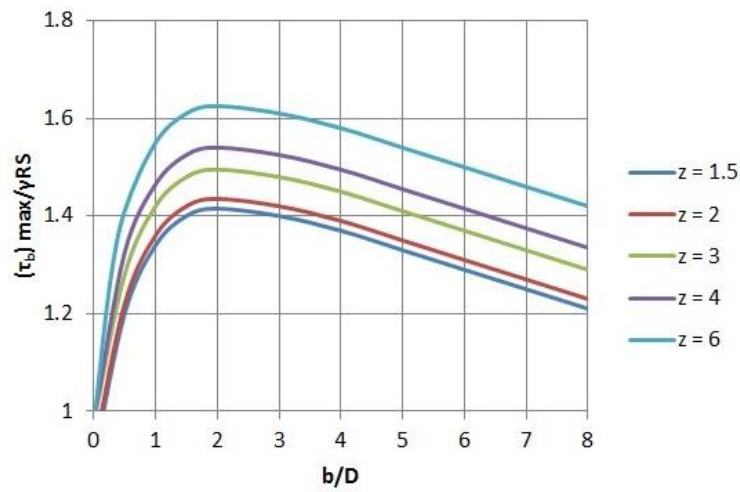
Figure 2.7 b (above) and Figure 2.7 c (below)
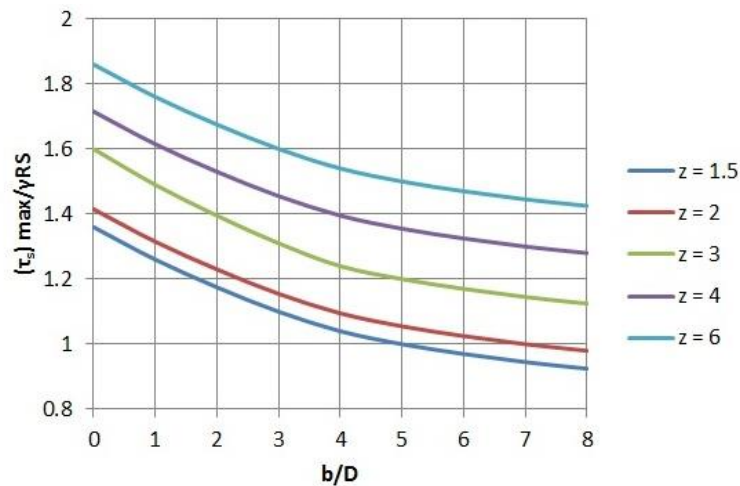
Figure 2.7 a,b & c: Distributions of boundary shear stress in a trapezoidal channel (a) with coefficients for maximum shear on bed (b) and banks (c) as a function of b/D (used with permission from Dr. Chang April 9th 2013, reproduced from Chang 1988)

2.3.2 Critical Shear Stress

If the forces applied on the particle exceed the resisting forces it will be set in motion (Richards 1982). The characteristics of the soil determine the resisting forces of the particles. In non-cohesive soils, such as sands and gravels, the gravitational forces of their submerged weight are their resistance against erosion (Richards 1982). The Shields curve (Figure 2.8) is commonly used to determine the critical shear stress of non-cohesive soils based on particle diameter. The curve is based on a series of flume experiments of water flowing over flat sand beds. It proposes a range of critical shear stresses for particles of 0.1 mm to 10,000 mm in diameter with shear stresses ranging from 0.1 Pa to 10 Pa. This curve has been expanded by several researchers to cover a larger range of particle diameters. However, the curve is only designed to provide the critical shear stress on the bed of the channel (Morisawa 1968).

Lane (1953) proposed an equation to quantify the critical shear stress on the side slopes of channels. Particles on a stream bed are subjected to a tractive force acting in the direction of the flow, whereas side slope particles are additionally subjected to a gravitational force parallel to the slope. The bed's critical shear stress is multiplied by K, which represents the ratio of the tractive force necessary to start motion on a side slope in relation to the force required to start motion on the bed. Equation 2.4 is used to calculate the value of K.

$$K = cos\varphi \sqrt{1 - \frac{tan^2\varphi}{tan^2\theta}}$$

Equation 2.4

where,
θ = soil friction angle
φ = side slope angle

Figure 2.8: Shields Diagram for determining the critical shear stress of cohesive soils (reproduced from Knighton 1998)

Cohesive soils' critical shear stress cannot be estimated from the Shields curve as their behaviour is not solely governed by gravity. Their resisting forces are related to physical and chemical surface effects, such as soil particle bonding and interaction with pore and eroding water (Arulanandan *et al*. 1980). The chart developed by Alizadeh (1974) and revised by Heinzen (1976) (shown in Figure 2.9) illustrates the relationship between critical shear stress (τ_c) and the soil's sodium adsorption ratio (SAR). SAR can be calculated using Equation 2.5, where the dielectric dispersion and total salt concentration of the eroding fluid is expressed in milliequivalents per liter (meq/l).

$$SAR = \frac{(Na^+)}{\sqrt{\frac{Ca^{++}+Mg^{++}}{2}}}$$ Equation 2.5

The dielectric dispersion provides a quantitative measure of the particle arrangement and pore spaces in the soil (Mitchell and Soga 2005). The decrease in dielectric constant is expressed as a function of the soil structure, defined by the type and amount of clay particles, water content, pore fluid composition and fabric. The soil can be characterized by taking into account the

21

compositional and environmental factors of the clay-fluid system and by measuring the magnitude of the dielectric dispersion (Arulanandan *et al*. 1975).

This figure has been removed due to copyright issues.
To view it, refer to its source.
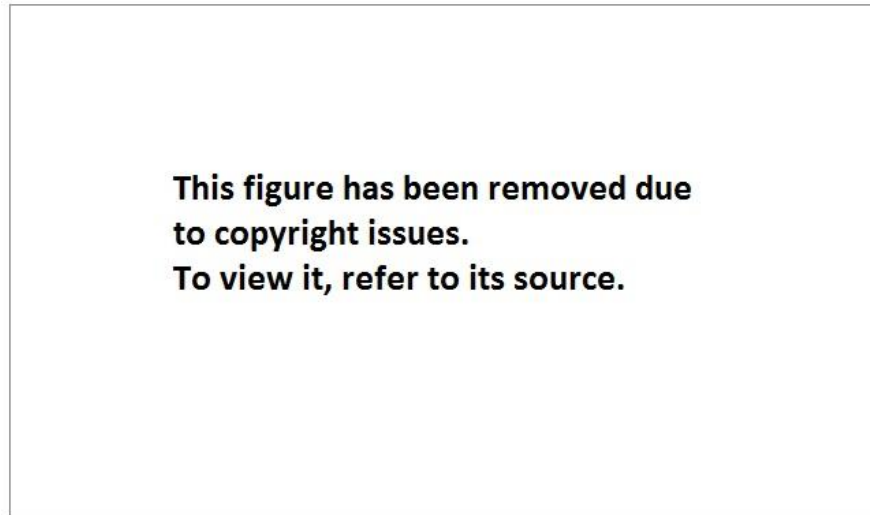
Figure 2.9: Critical Shear Stress as a function of SAR, $\Delta\varepsilon o$ and CONC (based on data from Arulanandan *et al*. 1980)

Sodium adsorption ratio measures the salt concentration of the pore fluid by measuring the concentration of sodium, calcium and magnesium cations. The surfaces of clay soils' particles are negatively charged and as a result attract positively-charged particles. The charged surface and the distribution of cations attracted to the surface are termed the diffuse double layer (Barbour and Fredlund 1989). Cations from overlapping double layers repel each other enough to overcome the attractive van der Waal's forces between particles, resulting in the repulsion of the clay particles. The attraction between clay particles is greater when the cations are bound tightly to the clay surface – the diffuse double layer is thinner, which leads to flocculation of clay particles and shrinkage of the soil (Mitchell and Soga 2005).

Cations with higher valence, such as Ca^{++} and Mg^{++}, are more tightly bound to the clay surface than lower valence ones such as Na^+, which promotes dispersion of the soils. This means that the higher the SAR value, the higher the degree of deflocculation and erosion.

Arulanandan *et al.* (1980) extended previous research by performing erosion experiments to measure critical shear stress. Thirty soil samples were taken from stream banks across the United States; half of the samples were from sites exhibiting erosion, and the other half were from stable sites. Three gallons of river water were collected at each site to act as the eroding fluid in the experiment. Erosion tests were performed on the samples by circulating the collected water on the undisturbed samples inserted in a hydraulic flume from the bottom. The flume was 6 inches wide, 12 inches deep and 8 feet long. Figure 2.10 shows a schematic of the system. The velocity head of the flow was measured using a pitot tube, which was used in an empirical equation by Preston (1954) to approximate the bed shear stress when particle movement is observed. The shear stress was calculated using Equation 2.6 (Arulanandan *et al.* 1980). This calculation was only valid for shear stresses lower than 14.6 dynes/cm^2.

$$log \frac{\tau_o d^2}{4\rho v^2} = -1.396 + \frac{7}{8} log \frac{(p_t - p_o)d^2}{4\rho v^2} \qquad\qquad\qquad \text{Equation 2.6}$$

where
$$4.5 < log \frac{(p_t - p_o)d^2}{4\rho v^2} < 6.5$$
τ_o = bed shear stress (dynes/cm^2)
d = outside diameter of pitot tube (cm)
ρ = mass density of fluid (g/cm^2)
v = kinematic viscosity of the fluid (cm^2/sec)
p_t = total head measured (dynes/cm^2)
p_o = static head measured (dynes/cm^2)

The average shear stress distribution across the surface of the samples was calculated by placing the pitot tube along different locations of the soil surface. After 2.5 minutes of testing, the soil

sample was removed from the apparatus and weighed. The same procedure was repeated for increasing flows to produce a graph of weight loss versus shear stress. Critical shear stress was defined at the point where the weight loss increased from zero.

This figure has been removed due to copyright issues.
To view it, refer to its source.
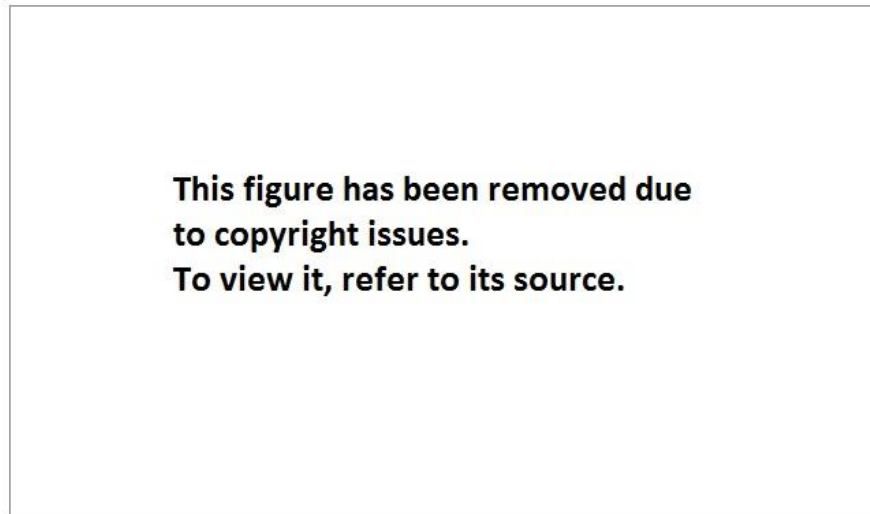
Figure 2.10: Representation of laboratory recirculating hydraulic erosion flume
(reproduced from Arulanandan *et al*. 1980)

Furthermore, remoulded samples were tested in a rotating cylinder apparatus as shown in Figure 2.11. The apparatus consisted of an axially-supported hollow plexiglass cylinder on a shaft rotated by an electric motor. Soil samples were placed inside the rotating cylinder, and the eroding fluid filled the chamber between the rotating cylinder and the sample. The outside cylinder was electrically rotated, which created a shear stress on the fluid within the cylinder and subsequently on the soil sample. Shear stress readings were recorded directly via measuring the total exerted force by the fluid on the sample as the cylinder was rotated. Arulanandan et al. (1980) compared the measured τ_c to predicted critical shear stress results shown in Figure 2.12 and Figure 2.13 for undisturbed and disturbed samples, respectively. The x-axis was used for measured τ_c and the y-axis for predicted τ_c, and a straight line was drawn on both charts with a 1:1 slope. If the measured and predicted results fall on the line they are the same. Predicted

values are too high if the results fall above the line, and too low if they fall below. The plots determined that the predicted values for τ_c were lower than the measured values for both undisturbed and remoulded samples.

This figure has been removed due to copyright issues.
To view it, refer to its source.
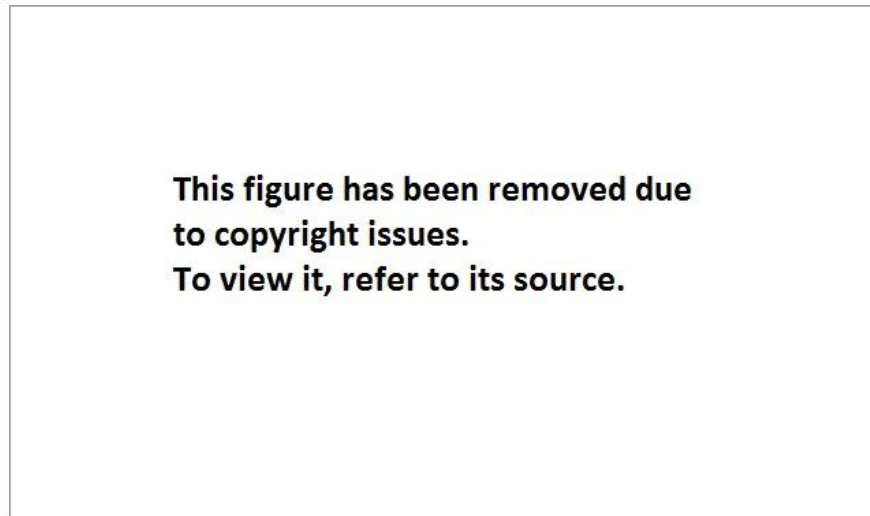
Figure 2.11: Cross-Section through rotating cylinder apparatus (reproduced from Arulanandan *et al*. 1980)

This figure has been removed due to copyright issues.
To view it, refer to its source.
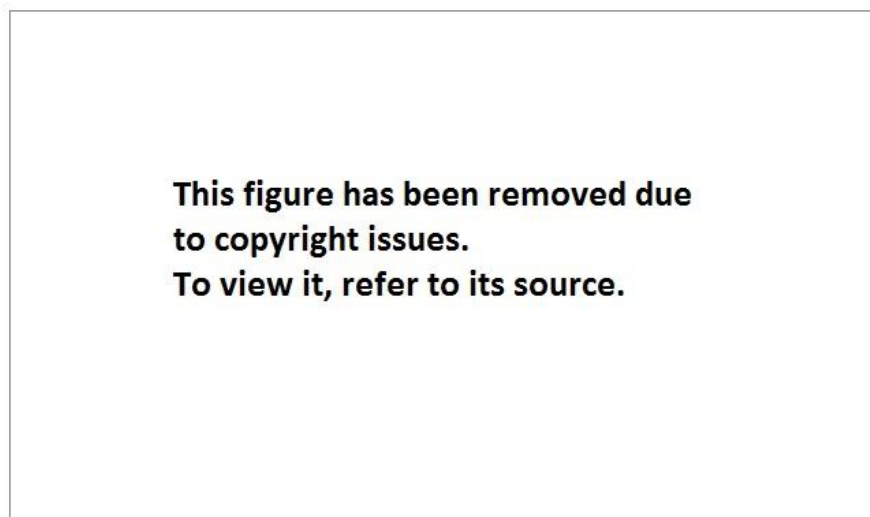
Figure 2.12: Predicted critical shear vs. measured critical shear for undisturbed soil samples (based on data from Arulanandan *et al*. 1980)

This figure has been removed due to copyright issues. To view it, refer to its source.

Figure 2.13: Predicted critical shear vs. measured critical shear for disturbed soil samples (based on data from Arulanandan *et al*. 1980)

The lower critical shear stress results of Alizadeh (1974) and Heinzen's (1976) chart may be related to distilled water used as the eroding fluid in their experiment. Arulanandan *et al*.'s (1980) experiments further proved that the salt concentration of eroding fluid significantly influenced the erosion of soil samples. As the salt concentration of the eroding water decreased, so did the critical shear stress. Therefore, the more material in the eroding water (such as suspended solids), the higher the critical shear stress. Arulanandan *et al*. 1980 explained this through the concept of osmotic pressure, which decreases when there is a decrease in the salt concentration gradients between the eroding fluid and pore fluid. This means that critical shear stresses are much higher for soils in distilled water (as opposed to soils in contact with water with an existing suspended load), due to the higher salt concentration gradient. Arulanandan *et al*. (1980) suggested that, because the critical shear stress increases as the salt concentration of the eroding fluid increases, the chart proposed by Alizadeh (1974) and Heinzen (1976) (Figure 2.9) would provide a reasonable estimate of the critical shear stress for a natural, undisturbed soil sample.

Briaud *et al*. (2001) proposed another similar method that involves the measurement of critical

shear stress through use of the Erosion Function Apparatus (EFA) shown in Figure 2.10. Soil

samples in a standard ASTM Shelby tube are pushed into one end of a rectangular pipe's circular

opening from the bottom until 1 mm is exposed into the flume using a piston. A flow of a given

velocity is run through the pipe, and the time and velocity required to erode the soil are

measured. The process is repeated at increasing velocities, and the shear stress is calculated

using Equation 2.7.

$$\tau = \frac{1}{8}f\rho v^2$$
<div align="right">Equation 2.7</div>

where,
τ = shear stress
f = friction factor obtained from a Moody chart
ρ = density of water
v = mean flow velocity in flume

Tap water can be used to run the tests. However, Briaud *et al*. (2001) suggested replicating the

actual site conditions by using the river water, or imitating the water's chemistry since this

influences the erodibility of cohesive soils. Results provided by Briaud *et al*. (2001) show the

values of τ_c for fine-grained soils vary between 0 and 5 Pa.

2.3.3 Erosion Rate

Erosion rate is the volume of soil scoured, during a certain period of time, when the applied

shear stress on the soil is higher than its critical shear stress. The quantity of erosion can be

back-calculated to estimate the retreats of bank using a measured erosion rate. Partheniades

(1965) proposed an excess shear stress approach to calculate erosion rates for cohesive soils by

using Equation 2.8.

$$\varepsilon = k(\tau_o - \tau_c)^a$$
<div align="right">Equation 2.8</div>

where
k = erodibility coefficient
τ_o-τ_c = Excess shear stress
a = an exponent often assumed equal to 1.0

The value of k is determined experimentally. Two hundred soil samples at stream sites from Nebraska, Iowa and Mississippi were tested, and it was determined that k could be estimated as a function of τ_c given by Equation 2.9 (Hanson and Simon 2001).

$$k = 0.1x10^{-6}\tau_c^{-0.5}$$

Equation 2.9

The Briaud *et al.* (2001) method for erosion rate is based on Equation 2.10, where h is the height of sample eroded and t is the amount of time required to erode the sample. The height of the sample is a standard 1 mm for all tests from the bottom of the flume.

$$\dot{z} = h/t$$

Equation 2.10

The final output is a curve of erosion rate vs. shear stress on the y and x axis, respectively. The critical shear stress is the point on the curve where the erosion rate first increases from zero. Briaud *et al.* (2001) indicated that erosion rates varied from 0.3 to 30 mm/hr and that the erosion rate of fine-grained soil is thousands of times slower than the erosion rate of coarse-grained soils.

Osmann and Thorn (1988) also proposed an equation based on the results of Arulanandan *et al.'s* (1980) experiments. As shown in Figure 2.14, Arulanandan *et al.* (1980) produced a graph of rate of change of erosion rate versus measured critical shear stress. To describe the behaviour of this graph, Osmann and Thorne (1980) developed Equation 2.11 in the transition region, where τ_c is greater than 0.6 Pa. The assumption is that soils with critical shear stresses lower than 0.6 Pa

will behave like cohesion-less soils. The final erosion rate is defined by substituting Equation 2.11 into Equation 2.12, where τ_c is in dynes/cm^2 and dW is in m/min.

$$R = 223\text{x}10^{-4}\tau_c e^{0.13T_c} \qquad\qquad \text{Equation 2.11}$$

$$dW = \frac{R}{\gamma}\left(\frac{\tau-\tau_c}{\tau}\right) \qquad\qquad \text{Equation 2.12}$$

Back-calculation can be performed to estimate the quantity of riverbank erosion once the erosion rate is obtained. The erosion of the bank can be calculated in meters by multiplying the erosion rate by the time over which the shear stress of the river has been greater than the critical shear stress.

This figure has been removed due to copyright issues.
To view it, refer to its source.
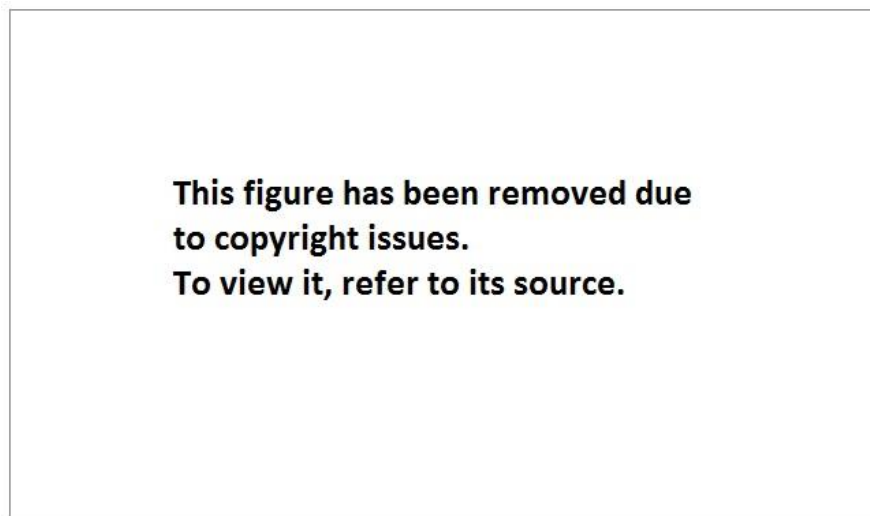
Figure 2.14: Rate of change of erosion rate vs. critical shear stress for undisturbed soil samples (based on data from Arulanandan *et al.* 1980)

2.3.4 Critical Shear Stress and Erosion Rate Related to Soil Properties

Briaud *et al.* (2001) hypothesized that a correlation existed between τ_c, erodibility and soil properties. In a review of literature dating back to 1960, no widely accepted correlation was found. The authors suggested that, if a correlation exists, it must involve several parameters and require many clay samples to be tested in order to validate the relationship.

Arulanandan *et al*. (1980) stated that the main property governing the erosion of clays is the concentration of dissolved sodium, calcium and magnesium cations in the pore water, represented by SAR. The correlations between SAR and erosion rate, and SAR and τ_c are shown in Figure 2.15, as proposed by Arulanandan *et al*. (1975). Higher erosion rates and lower critical shear stress are seen for soils with SAR values greater than 10, as shown by their steep lines and x-axis intercepts. For SAR values lower than 10, τ_c is shown to be as high as 38 dynes/cm^2 or 3.8 Pa with more gradual erosion rates. The concentration of dissolved salts in the eroding fluid is another main factor in erosion rates. As shown in Figure 2.16, if the salt content in the eroding water is low, the soil is more susceptible to erosion (Arulanandan *et al*. 1975). Arulanandan *et al.* (1975) also stated that erosion is a surface phenomenon where mechanical soil properties such as shear strength, moisture content and plasticity index do not accurately describe the state of the soil at the surface.

As the SAR of the soil samples increases, a corresponding increase to the erosion rate and decrease to the critical shear stress is observed.

SAR = 154
SAR = 12.4
SAR = 9.4
SAR = 1.4

Increased SAR of Soil Samples

Increased Erosion Rate

Decreased Critical Shear Stress
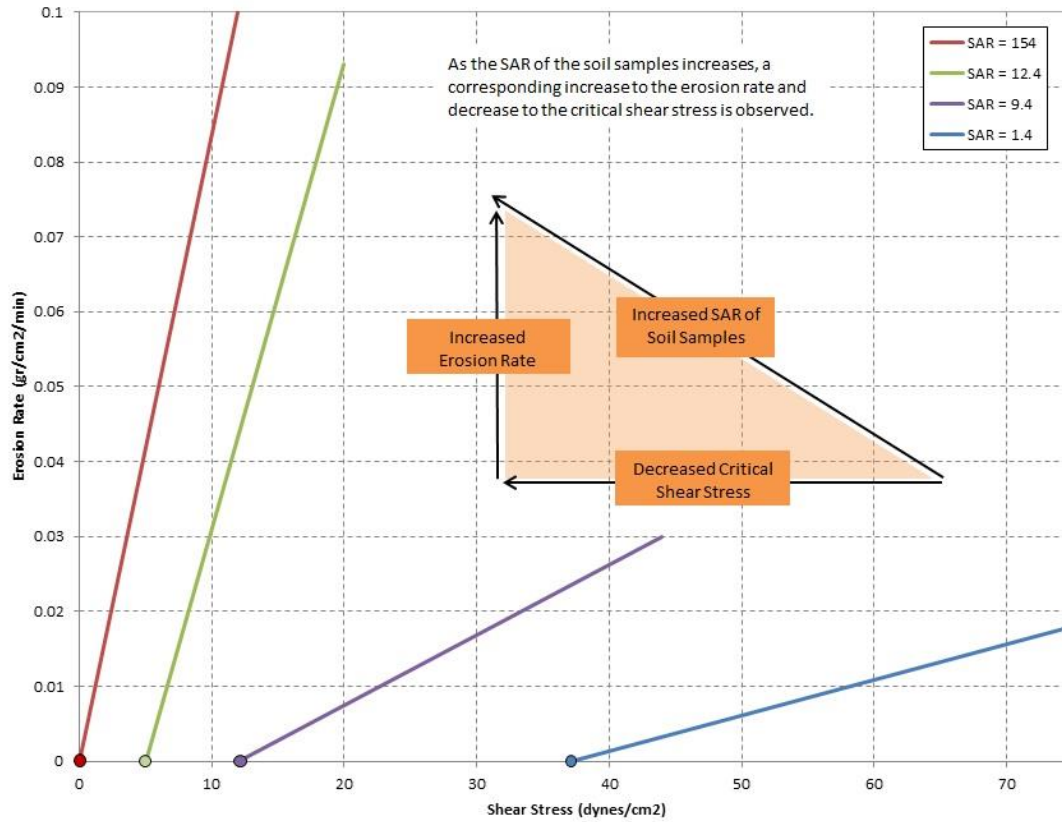
Figure 2.15: Effect of Sodium Adsorption Ratio (SAR) and Eroding Fluid Concentration (CONC) on Erosion Rate and Critical Shear Stress (used with permission from American Society of Civil Engineering April 4th 2013, based on data from Arulanandan *et al*. 1975)

31
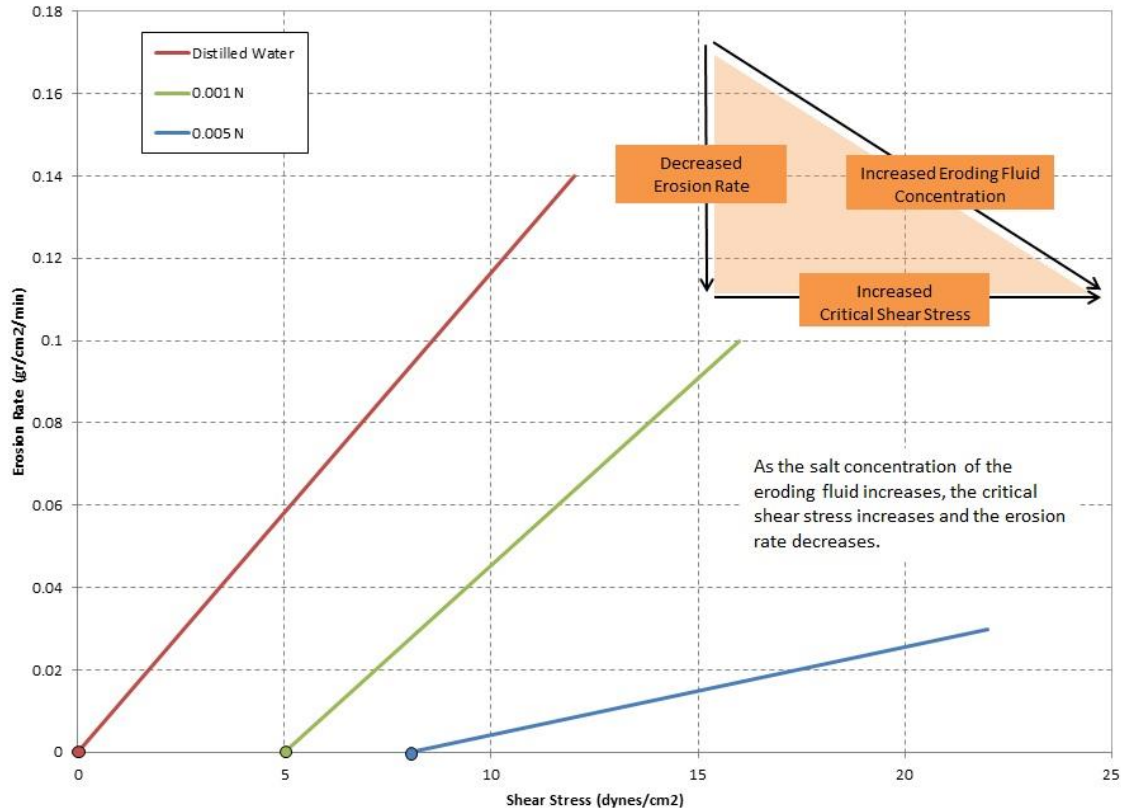
Figure 2.16: Effect of Eroding Fluid Concentration (CONC) on Erosion Rate and Critical Shear Stress (used with permission from American Society of Civil Engineering April 4th 2013,based on data from Arulanandan *et al*. 1975)

2.3.5 Numerical Methods to Quantify Erosion

Several numerical models for channel width adjustment exist, which incorporate the hydraulics of flow, sediment transport of bank material and bank stability. However, not all physical processes and mechanisms involved in channel adjustment have been represented successfully in one model. These numerical models have sophisticated solutions to describe the hydraulics of flow and sediment transport, but do not incorporate accurate analysis of riverbank stability. Assumptions are made that are not necessarily accurate regarding how failed bank material is deposited in the channel and/or carried away by the river flow. Since existing models have not been subjected to rigorous evaluation in terms of their ability to replicate laboratory data or

simulate field situations, more laboratory and field data are needed to evaluate and fine-tune them (Darby 1998).

2.4 Characteristics of the Red River

The Red River originates in the southern part of North Dakota and Minnesota, at the convergence of the Ottertail and Bois de Sioux Rivers. The river continues to meander from this point northward over a distance of 885 km to Lake Winnipeg (Red River Basin Investigation (RRBI) 1953). The river originally became established between 8200 and 7800 ^{14}C yr B.P. when Glacial Lake Agassiz receded northward. The Red River eroded a shallow valley approximately 15 m deep and 2500 m wide with a gentle gradient of 0.0001 (Brooks *et al*. 2005) in the lacustrine glacial lake deposits.

Red River has a drainage area of 287,500 km^2. Fifty-seven percent (or 163,000 km^2) are drained by the Assiniboine River, which is the major tributary to the Red River. Of the remaining 124,000 km^2, 102,000 km^2 are in the U.S. and 22,000 km^2 are within Canada (RRBI 1953). Predominantly a suspended sediment load composed 90% of silt and clay regardless of the sediment concentration and river discharge (Brooks 2000) is carried by the river. The minimum and maximum sediment concentrations fall within a range of 10 to 20 mg/L during December and February and 500 to 1900 mg/L from April to July (Brooks 2002).

2.4.1 Annual Flows and Elevations

Flow and elevation have been recorded at the Emerson International Gauging Station at the international boundary between Canada and the United States approximately 140 km south of Winnipeg since 1912. These records show a peak of flow and elevation in the Red River during the spring months of April to May. This is in response to the winter snowmelt run-off and spring

precipitation. Secondary peaks are also observed, generated by high rainfall events from June to October. Outside of the peak flow periods, Public Works Canada regulates the elevation of the Red River within the City boundaries with the use of the St. Andrews Lock and Dam (SALD) which is located at Lockport, Manitoba, 27 kilometers north of Winnipeg. SALD is operated each year after the spring peak inflows rise to 223.7 m. This elevation is maintained through the summer and fall to facilitate boat navigation over the outcrops of bedrock approximately 50 km downstream of Winnipeg, known as Lister Rapids. In the beginning of November, the dam is opened and the river's elevation is allowed to subside to its natural 221.9 m, in order to accommodate the following year's spring in-flows.

Reviewing historical flow records (available from 1912) shows the mean annual discharge has been 110 m^3/s with the highest discharge recorded at 3770 m^3/s in 1997 (Manitoba Water Resources 2005). The full discharge of the Red River is 600 m^3/s, and its return period is 2 years (Brooks 2003). Discharge higher than this amount would result in a state of flood in the City of Winnipeg. This has occurred 49 times (or 53%) over a 92 year record (Manitoba Water Resources 2005). Due to the shallowness of the valley and the insufficient capacity to contain high flows, flooding and overtopping of the banks is common along the Red River (Brooks and Nielsen 2000).

Even though floods are typically associated with spring snowmelt, prolonged periods of rain can also result in flood conditions in the late months of spring and early months of summer (RRBI 1953). The low valley gradient of the region results in slow rise and fall of floods over a period of up to 4 to 6 weeks (Brooks 2003).

When the river overtops its banks, the flat topography further increases the flood hazard as the river water spreads across many kilometers of prairie surface. Flow records and tree-ring dating show that the largest floods of the Red River have been in 1826 (5350 m^3/s), 1852 (3770 m^3/s), 1950 (2670 m^3/s), 1979 (2620 m^3/s) and 1997 (3740 m^3/s) (Manitoba Water Resources 2005, Brooks *et al*. 2003). The 1997 flood, which was the largest since 1852, flooded a total area of 2000 km^2, with sections up to 40 km wide, between the Canada/U.S. boarder and Winnipeg (Brooks 2003).

To alleviate the flood risk to the City of Winnipeg, the Red River Floodway was constructed and put into operation in 1968. The Floodway is an excavated channel that diverts a portion of the Red River around the City of Winnipeg. It has a design capacity of 1700 m^3/s. However, it managed to carry successfully a discharge of 2110 m^3/s in the flood of 1997 (Brooks and Nielsen 2000). Since the inauguration of the Floodway, the flows at the Emerson International Gauging Station have not been representative of the river's flows within the City of Winnipeg. The James Street Pumping Station (located inside the City of Winnipeg) is the alternative gauging station and has been recording daily flows and elevations since 1948.

2.4.2 River Pattern

A common characteristic of a mature river is its meandering morphology. The Red River's meandering has been interpreted to be relatively inactive by researchers who studied its aerial photographs over the past 130 years. Photographs of the floodplain show a single pattern of ridge and swale topography, indicating that the meanders went through a single sequence of expansion (Brooks 2003). Similar to ripples of sediment, surface ridges and swales are typical

features of meandering rivers. The widening of the valley cross-section is negligible when compared to timescales of several centuries (Brooks 2003).

2.4.3 Lake Agassiz Soils

The soils in the Winnipeg and southern Manitoba areas are what used to be the bed of Glacial Lake Agassiz. The Lake was formed between 13,500 and 8,000 years BP, when the Wisconsin continental glacier blocked the natural drainage north to the Arctic Ocean via the Hudson's Bay (Graham and Shields 1985). Lake Agassiz covered the greater part of Manitoba (Quigley 1980) and was formed by the combination of the melted water from the glacier, local rainfall, and rivers from the south and west. At its maximum range, this glacial lake covered an area greater than 521,000 km^2 and was the largest lake in North America. However, the lake's maximum size at any one time was 208,000 km^2 (Baracos *et al*. 1983). This great lake was more than 150 meters deep, above the present level of the City of Winnipeg (Macdonald 1937). Initially, Lake Agassiz drained southward into the Mississippi river system, but as the ice retreated north, the drainage of the lake transitioned northwards into Lake Superior and successively into the Hudson Bay. Lakes Winnipeg, Manitoba, Winnipegosis, and the Red Lakes in Minnesota are the remains of Lake Agassiz (RRBI 1953).

The Wisconsin glacier went through a series of advances and retreats. This resulted in the deposition of a heterogeneous till consisting of clay, sand, gravel and boulders, to a maximum depth of 90 meters in some areas (RRBI 1953). During the existence of Lake Agassiz, the lacustrine clay was deposited overtop of the till. This sediment was transported into the lake by rivers and spread over the bottom of the lake (RRBI 1953). The average depth of the clay is 9 to 13 meters and is found at depths varying from zero to 20 meters (Baracos *et al*. 1983). These

lacustrine deposits are high plastic clays. Since they have the ability to hold large quantities of moisture, they exhibit high swelling and shrinkage characteristics (RRBI 1953).

2.4.4 Soil Stratigraphy

Analyses of the Lake Agassiz deposits have classified them into two main categories: an upper complex zone and a silty clay unit (Baracos and Kingerski 1998). Till and bedrock underlie these deposits. Alluvial deposits overlie the Lake Agassiz deposits around riverbank areas.

2.4.4.1 Upper Complex Zone

The upper complex zone is the top portion of the soil stratigraphy and averages a depth of 1 m to 4.5 m. It was formed by post-glacial events, such as deposition and erosion (both due to flooding and river flow), vegetation growth and human activity (Baracos *et al*. 1983, Baracos and Kingerski 1998). The stratigraphy of these deposits consists of discontinuous thin layers of silt, silty clay and clay, characterizing them as complex (Baracos and Kingerski 1998).

The silty clay and clays are highly plastic and, due to repeated freeze-thaw cycles and shrinkage and swelling upon drying and wetting, reveal a nuggety structure (Baracos and Kingerski 1998). The silt is in discontinuous interlayers that vary in thickness within short distances and can be up to 3 m thick (Baracos *et al*. 1983). A layer of lacustrine silt defines the base of the complex zone.

2.4.4.2 Silty Clay Unit

The upper complex zone is underlined by a silty clay unit. Its thickness ranges from zero to 21 meters with an average thickness of 9 to 12 meters (Baracos and Kingerski 1998). This unit is divided into two distinct layers based on the soil colour – even though both layers are considered to be a part of a single depositional sequence, as there is no difference in clay fraction or

mineralogy (Baracos et al. 1983). The change in colour of the upper unit is the result of oxidation (Baracos et al. 1983). The upper clay has a brown to mottled grey-brown colour and ranges in thickness from 1.5 to 6 meters. The lower clay deposits are coarser and more bedded than the upper layer, with alternating layers of clay-rich and silt-rich sediments, and are generally grey (Baracos et al. 1983). The lower deposits also contain joints, fissures, rock fragments that approach boulder size, and uncemented silt inclusions.

2.4.4.3 Till

Till underlies the lacustrine clay and ranges from zero to 10 meters in thickness. The till sediments were deposited via Wisconsin Glacier's numerous advances and retreats (Baracos *et al*. 1983). This till layer is a heterogeneous mixture of particles ranging from clay to boulder-sized. The clay content decreases with increasing depth into the till. The till has two distinct layers which exhibit different properties. The upper portion is considered soft and the lower portion hard. The clay and moisture contents of the two layers differ, which influences their strength. Due to the upper layer's greater clay and moisture content, it has a lower strength in comparison to the lower layer (Baracos and Kingerski 1998). The undrained shear strength of the lower till layer approaches the strength of weak concrete (Baracos and Kingerski 1998). This is why end-bearing piles are often founded on the lower till. Regardless of their strength properties, both layers are classified as soils (Baracos *et al*. 1983).

2.4.4.4 Bedrock

Approximately 76 to 230 meters of Paleozoic limestone and dolomite bedrock are beneath all the soil layers (Render 1970). The upper 15 to 30 m of this bedrock are highly fractured and jointed, and contain bedding planes that provide a high degree of permeability, resulting in a major aquifer referred to as the Upper Carbonate aquifer (Render 1970). The upper 7.5 m of the

carbonate rock experience the greatest amount of flow, due to having the highest permeability (Render 1970). The low-permeable clay and till deposits on top and the low permeability of the bedrock below confine the aquifer from top and bottom (Baracos and Kingerski 1998). During the past 130 years the aquifer has been a major source of groundwater to the City of Winnipeg, during which over 200 commercial and municipal wells were installed (Render 1970). A large drawdown of the aquifer occurred under the City of Winnipeg due to increased consumption during the 1900's (Render 1970). The constant low temperature of the groundwater has made it ideal for commercial and industrial use for cooling (Render 1970), as well as irrigation and domestic purposes. However, groundwater usage in the Winnipeg area has been declining recently. This is mainly due to the fact that some major industrial companies are no longer located in the area and those that still use the aquifer return the water to it after use (Tutkaluk, 2000).

2.4.5 Riverbank Stratigraphy

High flows and flooding have deposited alluvial sediments on the Red River banks and its surroundings. Mixture of sand, silt and clay are what make up most of the deposits, with little to no coarse-grained materials (Brooks 1993). The alluvial deposit's fine texture is a reflection of the fine grain size of the Lake Agassiz clay, which comprises the majority of eroded sediments transported by the river (Brooks 1993). All sections (outside and inside bends, transitions and straight sections) of the Red River are subjected to erosion and deposition (Baracos and Lew 2001). Erosion is highest where flow velocities are greatest, as to be expected. Erosion activity occurs primarily in the lower parts of slopes and the bed during flood events (Figure 2.3 and Figure 2.4). At the same time, velocities are lowest near the top of the slope, among vegetation, and where the river has overtopped its banks. Since the velocity cannot support the suspended

load, this is where deposition occurs (Baracos and Lew 2001). Added erosion occurs when trees

and vegetation are undercut from fluvial and ice action.   Increased turbulence (caused by

exposed tree roots which interfere with the flows) result in further undercutting of the banks

(Baracos and Lew 2003).

The thickness of the 1999 flood deposits along the upper slope of the outside bends of both low

and steep angled slopes was studied by Brooks (2005). The 1999 spring peak flow overtopped

the bank by a depth of 0.5 m, resulting in the deposition of sediment behind the crest and on the

upper slope. Deposition was measured along both low-angled and steep-angled slopes, defined

as having gradients of less than 11° and between 23° and 27°, respectively. The study found that

the overbank deposits for low-angled slopes aggraded up to a thickness of 21 cm and generally

thinned with increasing distance from the river. The thickness of deposits varied from 3 to 21

centimeters within 30 meters from the channel's edge.   The thickness decreased to five

centimeters or less at distances greater than 50 meters from the channel. Grain size analyses

showed that the sediment was 60 to 80 percent silt particles. The deposits on the steeper slopes

were similarly silt-sized particles and thinned with increasing distance from the controlled

summer water level. However, the deposits were thinner in comparison to low-angled slopes.

The deposits ranged in thickness from 7 cm to less than 0.1 cm. The majority were along the

lower several meters of the bank.   They were deposited as water levels withdrew to the

controlled summer levels. Contrary to meander theory, the study concluded that deposition on

the banks of inside bends was minor in comparison to the accumulation on the outside bends

(Brooks 2005).

2.4.6 Riverbank Stability and Failures

Riverbank instability is observed to be seasonal and related to a combination of factors, such as river elevation, pore water pressures, and bedrock aquifer elevation (Baracos 1978, Tutkaluk 2000, Baracos and Lew 2003). Infiltration of snowmelt and rain during the spring and summer contribute to high pore water pressures within the banks. This results in a decrease in the shear strength available to mobilize the failure surface through the bank. However, due to the raised river elevation maintained by Public Works Canada through the summer and early fall with the use of St. Andrews Lock and Dam (SALD), the failure is often delayed (Baracos and Lew 2003). The weight of the river water bearing on the lower bank acts as a counter-balancing force to the high pore water pressures and helps stabilize the banks (Baracos and Lew 2003). Furthermore, the increased consumption of the groundwater during the summer, which decreases pore water pressures along the clay-till interface, also aids in stabilizing the banks.

Conversely, the decrease in consumption of the groundwater in the fall, the opened gates at SALD (to lower the river elevation in preparation for the following year's spring inflows) and the high pore water pressures from the spring (due to the low permeability of the clay) commonly result in riverbank failures in the fall, which continue at a decreased rate through the winter (Baracos 1978, Tutkuluk 2000, Baracos and Lew 2003).

Two other driving factors that add to the instability of the banks are the erosion around the toe of the banks and the deposition around the crest of the riverbanks due to high flows and ice forces. The spring and summer high flows exert higher shear stresses on the banks, causing erosion by entraining soil particles into the flow (Thorne 1982). The erosion reduces the forces supporting the upper banks, resulting in reduced stability of the banks (Baracos and Lew 2003). However,

most often the banks do not fail until the combined effects of both the river and aquifer are observed in the fall (Baracos 1978). Another factor that removes large amounts of soil from the bank during the spring is ice break-up and scouring. Ice lifts the frozen soil to which it is attached as it breaks up, allowing the soil to be carried away by the flow. Also, the impact of the ice sheets against the banks removes large chunks of material, resulting in tree root exposure. Exposed roots cause an increase in local turbulence, which leads to more erosion of the banks (Baracos and Lew 2003). It is common for the upper portions of the submerged bank to accumulate sediment during the spring flows. Roots of trees and vegetation also promote sediment deposition by reducing flow velocities. This deposition can accumulate to an appreciable loading in some locations over several years. If the loading is on the upper banks (adding to the driving forces causing sliding), the bank becomes more unstable; the opposite is true if the sediment deposition occurs at the bottom of the slope (Baracos and Lew 2003). Failure of riverbanks is not confined to the outside bends, but rather occurs also along inside bends, straight and transition sections of the Red River (Baracos and Lew 2003). These failures are explained through the change in thalweg location under low-stage and high-stage flows as shown in Figure 2.17. The thalweg approaches the outer banks during low-stage flows, whereas during high-stage flows the meander pattern is short-circuited and the flow goes over rather than around the inside bends.
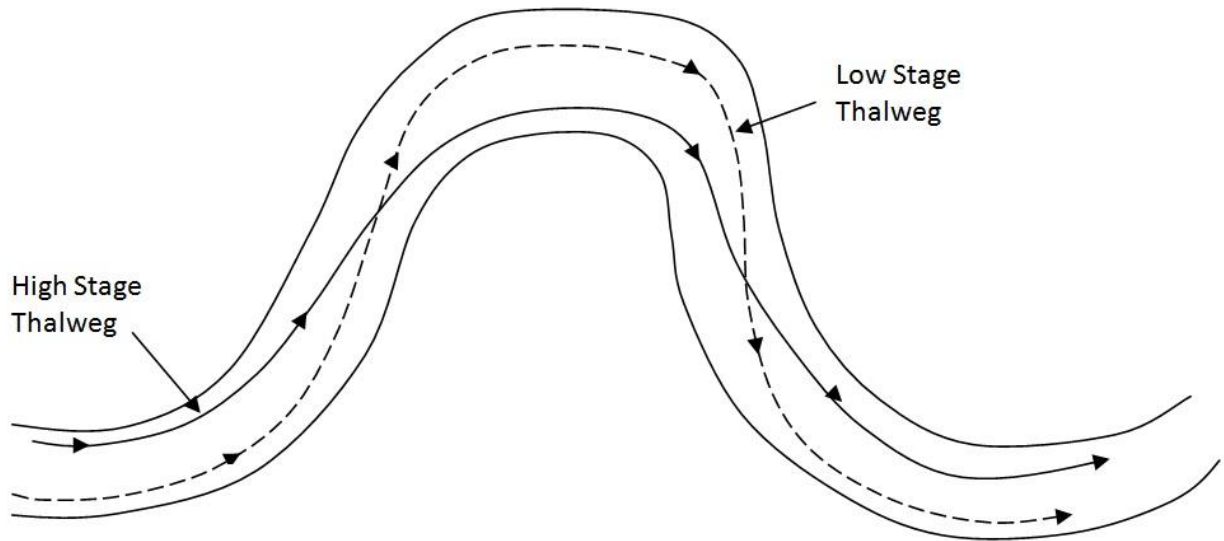
Figure 2.17: Location of thalweg at low and high stage flows

A number of factors are combined to cause riverbank instability and ultimately fail (Baracos and Lew 2003). As a bank fails, the soil moves toward the toe of the bank or directly into the channel and is removed from that point depending on the river's flow. The accumulation of the material at the toe depends on the frequency of failure and the ease of removal via flow. At locations where the flow is able to remove all debris, the toe continues to erode. This leads to an increase in the slope angle and induces further subsequent bank failures. However, if the flow is not able to remove the material, the debris accumulates at the toe and acts as a buttress, known as basal endpoint control, which tends to increase stability of the bank. The extra weight and the decreased slope angle support the upper bank to make the slope more stable (Thorne 1982). The new configuration of the bank is more stable than before the failure. This stable position is maintained as long as the flow is not sufficiently great to erode the material. Ultimately, the equilibrium of river banks is a balance between the supply and the removal of material at the base of the bank.

The commonly-observed stability of Red River's banks for a long period of time and their sudden subsequent failure can be explained by the progressive erosion over a number of years until the point of failure.

Red River bank slides have been observed to be deep seated and retrogressive, extending to the clay-till interface and up to 80 meters from the summer's water level (Baracos and Kingerski 1998). Due to the lower shear strength of the material above the till, the sliding is limited to the clay layer and usually does not extend into the till (Baracos and Lew 2003).

2.5 Applying the Theory

The previous sections discussed river systems in terms of the hydraulics of their flow, sediment transport and deposition, and morphology. Various factors and theories governing erosion where also presented followed by the characteristic of the Red River.

The variables presented, governing erosion, are just some of the possible variables in determining erosion rates. To be able to assess the impact of erosion more accurately, for a specific study site, empirical erosion rates are required.

CHAPTER 3: EROSION MEASUREMENT DEVICE

3.1 Introduction

The Erosion Measurement Device (EMD) was designed and built at the Geotechnical Laboratory of the University of Manitoba to measure the erodability of typical Red River sediments under flow velocities that are consistent with the velocity distributions during normal flow and flood conditions.

3.2 Design of the Erosion Measurement Device (EMD)

The EMD was built for this study to measure the erosion function for selected soil specimens using water from the Red River. This erosion function defines the relationship between the hydraulic shear stress (directly related to flow velocity) applied in the flow boundary layer at the riverbed and the erosion rate for the material.

The water that circulates in the EMD is contained in the storage tank which is 0.9 cubic meters in volume with a central baffle system and coarse filter in the middle to prevent large particles from entering the pump and in turn into the flume. The weir prevents larger and heavier particles from getting into the second half of the sump. The coarse filter that is placed in between the baffle system stops larger floating particles from flowing in the water which can damage the pump and the flume. This may provide more conservative results according to theory and the experiments performed by Merten *et al.* (2001) on erosion in rills. The study confirms larger sediments cover the soil bed during the erosion process would shield the soil from flow forces and thus reduce detachment of the soil sample particles which would result in lower erosion rates.

A frequency drive regulates the speed of the pump motor which produces the desired flow velocities. The velocity in the pipe is determined by an ultrasonic flow meter. An acrylic flume which is 243 centimeters long, 10 centimeters wide and 5 centimeters deep is in between the pump and the return pipe to the sump. The flume is contained by a lid that has two grooves at the bottom, lined with a rubber gasket, which fits on top of the flume walls to prevent it from bowing out when the flume is pressurized (Figure 3.1). The lid is clamped in place with eleven clamps across the length of the flume to prevent any leakage. At the end of the flume the soil sample extrudes into the flume from the bottom. The return pipe is located after the flume. A junction connection in line with the return pipe allows emptying the water from the flume when the pump stops. Figure 3.2 shows the overall schematics of the EMD.
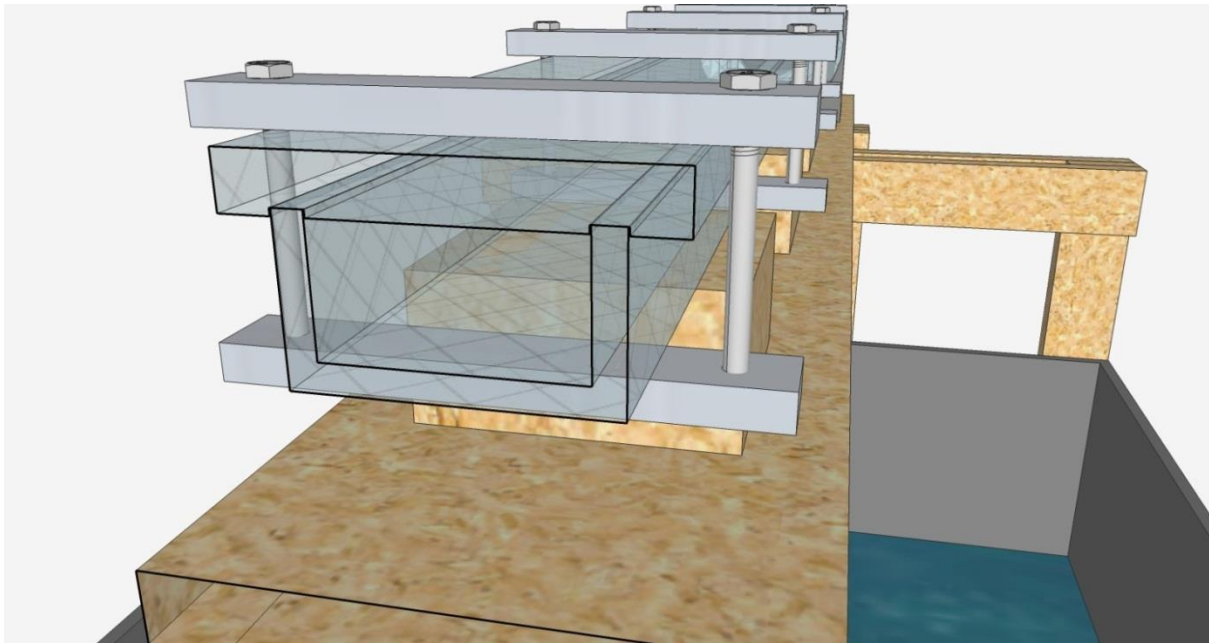
Figure 3.1: Cross section of flume and lid
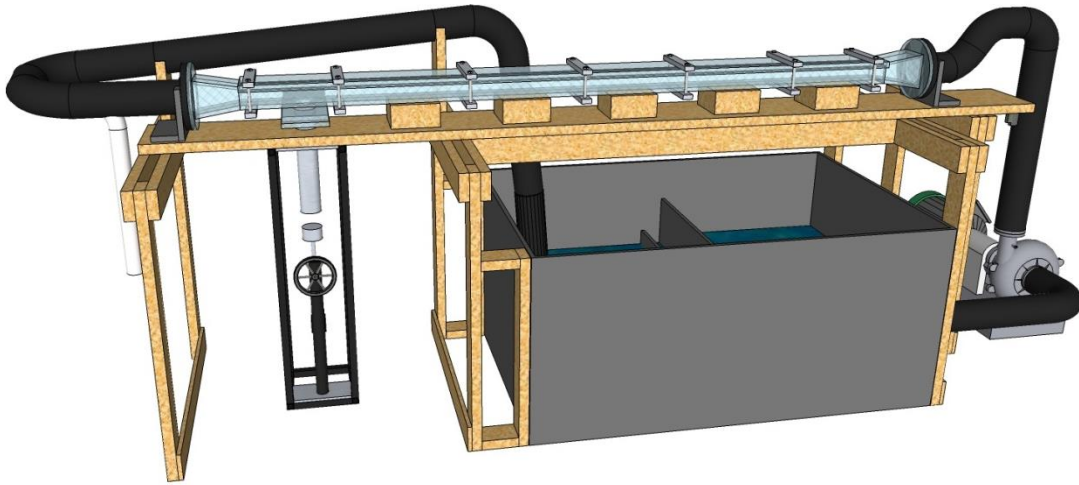
Figure 3.2: Overall look of EMD

The device includes a number of key components. Figure 3.3 displays the right end of the device, where the pump and the frequency drive regulate the flow into the flume and the ultrasonic flow meter that displays the flow in the pipe is located. The flow velocity in the flume is then calculated using the flow volume and the cross-sectional area of the pipe and the flume.

Figure 3.3: Pump and Ultrasonic Flow meter

Figure 3.4 shows the end of the flume where the tube with the sample being tested is fastened to the bottom of the flume and extruded with the screw jack. The sample is observed in the dark with a flashlight and lasers mounted on the platforms on both sides of the flume. This allows for visual observation of the erosion at positions on the specimen in the flow field.

Figure 3.4: Extrusion System and Observation Deck

Figure 3.5 illustrates the extraction of a Shelby tube sample into the customized pipe that fits under the flume with O-rings to prevent leakage.

Figure 3.5: Shelby Tube Extraction Device

3.3 Methodology

A roughness of 1.5 µm was assumed to determine the shear stress that a certain flow velocity would produce. Each frequency was then set and the average flow velocity in the pipe measured using the Ultrasonic Flowmeter. The velocity in the pipe was converted to the average flow velocity in the flume using the cross sectional area of the two conduits. The flow velocity in the flume was then used to calculate the shear stresses applied to the specimen. The equation used was obtained from Briaud *et al.* (2000) (Equation 2.7). The pipe velocity was calculated and the required frequency to achieve that pipe flow velocity was calculated for the desired shear stresses to be applied to the samples from the obtained shear stresses and their corresponding flume velocities.

$$\tau = \frac{1}{8}f\rho v^2$$ Equation 2.7

3.3.1 Phase I

River water was used as the eroding fluid in this phase of testing. The water was collected from St. Vital Park's boat launch area. Figure 3.6 shows the approximate location where the sample water was collected by a red dot. A floatation device was used to suspend the pump and not allow it to sink to the bottom of the river. The water was pumped into three barrels and transported back to the laboratory. The methodology of the first phase of testing is outlined as follows:

- A plug was placed in the Shelby tube hole in the flume, the lid system fastened and the frequency drive turned on to mix the sump water. The pump was turned on and off at low

frequencies (about 18 Hz) to prevent damage to the pump and EMD due to higher hydraulic forces.

- A Shelby tube sample was then extracted using the restriction system placed on top of the Shelby tube extruder (Figure 3.5).

- A sample was taken from the top of the tube and the surface was maintained flat using the wire or hacksaw. The sample was then used to determine moisture content. The bottom of the tube was also cleared of the sealing wax and prepared for the plunger.

- The pump was turned off, the flume drained; and the clamps, lid, and the plug were removed.

- A sample of the water in the sump was taken to perform a hydrometer test.

- The tube was fastened under the flume and the plunger was inserted into the tube. The sample was extruded to the same level as the bottom of the flume and the lid was replaced and clamped.

- The pump was turned on at a frequency of approximately 20 Hz to push out air in the pipes and flume.

- The frequency was then adjusted to achieve the required flow velocity to produce the desired shear stress on the soil sample. The ultrasonic flow meter was used to determine the velocity in the pipe.

- Depending on the erosion rate observed and the amount of sample available, the erosion was timed. At low shear conditions, when the erosion rates are low, the sample was eroded for half an hour to an hour. Higher shear stresses erode samples faster; hence the sample was eroded for shorter periods (five to fifteen minutes).

- The measuring device attached to the screw jack was monitored at the beginning and the end of the timed erosion. This provided the total erosion during the measured time.
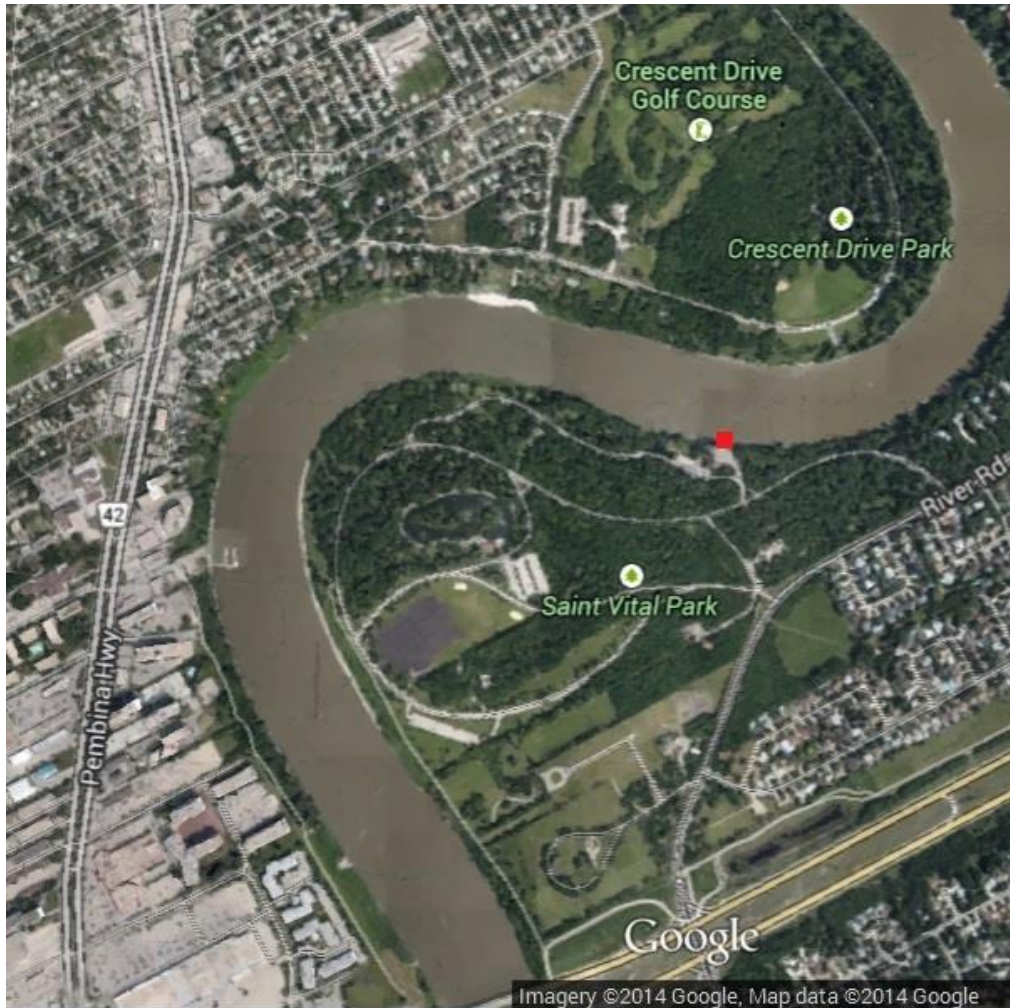
Figure 3.6: Approximate location of collection of Red River water sample (marked in red)

3.3.2 Phase II

The general procedures used in the Phase II of tests were the same as the first phase of testing with a few exceptions to allow examination of the specific condition of interest. The changes required for this phase are as follows:

- Samples were taken from Shelby tubes and air dried to determine moisture content and grain size distribution. The liquid limit and plastic limit were determined for each sample. A hydrometer test was also performed to determine the grain size distribution of the fines.

- A coarse filter was used in the sump to allow suspended particles to pass to the second chamber of the sump and remain in the system. The coarse filter was kept in place to prevent larger soil particles and twigs and other plant matter from causing damage.

- The erosion rate was determined by measuring the time that was taken to erode 10mm of sample.

- Sediments were added to the water to increase the sediment load to desired target levels. The sediments used were predominantly clay sized.

- To speed up the mixing of additional sediment a known concentration was premixed and added to the sump where a circulating pump mixed the sump water.

- A hole was drilled in the pipe between the pump and the flume, to allow extraction of more representative samples of water going into the flume.

- The mass of suspended solids was measured by taking a one litre sample of the water prior to and after measuring the erosion rate for a specific shear stress and the sediment load increment. Additional samples of the water were also taken throughout the testing.

- In the test runs it was observed that the sediment load in the water was decreasing since the flow velocities were low and was not causing enough mixing effect in the sump. As a result the water in the sump was mixed every half hour to keep the sediment load more consistent.

- Some samples were taken from both sides of the sump after some of the tests and grain size analysis performed on them to examine the effect of the weir in the sump.

CHAPTER 4: SITE SELECTION AND LABORATORY RESULTS

4.1 Introduction

Locations and cross sections of selected sites along with the laboratory testings performed on the disturbed and Shelby tube samples (two per site) are presented in the following sections.

4.2 Site Selection

A series of specimens from nine sites along the Red River were tested using the new apparatus to measure erodability at representative locations along the river and on varying types of riverbank profiles and geometries. The nine sites and their classifications are as follows: Crescent Park (inside), St. Mary's Road (outside), Howden Road (inside), Red River Drive (outside), St. Adolphe (outside / transition), Prefontaine Road (outside), Agriculture Canada (inside), Nolette Road (straight), St. Jean Baptiste (outside / transition). These sites were selected by KGS Group for a study to better understand the floodgate operation impacts.

4.2.1 Nine Sites along the Red River

Figure 4.1 shows the map of Southern Manitoba. Two sites were chosen within the City of Winnipeg: Crescent Park and St. Mary's Road, as shown in Figure 4.2. Two sites from the south of the city: Howden Road and Red River Drive, shown in Figure 4.3. Further south, in Figure 4.4, are the next four sites of the study: St. Adolphe, Prefontaine Road, Agriculture Canada, and Nolette Road. Figure 4.5 shows the location of the ninth site in the southern regions of Manitoba, St. Jean Baptiste.

Table 4.1 summarizes the orientation of the sites from where the samples were taken to the meandering of the river (inside, outside, transition bend or straight sections).
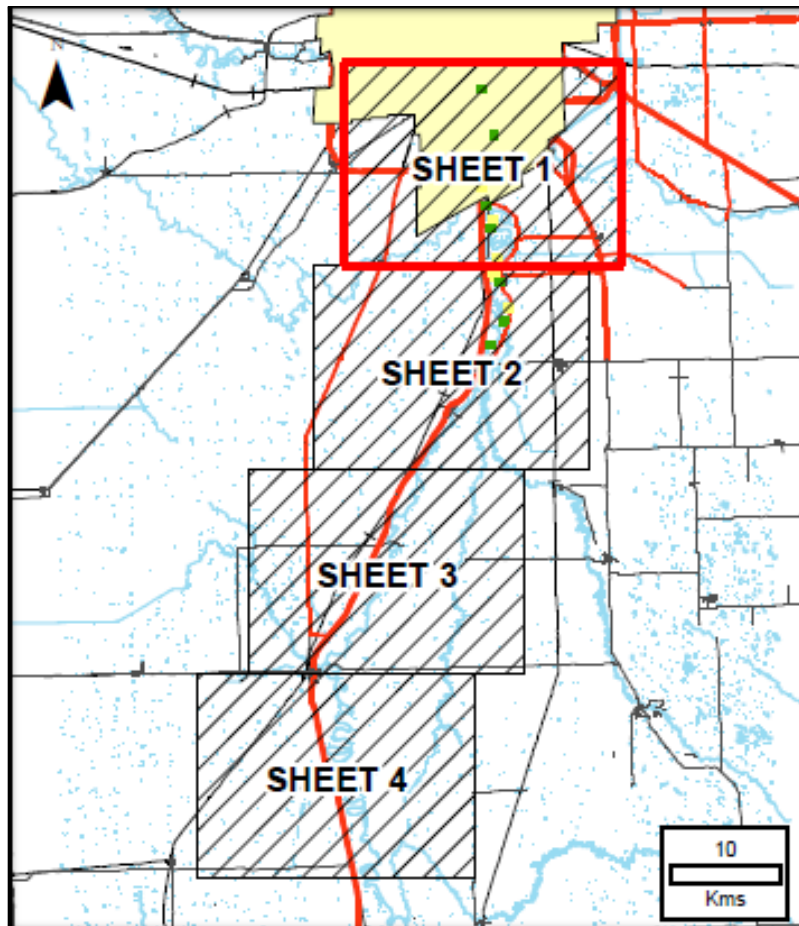
Figure 4.1: Map of Southern Manitoba (used with permission from KGS Group April 8th 2013)
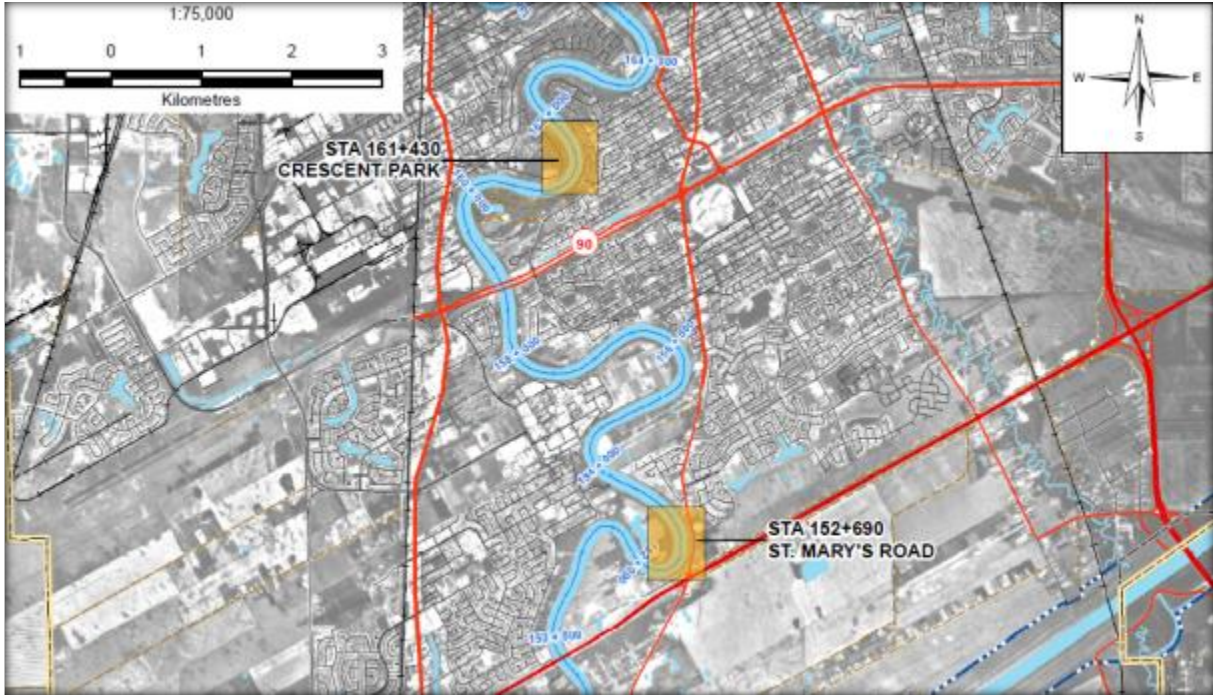
Figure 4.2: Sites in SHEET 1 of Figure 4.1 (within Winnipeg) (used with permission from KGS Group April 8th 2013)
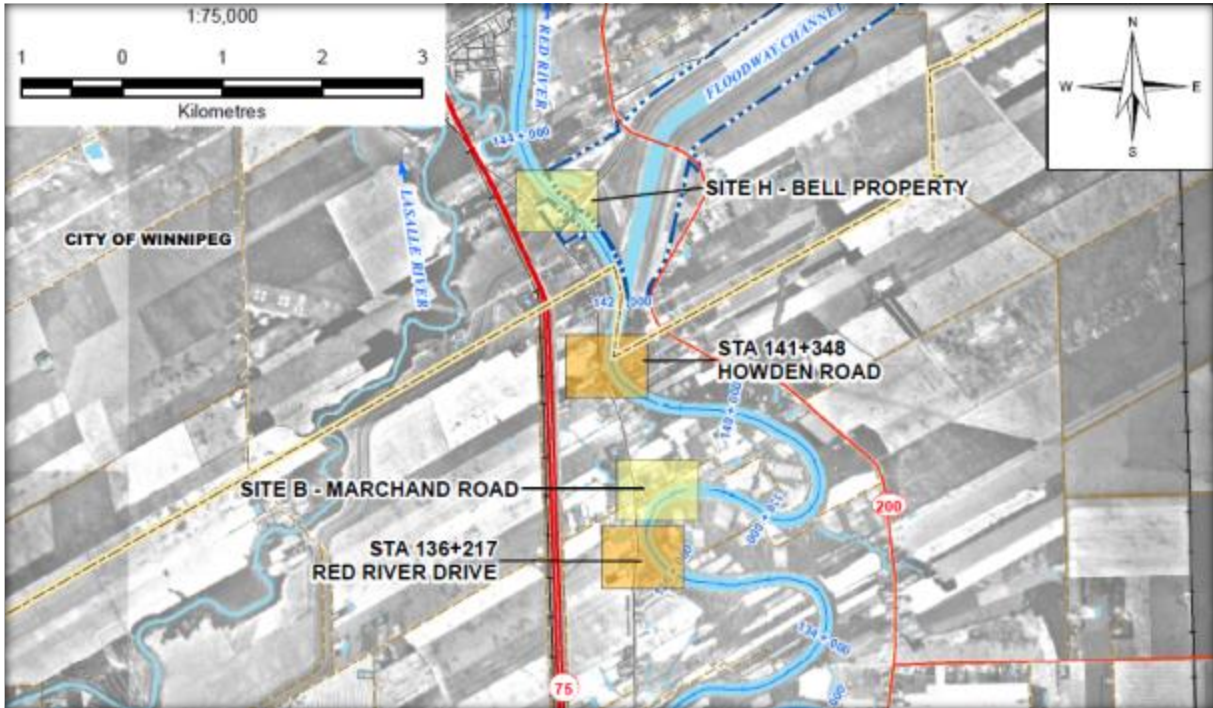
Figure 4.3: Sites in SHEET 1 of Figure 4.1 (just South of Winnipeg) (used with permission from KGS Group April 8th 2013)
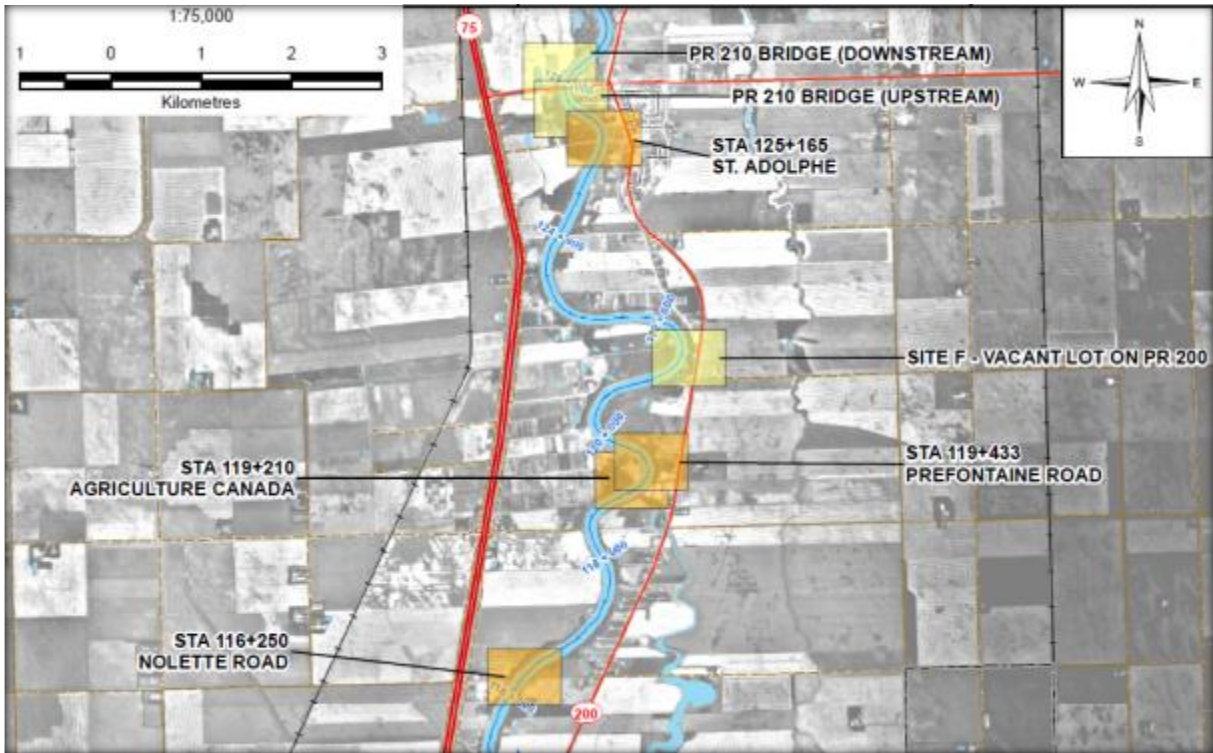
Figure 4.4: Sites in SHEET 2 of Figure 4.1 (used with permission from KGS Group April 8th 2013)
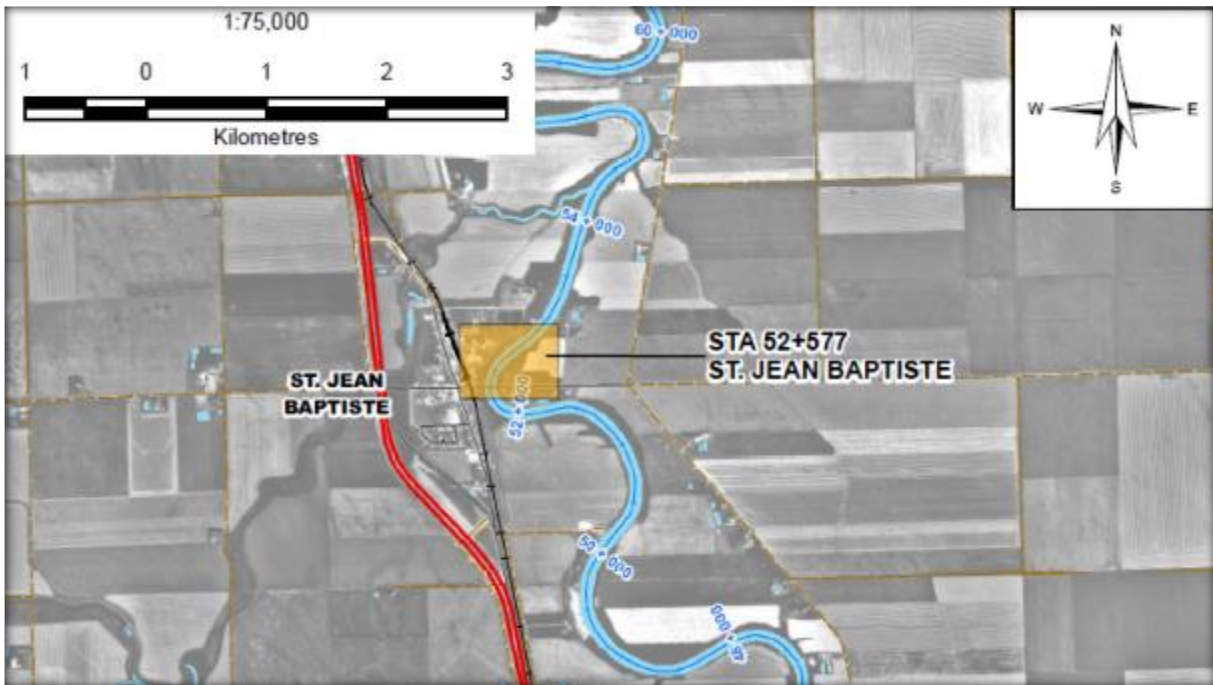
Figure 4.5: Site in SHEET4 of Figure 4.1 (used with permission from KGS Group April 8th 2013)

Site	Inside/Outside/Transition/Straight
Crescent Park	Inside
St. Mary's Road	Outside
Howden Road	Inside
Red River Drive	Outside
St. Adolphe	Outside / Transition
Prefontaine Road	Outside
Agriculture Canada	Inside
Nolette Road	Straight
St. Jean Baptiste	Outside / Transition

Table 4.1: Orientation of the sites along the meandering of Red River

4.2.2 Riverbank Cross-Sections

The cross sections of the nine studied sites are provided in Appendix A.

4.3 Laboratory Results

Since there were two Shelby tube samples obtained from each site there were two sets of tests performed on them. There were also hydraulic conductivity tests performed on remaining samples after the erosion tests.

4.3.1 Grain Size

4.3.1.1 Phase I

The Sieve and hydrometer analyses were combined to produce the grain size distributions presented in the figures in Appendix B for the nine study sites. As illustrated in those figures the soil types are all very similar. Figure 4.6 illustrates the combined grain size distribution of the nine site's disturbed samples.
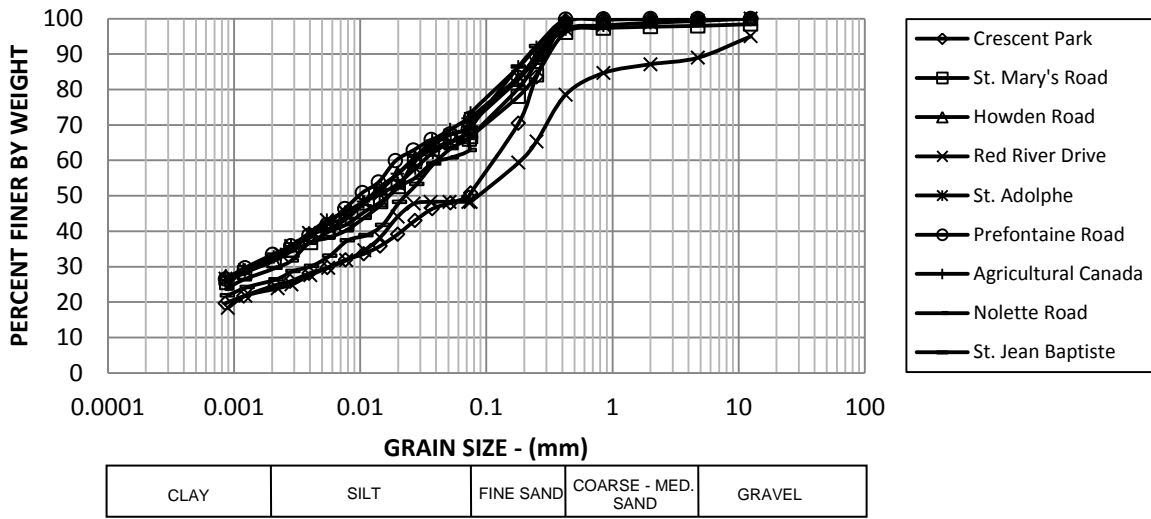
Figure 4.6: Phase I Grain Size Analysis of Nine Study Sites

4.3.1.2 Phase II

The Sieve and hydrometer analyses were combined to produce the grain size distributions for the nine remaining Shelby tubes of the nine study sites (Appendix C). The combined grain size distributions are presented in Figure 4.7.
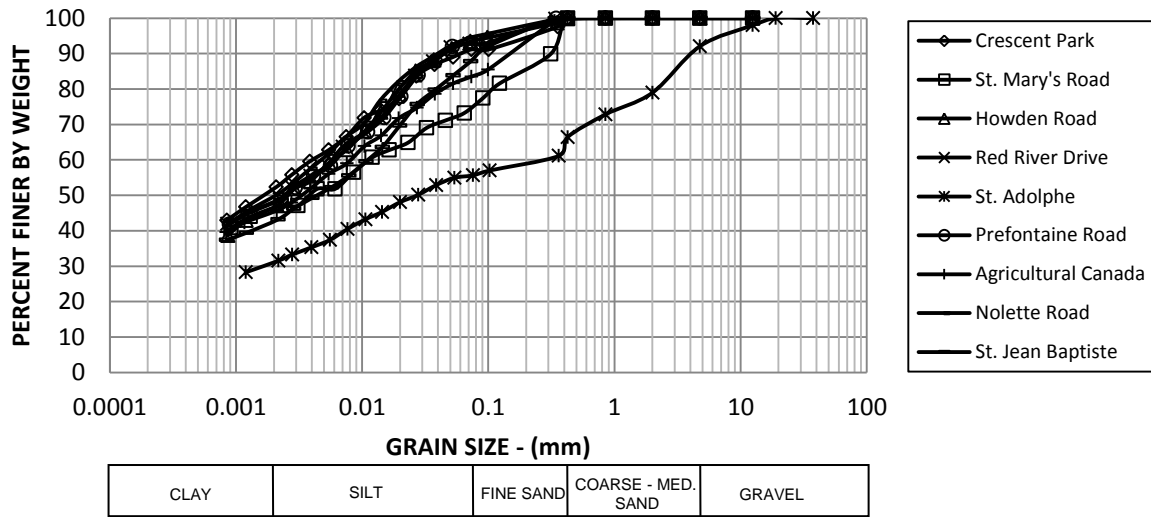
Figure 4.7: Phase II Grain Size Analysis of Nine Study Sites

4.3.1.2.1 Grain Size Analysis of Sump Samples

Three samples of the sediment of the left (return) and right (intake) sides of the sump were obtained after the testing of Shelby Tubes 1, 8, and 14, corresponding to Crescent Park, St. Adolphe, and Red River Drive, respectively, and their grain size distribution were determined (Appendix D). This was done to see the effect the weir and filter in the middle of the sump had on the sediment load. The combined grain size distributions are demonstrated in Figure 4.8.

It should be noted that these analysis would most likely show lower fine soil content, even though they were collected after the sump water had settled over night (at least 8 hours). This is due to finer particles still being suspended in the water, being sucked out while the water was being emptied, and while scooping up the material the fines being more difficult to completely be gathered.

The difference in the grain sizes is most noticeable for Shelby tube ST14 St. Adolphe which was the most granular of the samples.

4.3.1.2.2 Grain Size Analysis of Flume Water Samples

Hydrometer analyses were performed on two samples of water taken directly from the flume. Figure 4.9 and Figure 4.10 illustrate the results. It can be seen that the flume water contains mostly clay and some silt.
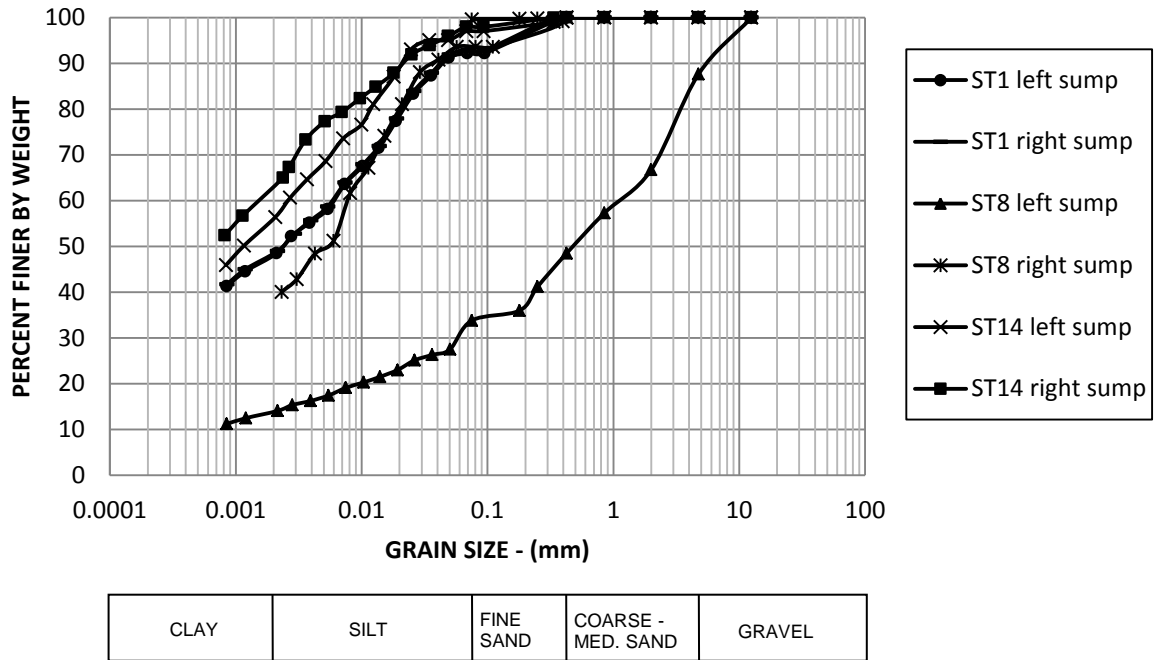
Figure 4.8: Grain Size Analysis of Sump Water Samples
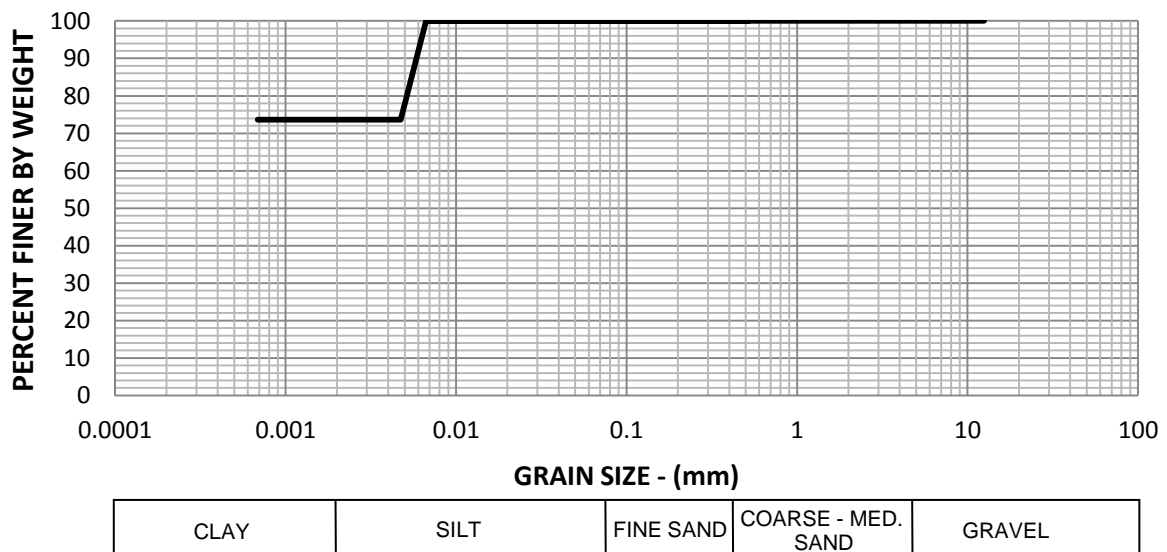
Figure 4.9: Grain Size Analysis of Flume Water end of ST1
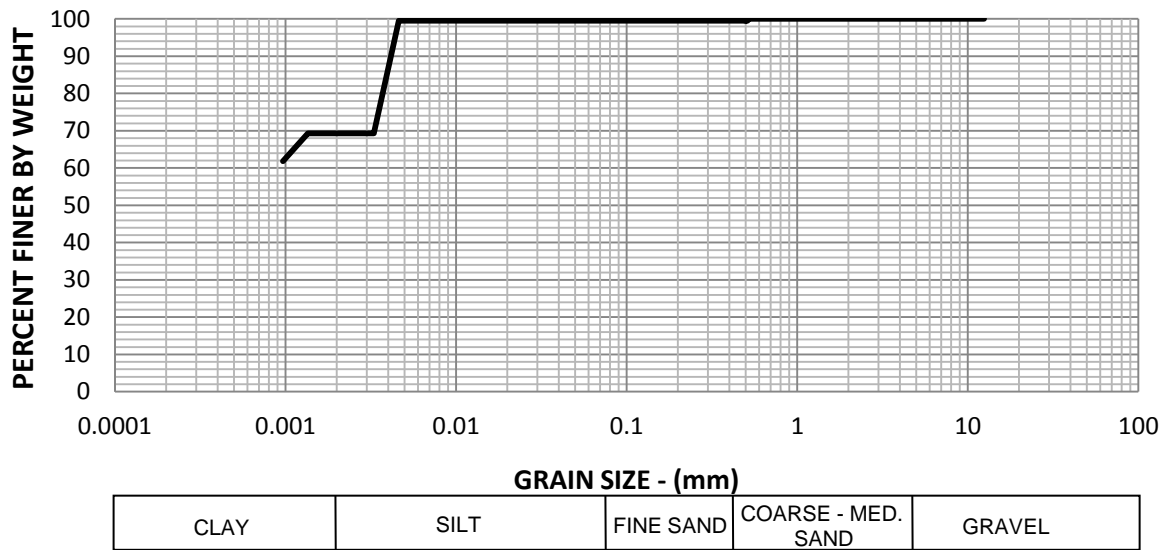
Figure 4.10: Grain Size Analysis of Flume Water end of ST16

4.3.2 Plasticity Indexes, Hydraulic Conductivity, and SAR Results

4.3.2.1 Phase I Moisture Contents, Atterberg Limits, and Soil Classifications

Moisture content, Atterberg limits, and their Unified Soil Classification System (USCS) classification have been summarized in Table 4.2. The classification obtained, since the majority of the particles were silt and clay, was derived from the corresponding liquid limit and plasticity index, and Plasticity chart (Figure 4.11).

Site	Shelby Tube	Moisture Content %	Liquid Limit %	Plastic Limit %	Plasticity Index %	USCS
Crescent Park	ST 2	37.8	55.8	20.2	35.6	CI
St. Mary's Road	ST 3	37.9	72.9	27.2	45.8	CI
Howden Road	ST 5	50.3	68.9	28.0	40.9	CI
Red River Drive	ST 13	33.3	64.5	24.6	39.9	CI
St. Adolphe	ST 7	46.3	67.3	27.0	40.3	CI
Prefontaine Road	ST 9	47.5	66.4	26.4	40.0	CI
Agriculture Canada	ST 15	42.9	63.8	25.0	38.8	CI
Nolette Road	ST 12	50.6	70.9	27.2	43.7	CI
St. Jean Baptiste	ST 18	36.0	56.7	23.8	32.9	CI

Table 4.2: Phase I Moisture Contents, Atterberg Limits, and Soil Classifications
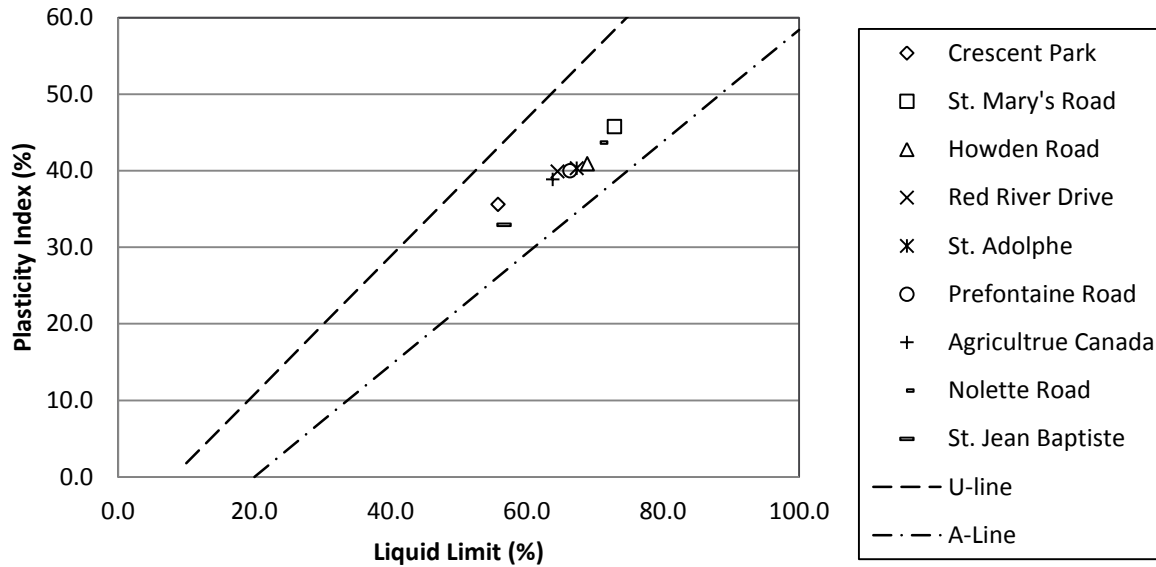
Figure 4.11: Phase I Plasticity Chart of the Nine Study Sites

4.3.2.2 Phase II Moisture Contents, Atterberg Limits, and Soil Classifications

Moisture content, Atterberg limits, and their Unified Soil Classification System (USCS) classification have been summarized in Table 4.3. The classification obtained, since the majority of the particles were silt and clay, was derived from the corresponding liquid limit and plasticity index, and Plasticity chart (Figure 4.12).

Site	Shelby Tube	Moisture Content %	Liquid Limit %	Plastic Limit %	Plasticity Index %	USCS
Crescent Park	ST 1	36.6%	64.6%	25.2%	39.4%	CI
St. Mary's Road	ST 4	36.0%	63.4%	24.0%	39.5%	CI
Howden Road	ST 6	29.5%	62.1%	25.4%	36.7%	CI
Red River Drive	ST 14	36.5%	63.6%	26.1%	37.5%	CI
St. Adolphe	ST 8	19.2%	59.8%	25.4%	34.4%	CI
Prefontaine Road	ST 10	39.8%	68.4%	25.4%	43.0%	CI
Agriculture Canada	ST 16	37.9%	61.3%	23.7%	37.6%	CI
Nolette Road	ST 11	34.1%	64.5%	24.8%	39.7%	CI
St. Jean Baptiste	ST 17	31.8%	56.4%	21.9%	34.5%	CI

Table 4.3: Phase II Moisture Contents, Atterberg Limits, and Soil Classifications
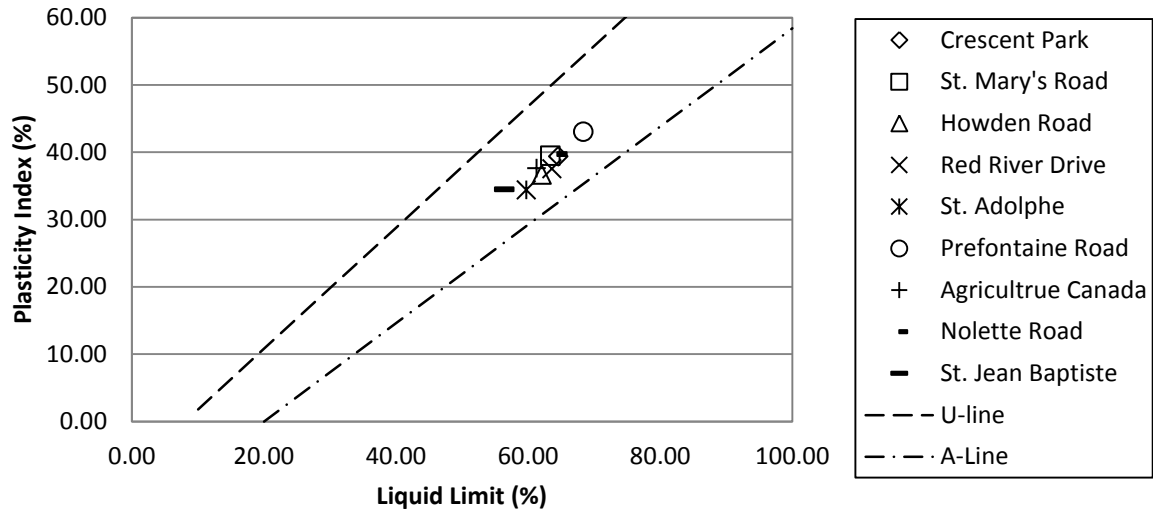
Figure 4.12: Phase II Plasticity Chart of the Nine Study Sites

4.3.2.3 Hydraulic Conductivity

The results obtained from permeameter tests performed on remaining samples after erosion tests are listed in Table 4.4. The samples were first tested with and effective pressure of 2 psi (13.8 kPa) and a gradient of 1 psi (6.9 kPa) and then reconsolidated to an effective pressure of 5 psi (34.5 kPa) and a gradient of 2 psi (13.8 kPa).

4.3.2.4 SAR Results

Samples were sent to ALS Environmental for SAR testing. The results are listed in Table 4.5.

| Site | Shelby Tube | Effective and Gradient | | K [m/sec] |
		psi	kPa	
Nolette Road	ST 12	2 & 1	13.8 & 6.9	3.1E-10
Nolette Road	ST 12	5 & 2	34.5 & 13.8	2.7E-10
St. Adolphe	ST 7	2 & 1	13.8 & 6.9	2.3E-10
St. Adolphe	ST 7	5 & 2	34.5 & 13.8	1.2E-10
Prefontaine Road	ST 10	2 & 1	13.8 & 6.9	2.3E-10
Prefontaine Road	ST 10	5 & 2	34.5 & 13.8	1.6E-10
Crescent Park	ST 1	2 & 1	13.8 & 6.9	5.6E-10
Crescent Park	ST 1	5 & 2	34.5 & 13.8	4.6E-10
Red River Drive	ST 14	2 & 1	13.8 & 6.9	1.9E-10
Red River Drive	ST 14	5 & 2	34.5 & 13.8	1.6E-10
St. Mary's Road	ST 3	2 & 1	13.8 & 6.9	2.6E-10
St. Mary's Road	ST 3	5 & 2	34.5 & 13.8	1.9E-10
St. Jean Baptiste	ST 17	2 & 1	13.8 & 6.9	2.0E-10
St. Jean Baptiste	ST 17	5 & 2	34.5 & 13.8	1.6E-10
Howden Road	ST 5	2 & 1	13.8 & 6.9	4.0E-10
Howden Road	ST 5	5 & 2	34.5 & 13.8	3.6E-10
Agriculture Canada	ST 16	2 & 1	13.8 & 6.9	9.2E-10
Agriculture Canada	ST 16	5 & 2	34.5 & 13.8	5.0E-10

Table 4.4: Hydraulic Conductivity of Soil Samples

B #	Site	Ca mg/L	K mg/L	Mg mg/L	Na mg/L	SAR	% Saturation	pH	Conductivity
1	Crescent Park	252	22.8	121	71.5	0.93	72.2	7.61	2.31
2	St. Mary's Road	109	18.6	45.6	37.3	0.76	87.9	7.56	1.05
3	Howden Road	147	15.1	60.4	45.3	0.79	83.7	7.77	1.55
7	Red River Drive	96.5	31.5	49.2	48.2	1	77.5	7.82	1.14
4	St. Adolphe	149	18.2	66.6	49.4	0.85	74.2	7.76	1.48
5	Prefontaine Road	78.5	11	33.1	61.4	1.46	81.6	7.67	0.95
8	Agriculture Canada	92.3	17.6	40.8	25.7	0.56	77.2	7.63	0.91
6	Nolette Road	103	10.8	42.3	47.7	1	87.9	7.88	1.05
9	St. Jean Baptiste	135	13.4	49.2	43.7	0.82	72.9	7.60	1.22

Table 4.5: SAR Testing Results

4.3.3 Erosion Rates

4.3.3.1 Phase I

The figures in Appendix E show erosion rate (millimeters per hour) versus shear stress (Pascals) obtained from all the individual tests. Their corresponding tables present additional information regarding the material during each increment of the testing and provide the values of erodability obtained for the materials under specified shear stresses.

At lower shear stress, when the erosion rates were low, the sample was eroded for half an hour to an hour time period. At higher shear stress the samples eroded faster, hence the samples were eroded for shorter periods (five to fifteen minutes). The measuring device attached to the screw jack was observed at the beginning and end of the timed erosion to determine amount of sample eroded during the measured time.

Figure 4.13 compares the nine study sites' erosion rates and in Figure 4.14 the erosion rates are compared to Fernando (2007) results which were taken from Kingston Crescent and tested at Texas A&M University. This comparison has simply been made to indicate, although based on limited data, that the sediment load does not appear to have a notable effect on erosion rates over tap water. This was further examined in the second phase of the study. The erosion rates are grouped together in Figure 4.15 and Figure 4.16 depending on if the samples were taken from inside or outside/transition bends and straight sections along the Red River.
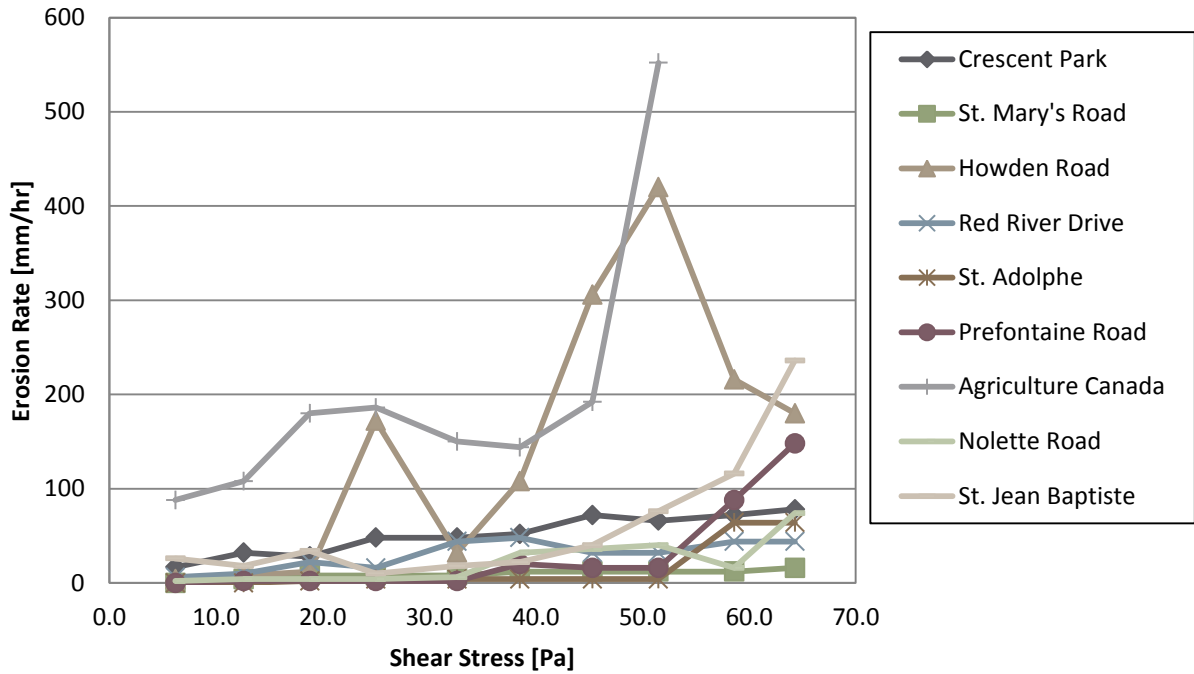
Figure 4.13: Erosion Rate vs. Shear Stress of Nine Study Sites
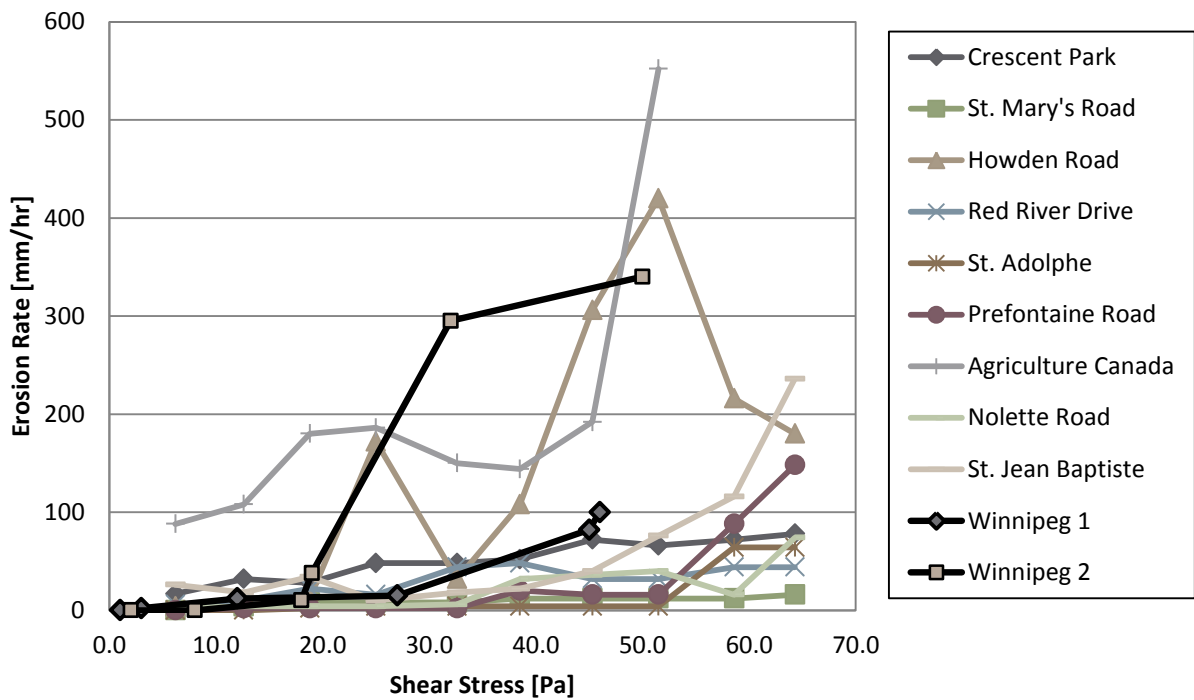
Figure 4.14: Erosion Rate vs. Shear Stress of Nine Study Sites and Fernando 2007 data

66
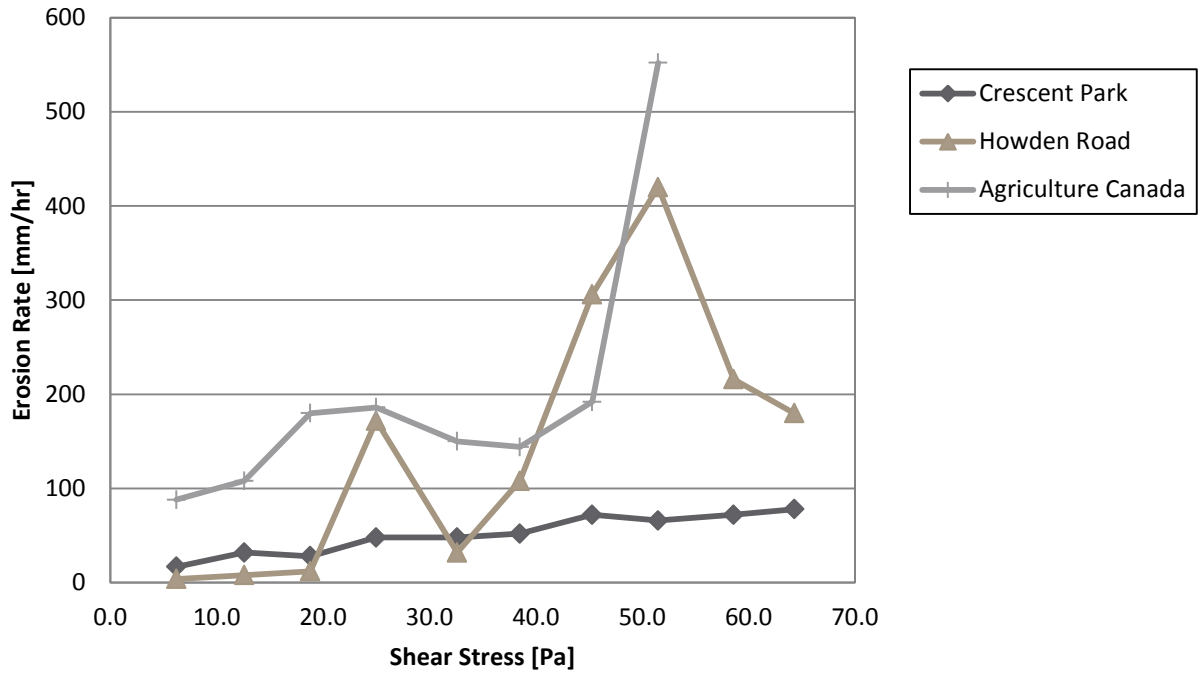
Figure 4.15: Erosion Rate vs. Shear Stress of the Inside Bend
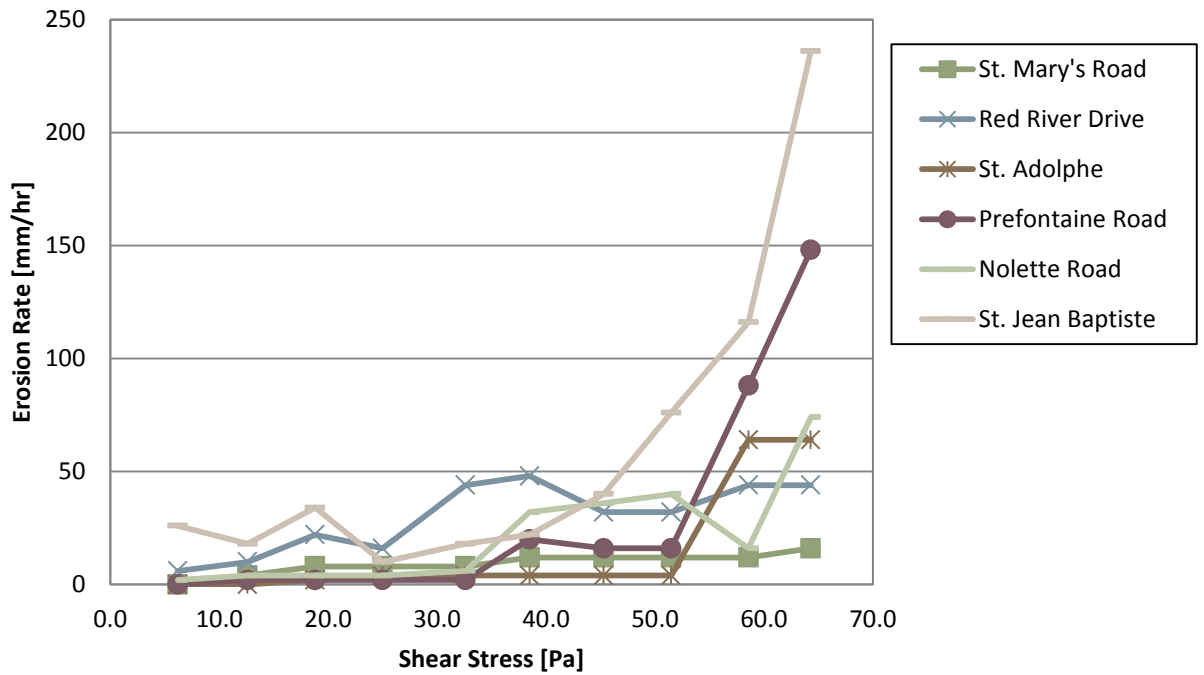
Figure 4.16: Erosion Rate vs. Shear Stress of the Outside Bend and Transition Sites

67

4.3.3.2 Phase II

During the second phase of testing range of shear stress was tested which was closer to the shear stress that occurs on the Red River's banks and bed. Shear stresses of 10.1 Pa, 13.7 Pa, and 17.5 Pa were applied to the samples. The obtained erosion rates for the three sediment loads and shear stresses are listed in Table 4.6.

Site Names	Shelby Tube	Sediment Loads [g/m^3]								
		0			100			200		
		Shear Stresses [Pa]								
		10.1	13.7	17.5	10.1	13.7	17.5	10.1	13.7	17.5
		Erosion Rates [mm/hr]								
Crescent Park	ST1	0.8	4.0	10.0	3.0	4.4	6.3	4.0	3.6	7.2
St. Mary's Road	ST4	60.0		60.0	26.1		13.3	7.5		12.0
Howden Road	ST6	0.0	0.3	0.3	0.5	1.3	2.0	0.0	5.0	6.0
Red River Drive	ST14	2.0	3.5	5.7	2.0	4.0	10.0	6.0	10.0	9.2
St. Adolphe	ST8	5.7	22.2	12.0	37.5	23.1	10.0	19.2	20.7	10.7
Prefontaine Road	ST10	0.0	0.0	0.0	2.0	2.7	3.3	2.0	5.3	6.0
Agriculture Canada	ST16	6.7	30.0	34.3	14.3	30.0	78.0	30.0	20.0	24.0
Nolette Road	ST11	0.0	0.0	1.0	1.5	3.5	4.0	1.0	2.0	1.5
St. Jean Baptiste	ST17	2.5	5.2	7.3	5.0	9.4	17.8	12.0	27.3	31.6

Table 4.6: Summary of Erosion Results of Phase II

The erosion rates are also demonstrated and the observations made during testing are presented in Appendix F.

4.3.3.2.1 Combined Results:

The combined erosion results are grouped into the shear stresses and sediment loads tested and are presented in Figure 4.17 to Figure 4.22.
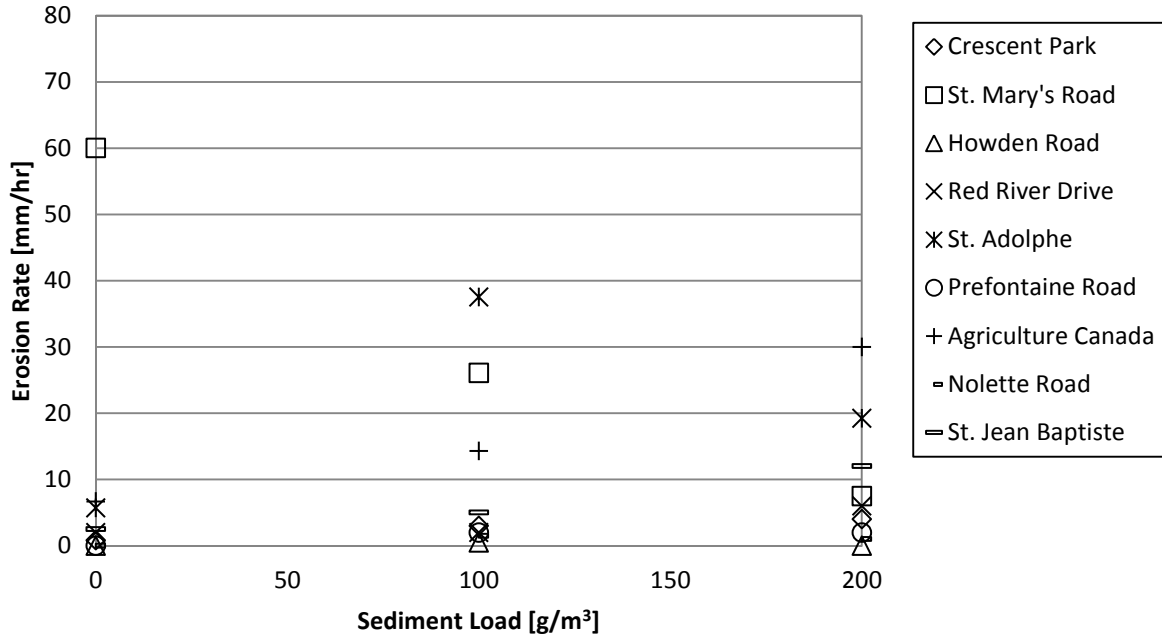
Figure 4.17: Combined Erosion Rates Tested at 10.1Pa Shear Stress
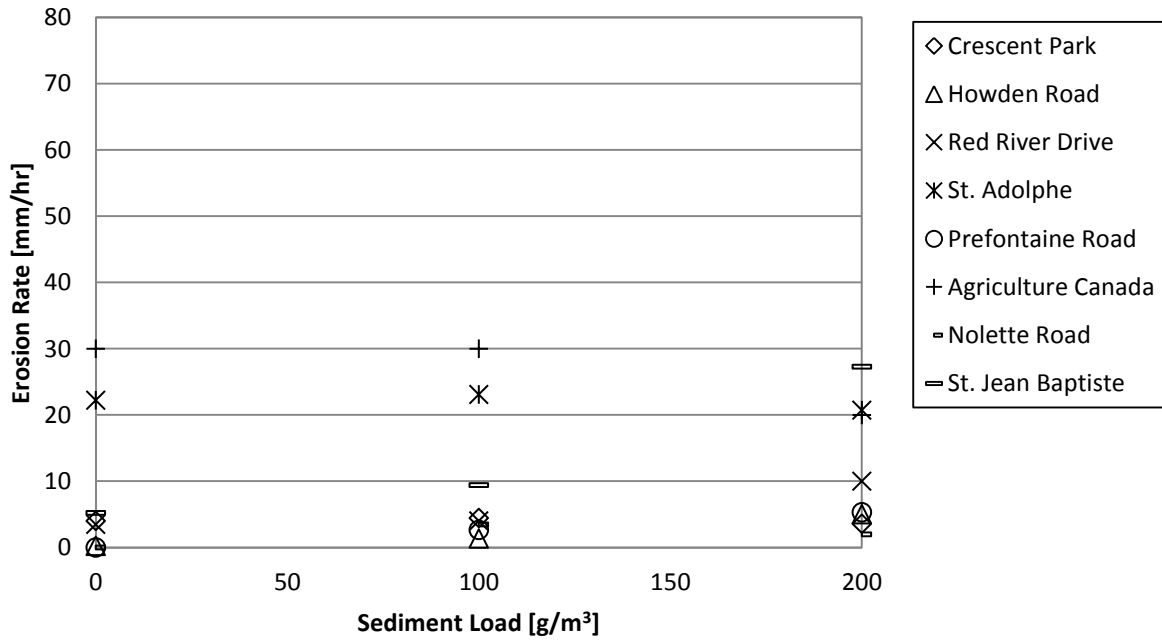
Figure 4.18: Combined Erosion Rates Tested at 13.7Pa Shear Stress
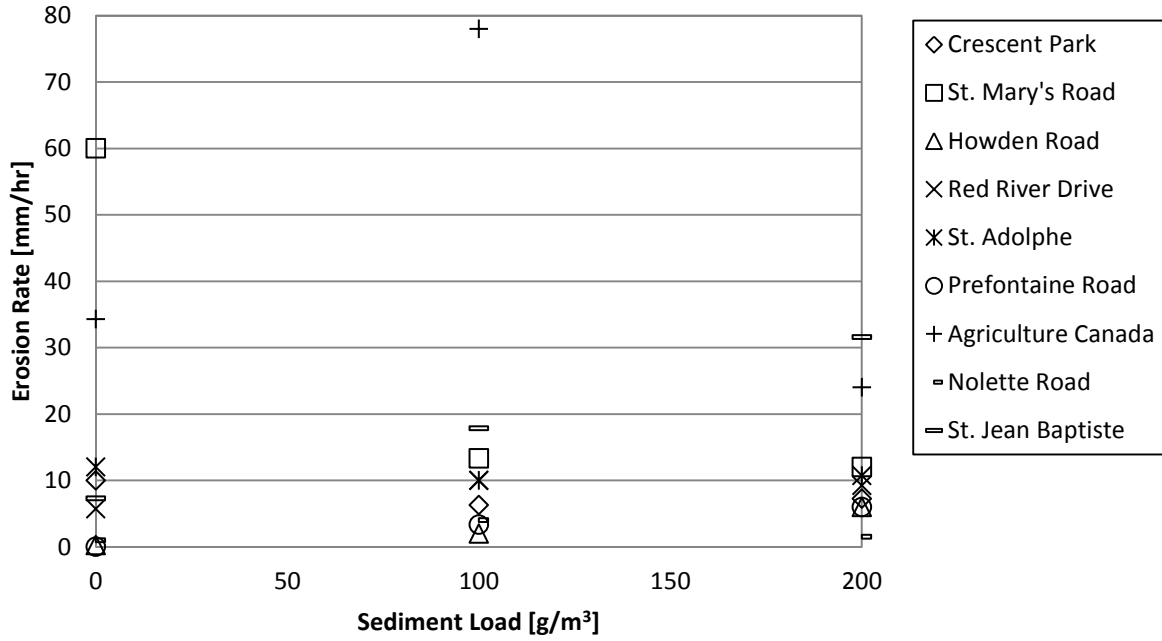
Figure 4.19: Combined Erosion Rates Tested at 17.5Pa Shear Stress
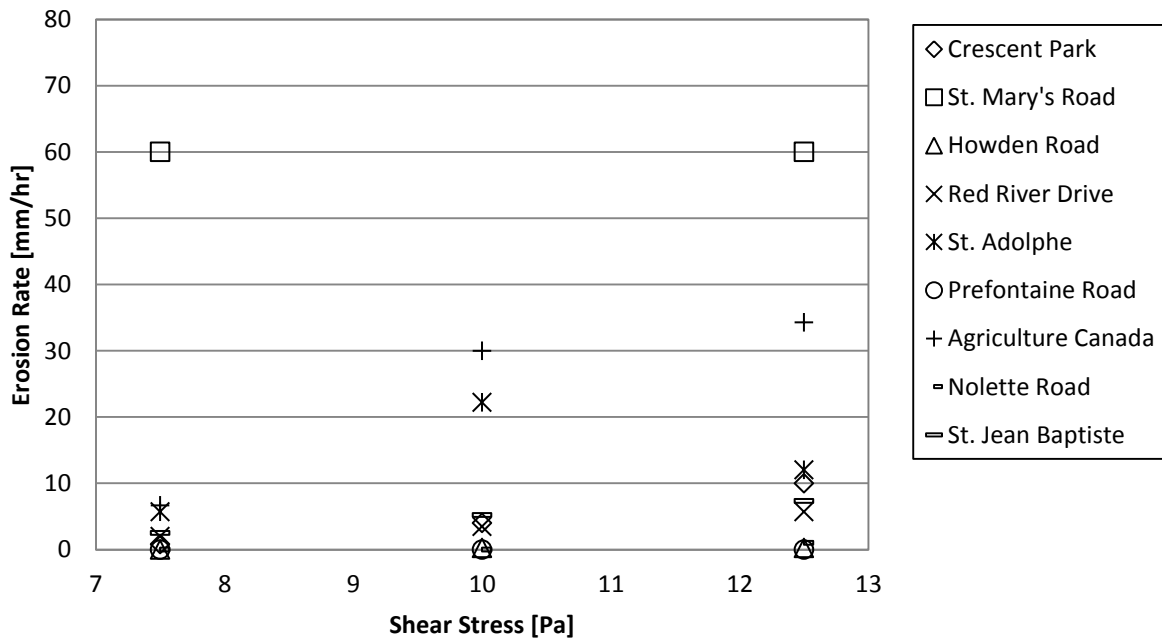
Figure 4.20: Combined Erosion Rates Tested with Sediment Load of 0g/m³

70
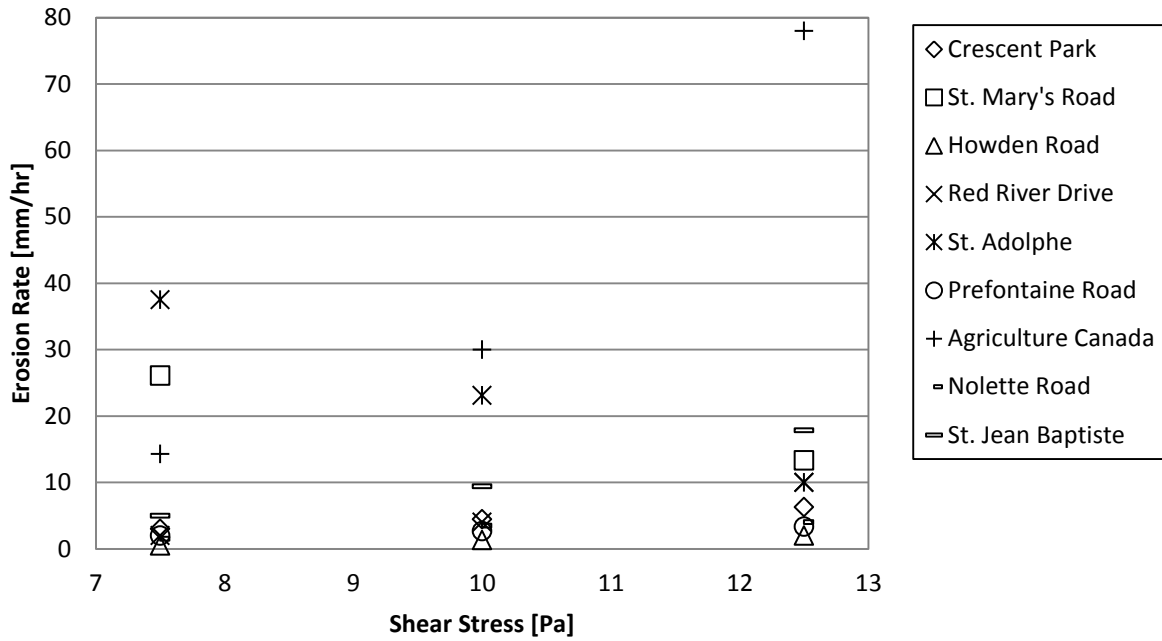
Figure 4.21: Combined Erosion Rates Tested with Sediment Load of $100g/m^3$
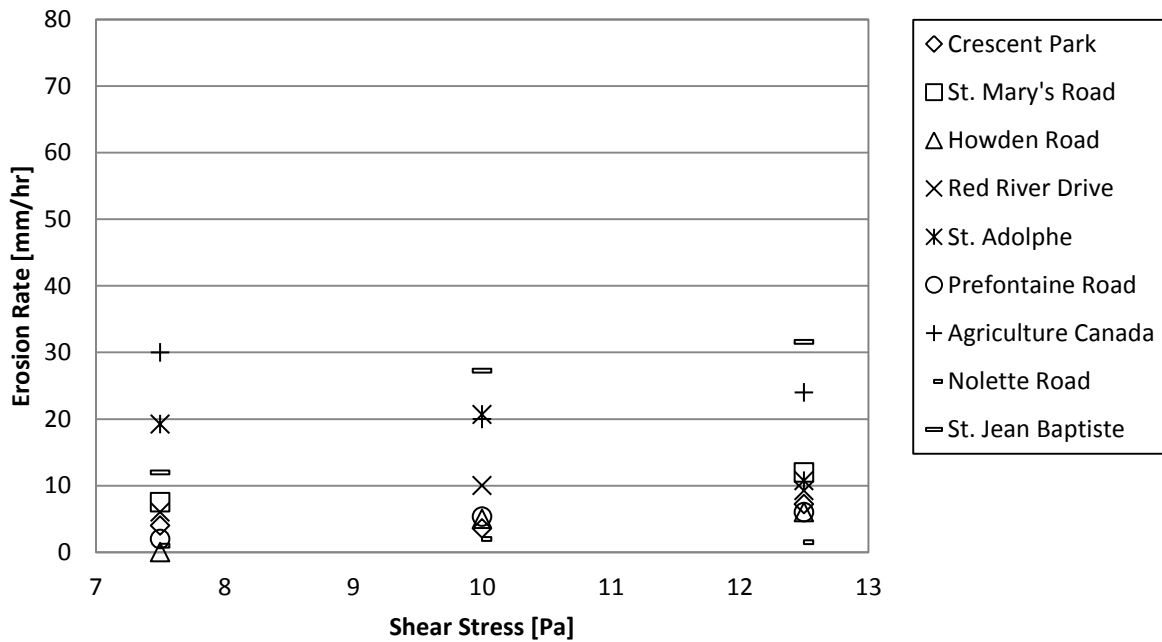
Figure 4.22: Combined Erosion Rates Tested with Sediment Load of $200g/m^3$

4.3.3.2.2 Comparison to First Phase of Testing:

The erosion rates obtained in the second phase of testing have been compared to the first phase

of testing in the approximate range of shear stress and are demonstrated in Figure 4.23 to Figure

4.31.
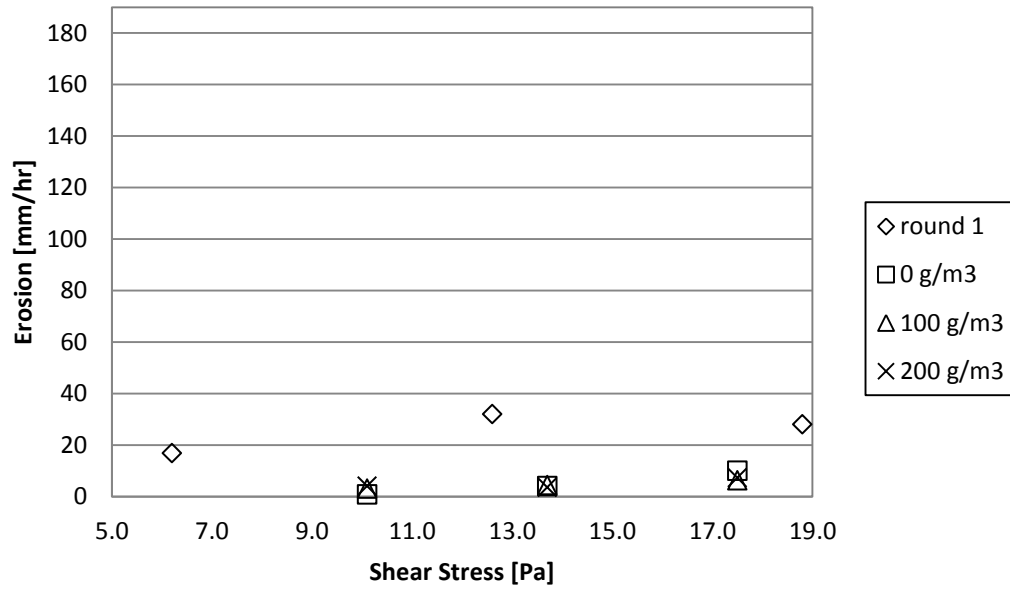
Figure 4.23: Phase I and II Comparison of Erosion Rates of Crescent Park
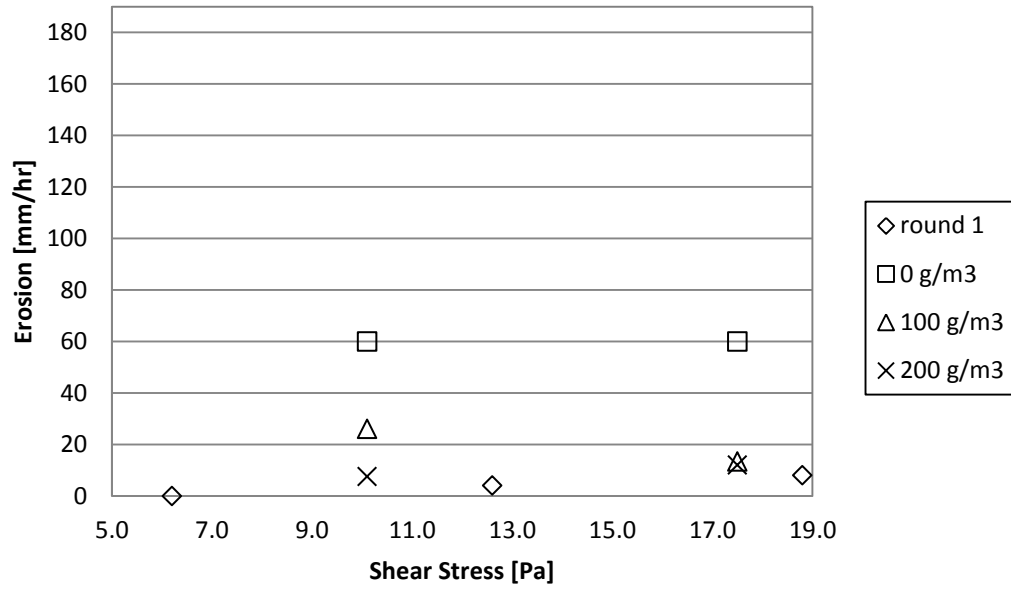
Figure 4.24: Phase I and II Comparison of Erosion Rates of St. Mary's Road
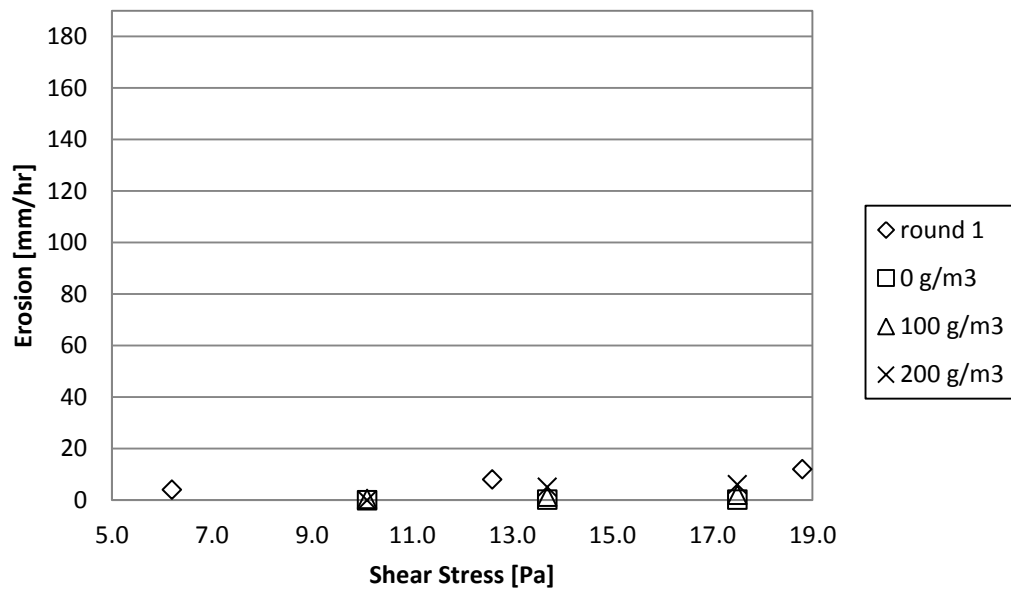
Figure 4.25: Phase I and II Comparison of Erosion Rates of Howden Road
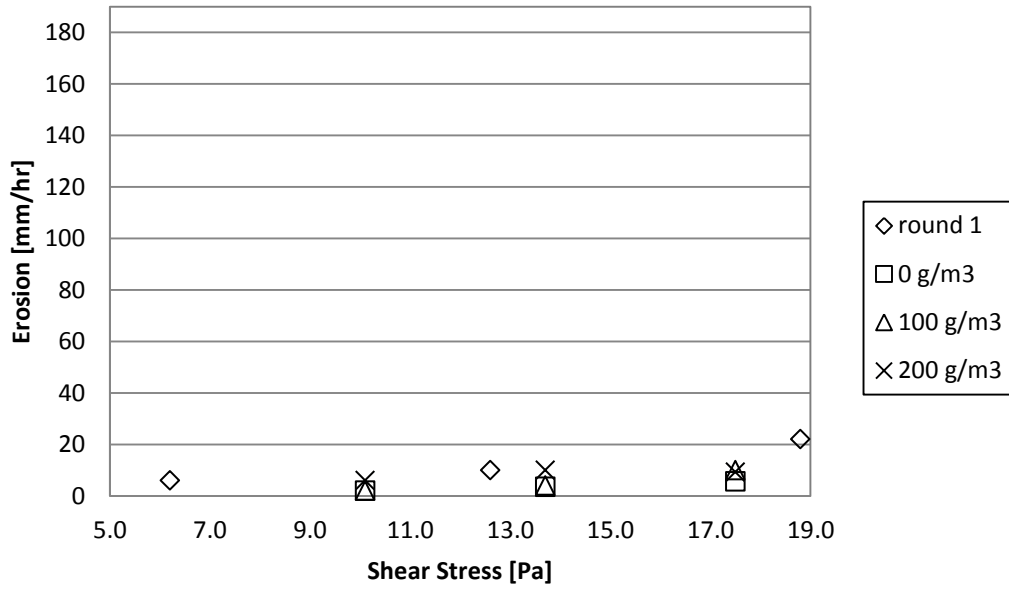
Figure 4.26: Phase I and II Comparison of Erosion Rates of Red River Drive
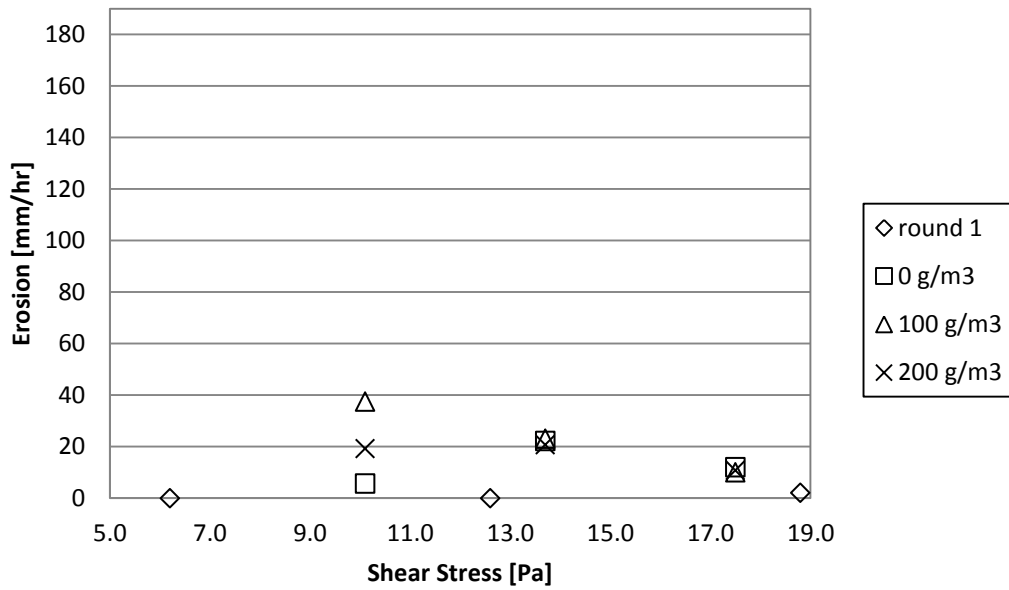
Figure 4.27: Phase I and II Comparison of Erosion Rates of St. Adolphe
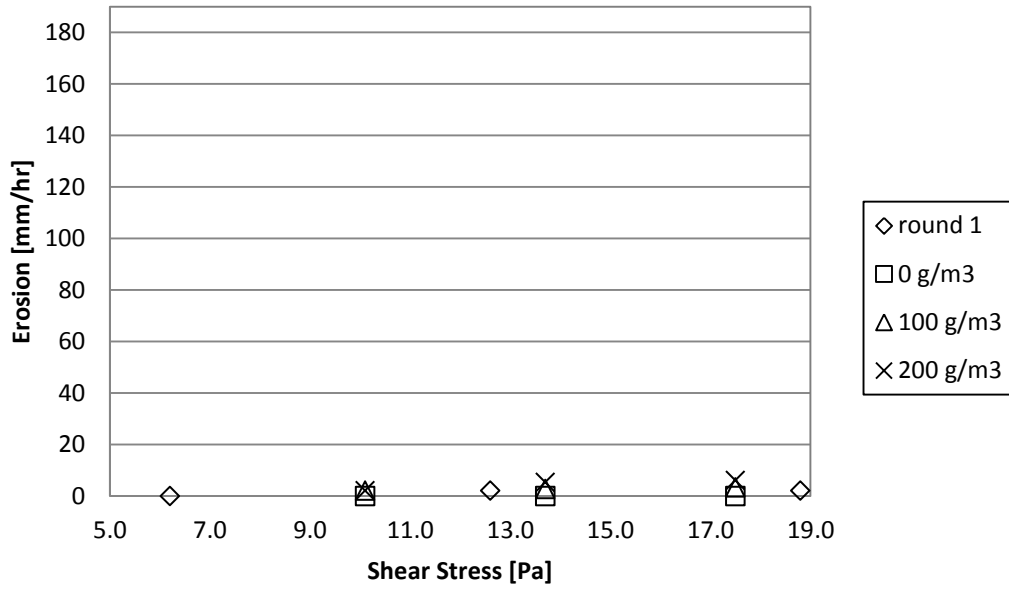
Figure 4.28: Phase I and II Comparison of Erosion Rates of Prefontaine Road
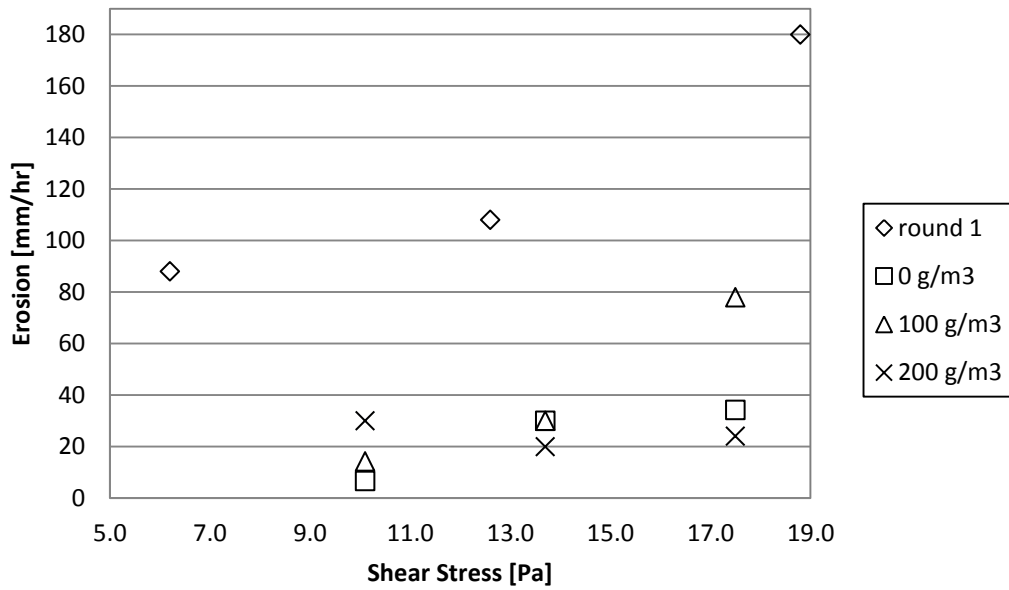
Figure 4.29: Phase I and II Comparison of Erosion Rates of Agriculture Canada
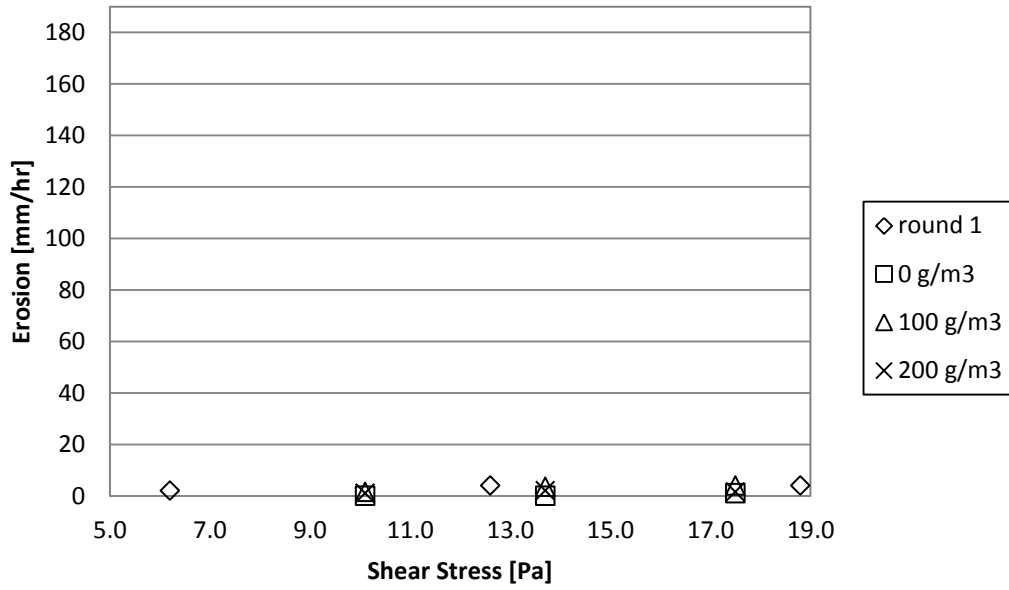
Figure 4.30: Phase I and II Comparison of Erosion Rates of Nolette Road
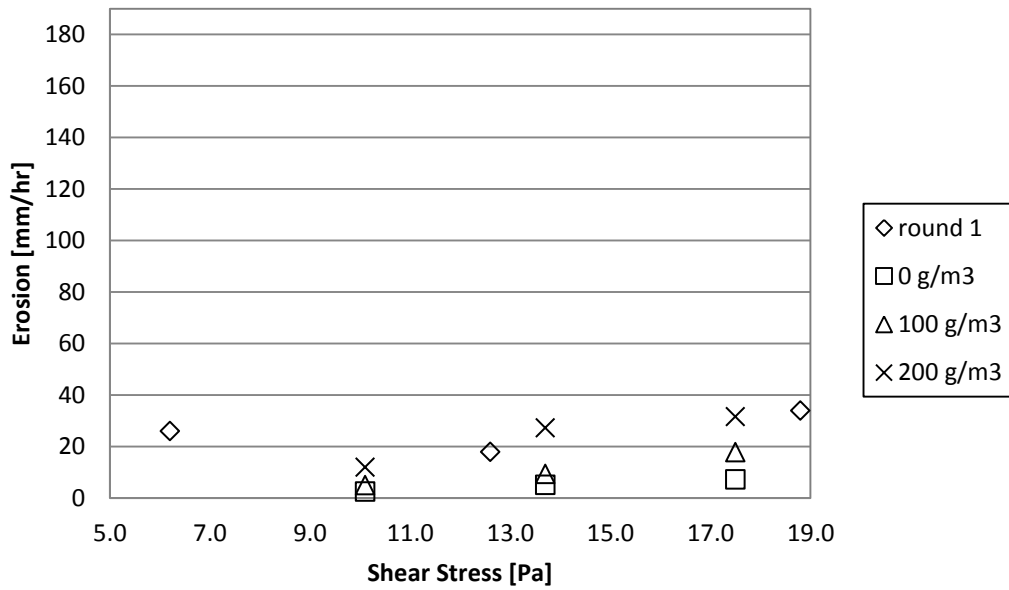
Figure 4.31: Phase I and II Comparison of Erosion Rates of St. Jean Baptiste

4.3.3.2.3 Sediment Loads:

Figure 4.32 illustrates the expected versus measured sediment load using over 120 samples that were taken. The results show a strong correlation given the accuracy of the measurements involved.
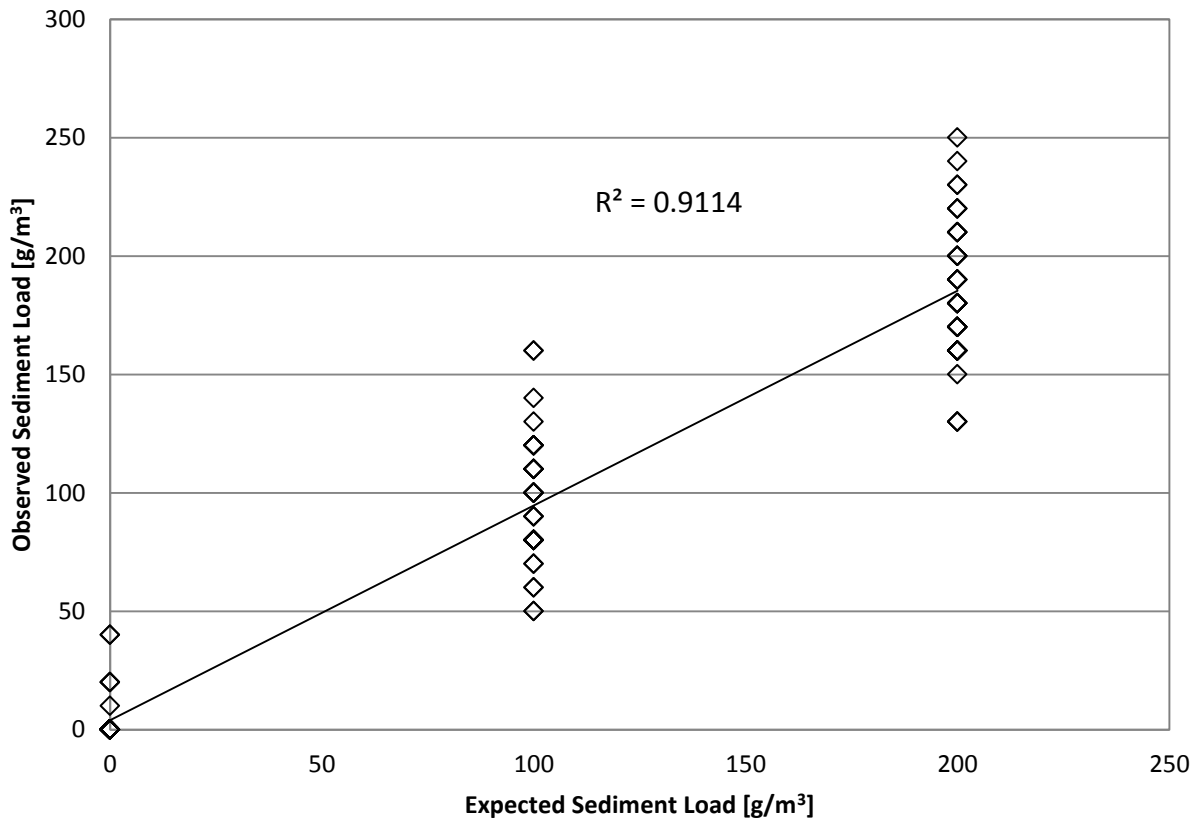
Figure 4.32: Observed vs. Expected Sediment Loads

CHAPTER 5: NUMERICAL MODELING OF EROSION IMPACT ON RIVERBANK

5.1 Introduction

Red River Drive was selected as the representative site to be used for analysis. This site was chosen since KGS Group had performed snapshot analyses using FLOW-3D software to calculate the flow velocities and shear stresses of that part of the rivers meander. The first step of the modeling process was to calibrate the model. Once that was satisfactorily achieved two flood scenarios were modeled: one with natural conditions and one with the operation of the floodway. The hydrograph and sensor data obtained by KGS Group for the Red River Drive site can be found in the figures in Appendix G. GeoStudio 2007 SEEP/W and SLOPE/W were used for the seepage and slope stability of the models, respectively.

5.2 Model Calibration

The 2010 fourty seven day flood event (between March 24th and May 5th) was used to calibrate the model since sensor data were available for the duration of that event.

5.2.1 List of Assumptions

The following are the list of the assumptions made in the calibration and simulation of the models:

- The analysis software considers the cross sections to be infinite depth into the page.
- Roots and their stabilizing capabilities were not considered.
- Deposition on the upper portions of the bank was neglected.
- The details and effects of precipitation were not considered.

- Erosion was applied horizontally to the cross sections.

5.2.2 Properties Used

The soil properties used in SEEP and SLOPE are listed in Table 5.1 and Table 5.2. The values obtained in Table 5.1 are the result of model calibration to get similar results in the points where the sensors were placed to the measured values in-situ. Typical values of unit weight, cohesion and friction angle (Anderson *el al*. 2004) of the Winnipeg area were used with slightly lowered values for the mid and toe section of the bank due to previous failures of the slope and effects of disturbance and weathering.

Name	Model	K-function	K-Ratio
unsaturated silty clay toe	Saturated / Unsaturated	clay 1e-4 m/s	1
unsaturated silty clay mid bank	Saturated / Unsaturated	clay 1e-6 m/s	10
unsaturated silty clay upper bank	Saturated / Unsaturated	clay 1e-10 m/s	10
unsaturated silt till	Saturated / Unsaturated	till 1e-4 m/s	0.03

Table 5.1: Soil Properties Used in SEEP/W

Name	Unit Weight	C	φ
unsaturated silty clay toe	18	3	12
unsaturated silty clay mid bank	18	4	13
unsaturated silty clay upper bank	18	5	15
unsaturated silt till	22	5	30

Table 5.2: Soil Properties Used in SLOPE/W

5.2.3 Boundary Conditions

Figure 5.1 demonstrates the boundary conditions obtained after the calibration process. The upper, middle, and lower sections of the clay bank and the underlying till layer are also seen in Figure 5.1. Total head of 230 m and 231 m were applied to the bottom of the modeled till layer and toward the left vertical edge of the model, respectively. A river elevation of 223.6 m was

used for the baseline calibration model and the hydrograph in Figure 5.2 was used in the transient portion of calibrations.
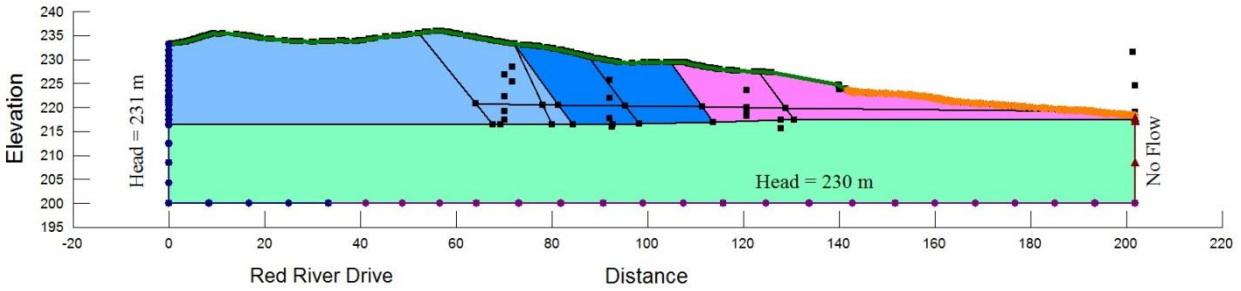
Figure 5.1: Boundary Conditions of Calibrated Model
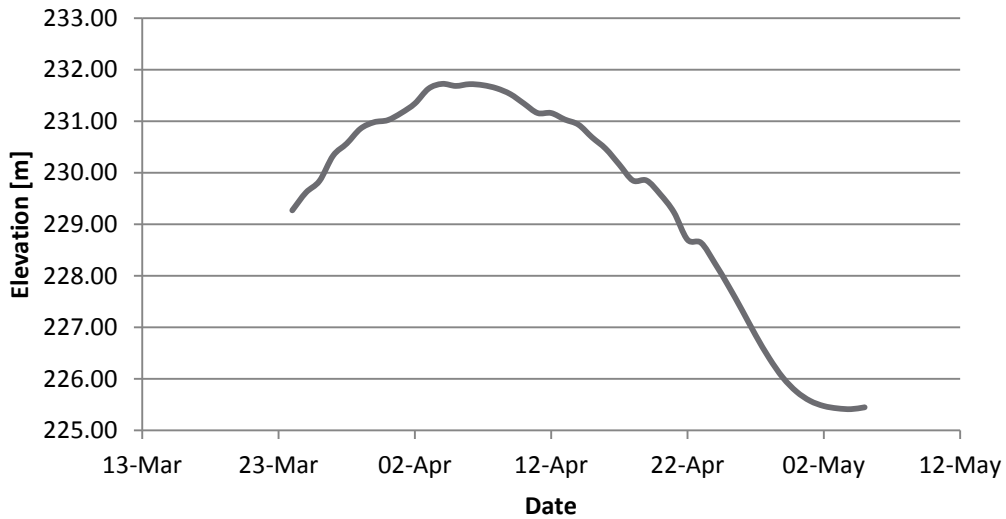
Figure 5.2: Hydrograph Used for Model Calibration

5.2.4 Calibrated Flood Event

Vibrating Wire Piezometers were installed in the upper, middle, lower and toe of the river bank, as detailed in the Red River Drive cross section in Appendix A and summarized in Table 5.3. The comparison of the measured data to the transient modeled results can be seen in Figure 5.3.

Vibrating Wire Piezometer	Location
vw98477, vw98556, vw98480, vw98479, vw98481, vw98478	Upper Bank
vw09-1290, vw09-1531, vw09-1329, vw09-1530	Mid Bank
vw09-1522, vw09-1330, vw09-1289, vw09-1521, vw95409	Lower Bank
vw98560	Toe

Table 5.3: Vibrating Wire Piezometer Installed Locations

In Figure 5.3 the first column of graphs is the upper bank, the second the mid bank, the third the lower and the forth the toe piezometers. Piezometers vw98477 and vw98480 both had the same recorded data and were assumed to have been damaged. The data for piezometer vw98556 was also determined to not be repeatable and as such was ignored due to unknown factors that may have caused this discrepancy such as instrument damage. The graphs for these three sensors are shaded gray in Figure 5.3.

The measured (in red) and modeled total heads (in blue) in Figure 5.3 show that the model was calibrated to an acceptable range.
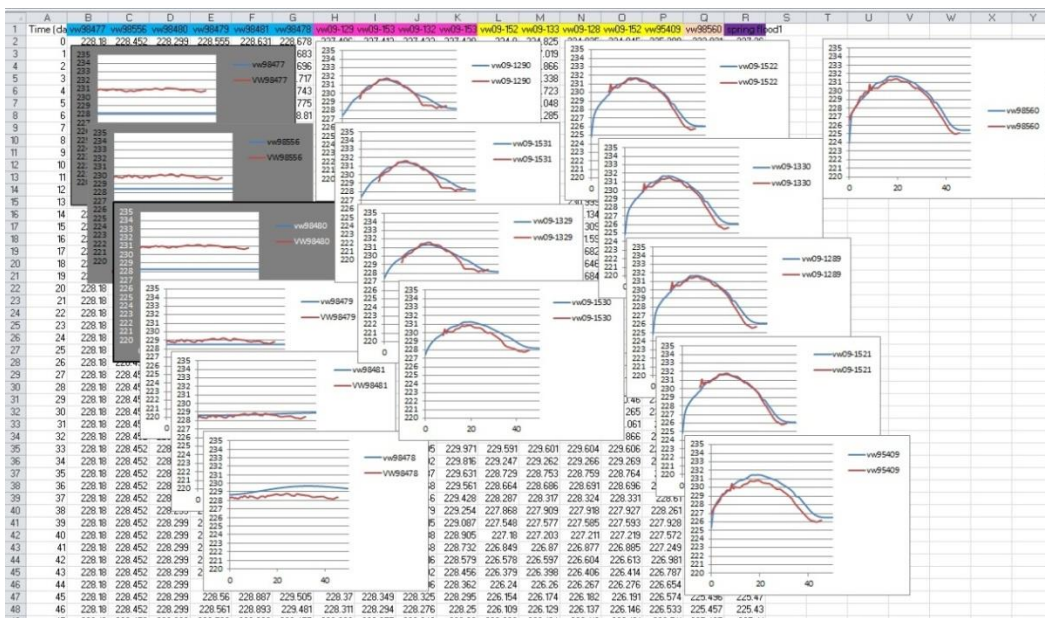
Figure 5.3: Comparison of Measured Head to Modeled Head

5.3 Modeled Flood Event

After the model was calibrated using the 2010 flood the second peak of the 2009 flood was analysed. The hydrograph presented in Appendix G for the second peak of the 2009 flood is under natural conditions (i.e. no Floodgate operation). KGS Group performed two snapshot FLOW-3D analyses of this flood: one with natural conditions and one with the Floodway in operation. Results of shear stress generated on a cross section closest to our study site are presented in Figure 5.6 and Figure 5.7.

5.3.1 Critical Shear Stress and Erosion Rate

The erosion rates obtained in Phase I and Phase II (for the same range of shear stresses) for Red River Drive are presented in Figure 5.4. The trend line of the erosion rates from Phase I was selected since it was conservative and the eroding fluid used in Phase I was river water obtained from Red River (with suspended sediments). Equation 5.1 is the erosion function used which results in a critical shear stress of approximately 2.5 Pa.

$$\dot{e} = 1.2664\,\tau - 3.2052 \qquad\qquad \text{Equation 5.1}$$

where
$\dot{e}$ = erosion rate in mm/hr
τ = shear stress in Pa

Due to the limited amount of sample material available sparse testing was performed in the range of shear stresses. Even then the samples were not homogenous which resulted in fluctuations in the erosion rates measured. Therefore there is a range of possible erosion rates for each shear stress tested. Equation 5.1 was used as it was the only measured erosion rate available for this location.
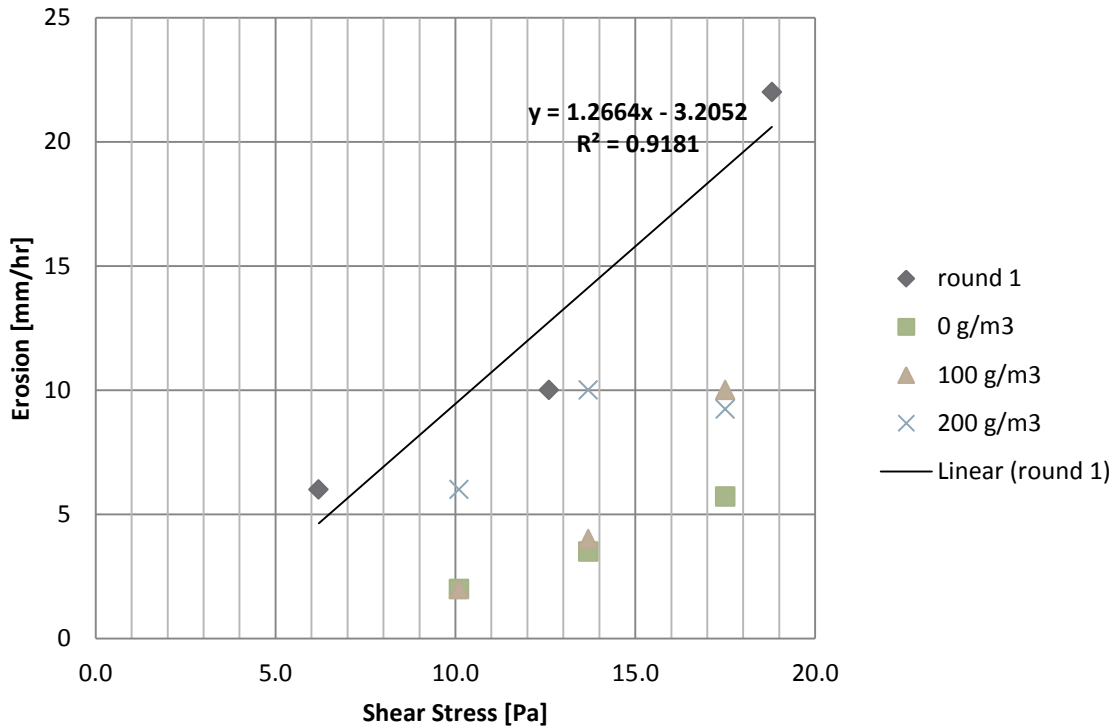
Figure 5.4: Red River Drive Erosion Rates

5.3.2 Fluid Shear Stress

The two scenarios modeled would generate different shear stresses along the bed and the banks of the Red River. The shear stresses considered were for natural condition and one under the operation of the floodway. Figure 5.5 presents the hydrographs used for both cases. The natural condition hydrograph was taken from the data KGS Group had provided and the one used for the Floodgate operation scenario was produced assuming maximum elevation at the same maximum of the natural condition hydrograph and applying a linear increase to each increment from the same elevations as the natural conditions' hydrograph's start and end.
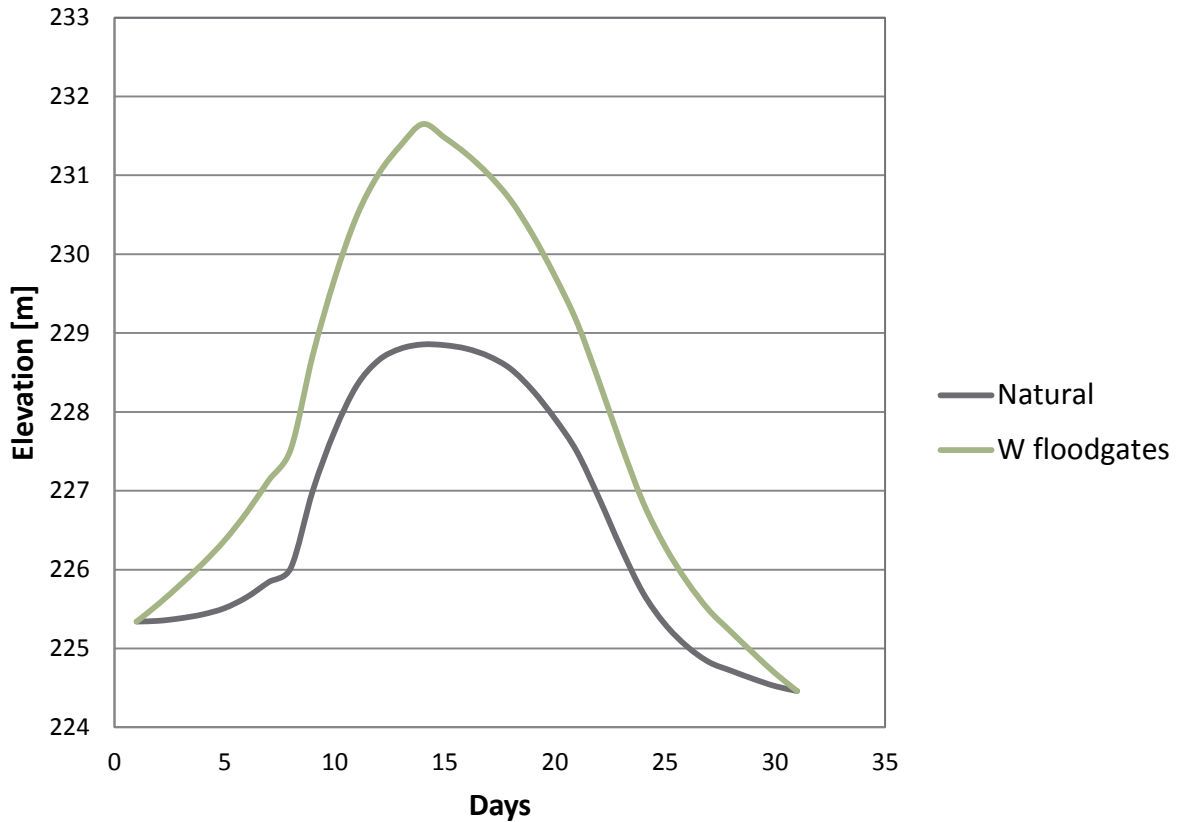
Figure 5.5: Hydrographs Used for Models

5.3.2.1 Natural Condition

Olsen and Florey's (1952) work (Figure 2.7) was used to calculate the shear stresses and resulting erosion of the river bank's cross section since the natural hydrograph of the flood was available. In the calculations b/D was assumed to be 14 and the slope of the river bank was rounded to 7 which give 1.3 as the coefficient. The maximum shear stress calculated match well with the FLOW-3D calculations (Figure 5.6) made and therefore was used for erosion calculations. The details of the calculations are presented in Appendix H and the summary of the values used to cut the river bank cross section are presented in Table 5.4.

Even though in this case it was not applied, as the calculated shear stresses were the same as FLOW-3D results, Olsen and Florey's method should be modified by a coefficient that depends on whether the embankment is on the inside or outside of the meander and the meander's radius.

Elevation	Erosion [m]	
	Day 16	Day 31
223.2	1.552	2.549
223.7	1.367	2.245
224.2	1.183	1.941
224.7	0.999	1.636
225.2	0.814	1.335
225.7	0.652	1.065
226.2	0.524	0.838
226.7	0.406	0.632
227.2	0.292	0.439
227.7	0.187	0.266
228.2	0.094	0.122
228.7	0.015	0.015

Table 5.4: Calculated Erosion after Day 16 and Day 31
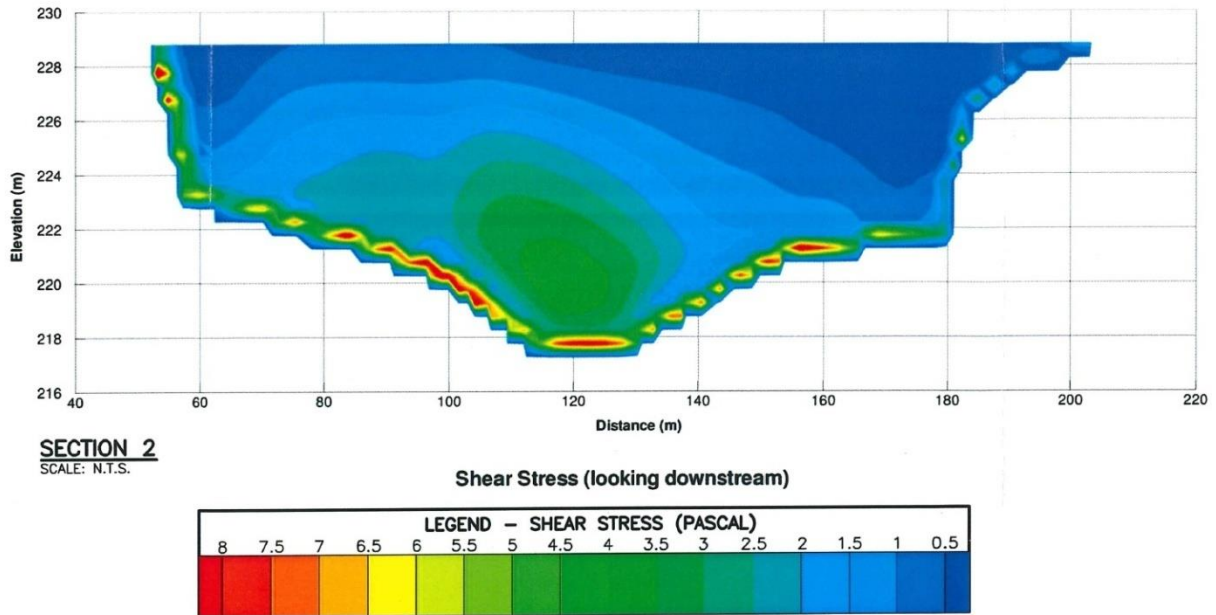
Figure 5.6: Shear Stress Profile under Natural Conditions - Water Level 228.67 m (used with permission from KGS Group April 8th 2013)

5.3.2.2 Floodgate in Operation

Since the only data available was KGS Group's FLOW-3D snapshot calculation (Figure 5.7) of the shear stress the maximum of those where chosen and assumed for the whole flood event simulated. This is most conservative assumption and the calculated erosions are listed in Table 5.5.

Bank Elevation	τ [Pa]	$\dot{e}$ [mm/hr]	Total [m]
up to 222	4	1.86	1.384
up to 228	3	0.59	0.442
up to 231.65	2	0	0

Table 5.5: Shear Stress and Erosion Calculations for Scenario with Floodgate in Operation
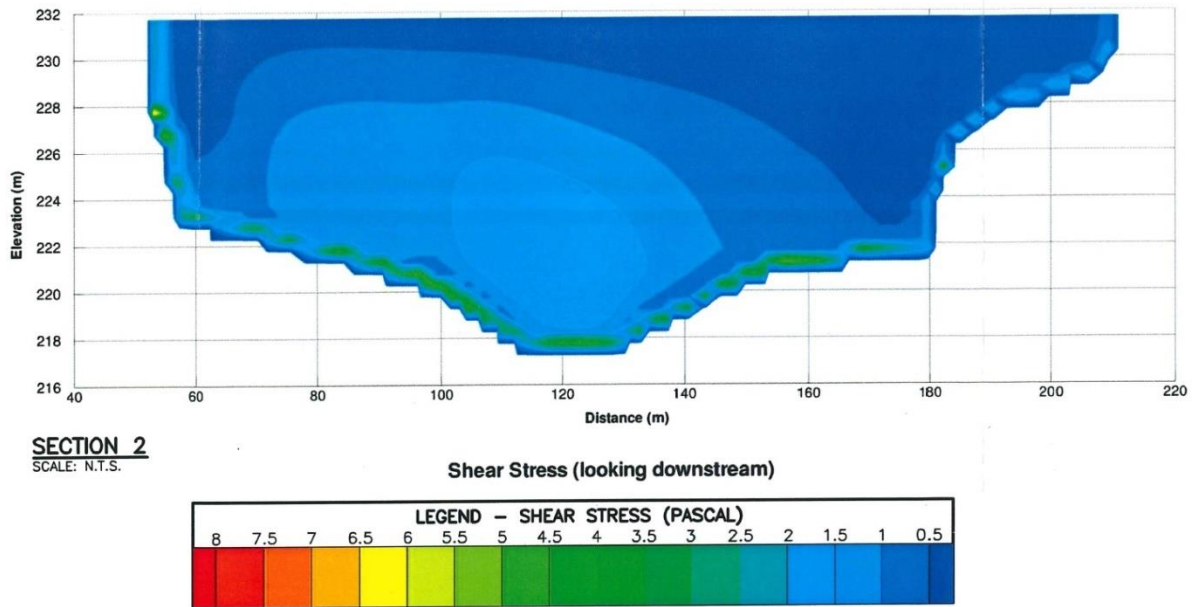
Figure 5.7: Shear Stress Profile with Floodgate in Operation – Water Level 231.65 m (used with permission from KGS Group April 8th 2013)

5.3.3 Results of Flood Event Modeled

The results of the two scenarios modeled are described in the following subsections. A baseline steady state model was needed for both models. The elevation at the start of the flood (225.34

m) was used. Figure 5.8 demonstrates the result of the seepage and Figure 5.9 the slope stability analyses. The factor of safety on the baseline slope stability analysis is 1.256 as seen in Figure 5.9.
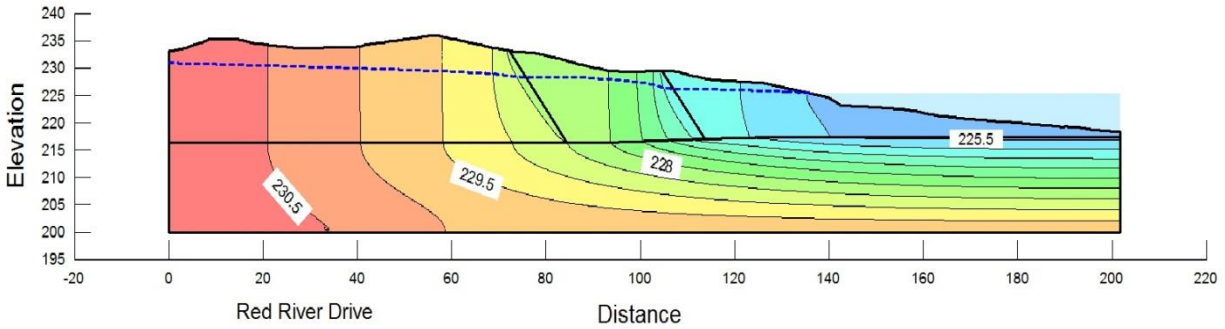
Figure 5.8: Baseline Seepage Model Result
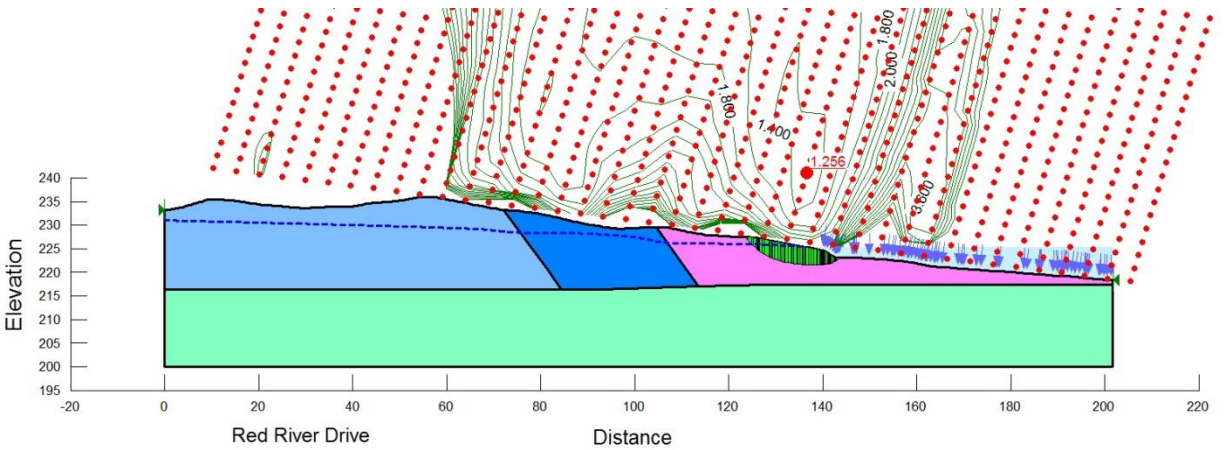
Figure 5.9: Baseline Slope Stability Model Result

5.3.3.1 Natural Condition

The transient seepage analysis was set to be calculated on daily increments. The snapshot of the seepage analysis after the peak of the flood (on the 16th day) is demonstrated in Figure 5.10. This result was coupled with a slope stability analysis of the eroded cross section. Its result is presented in Figure 5.11. The factor of safety calculated is 1.587 and is located in the middle section of the river bank. Similar analysis was performed on the seepage result and eroded cross

sections of the last (31st) day of model whose results are presented in Figure 5.12and Figure 5.13.

The factor of safety calculated is 1.097 and is at the lower sections of the river bank.
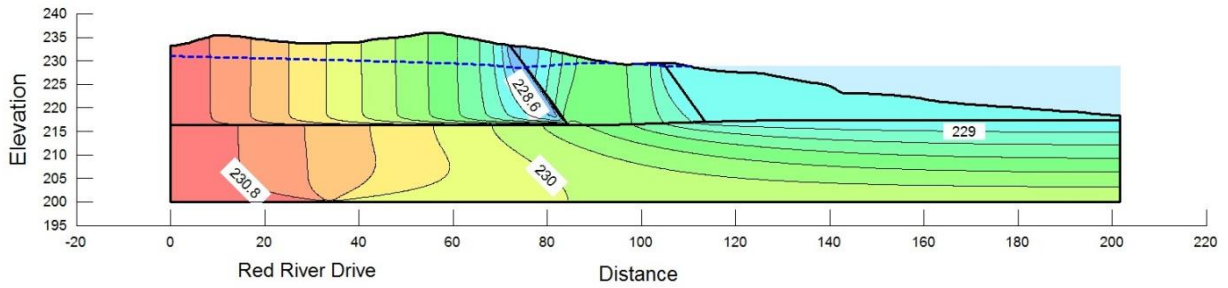
Figure 5.10: Natural Condition 16th Day Seepage Model Result
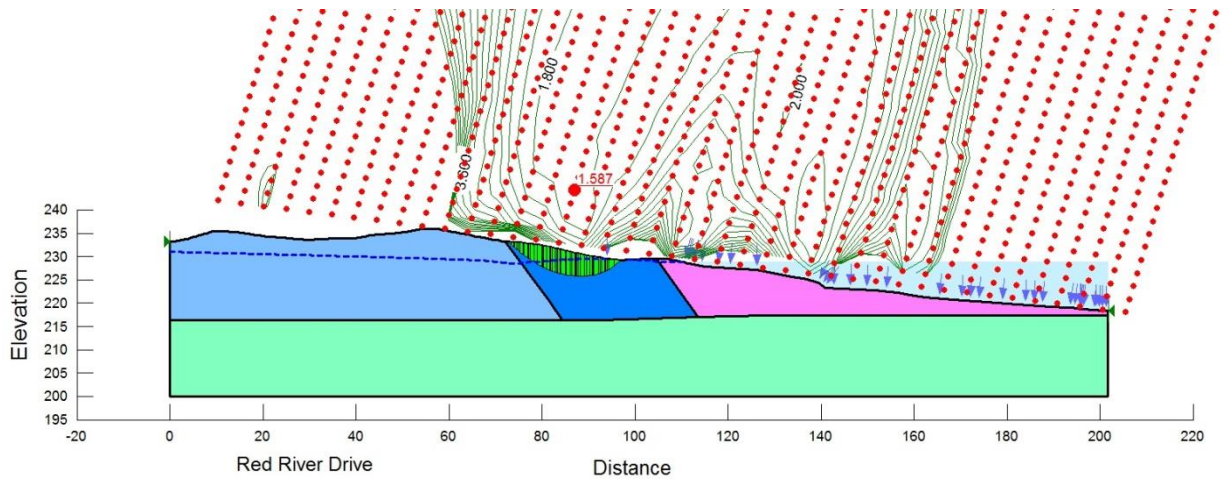
Figure 5.11: Natural Condition 16th Day Slope Stability Model Result
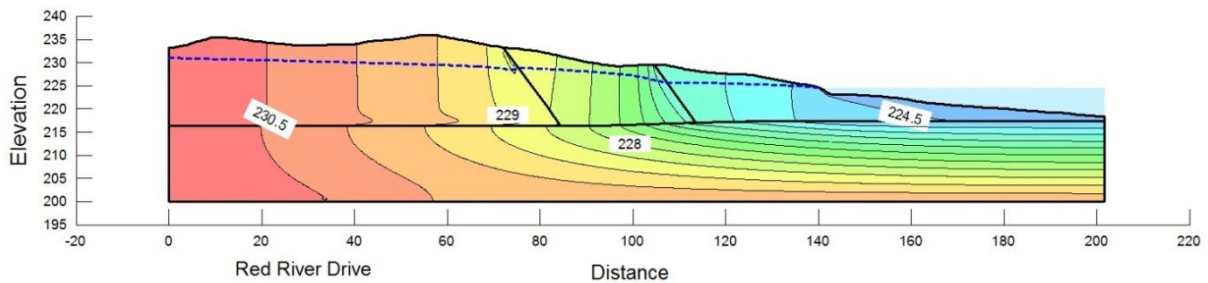
Figure 5.12: Natural Condition 31th Day Seepage Model Result
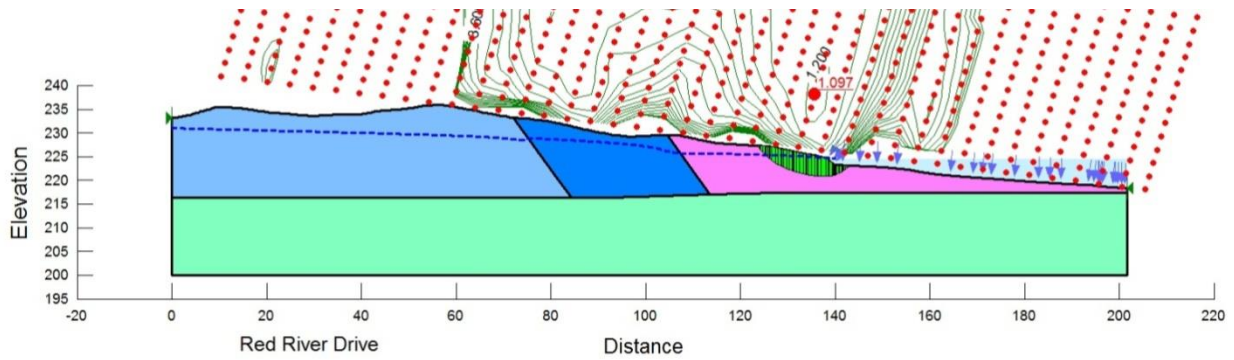
Figure 5.13: Natural Condition 31th Day Slope Stability Model Result

5.3.3.2 Floodgate in Operation

Similar analyses were performed with the assumed hydrograph for the scenario with the floodway in operation and its corresponding eroded cross section. The results of the analyses are presented in Figure 5.14 and Figure 5.15. The factor of safety at the end of this model (31st day) was 1.141 and is located at the lower section of the river bank.
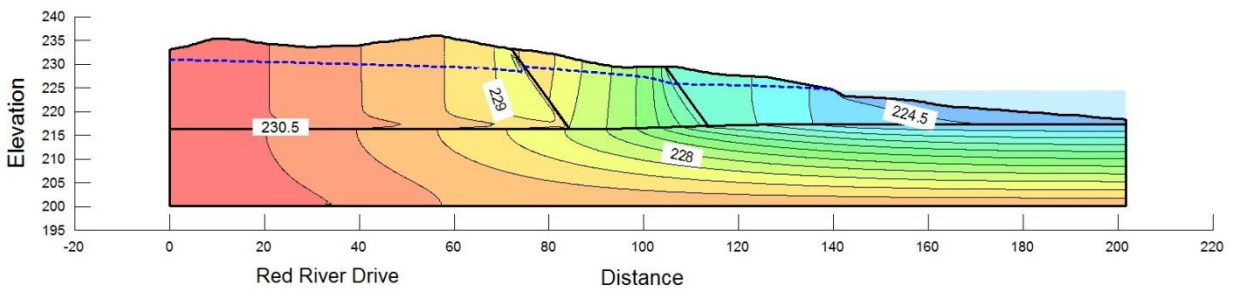
Figure 5.14: With Floodgate 31th Day Seepage Model Result
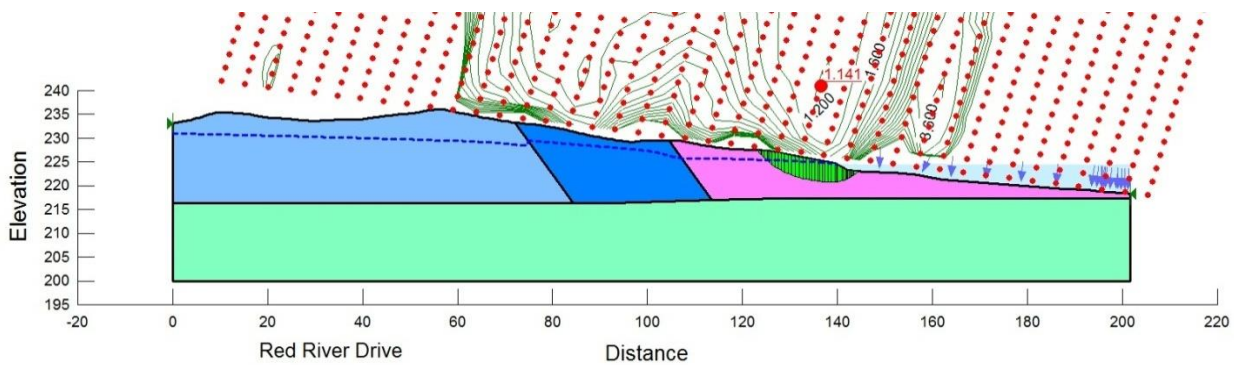
Figure 5.15: With Floodgate 31th Day Slope Stability Model Result

89

5.3.3.3 Summary of Results

The calibration of the model to obtain results in the same range of instrumentation measurements as made on site allowed confidence in the material properties and boundary conditions used in the model. The base line model was the same for both the Natural Condition and Floodgate in Operation scenarios with a global factor of safety of 1.256 at the lower toe.

In the Natural Condition scenario seepage and slope stability analyses were performed for day 16 and 31, corresponding to the end of peak flow and end of flood, with global factors of safety of 1.587 and 1.097, respectively. The critical slip surface for day 16 is located at the mid-bank. This is due to the slightly higher strength of the soil at that region and also the stabilizing effect of the weight of the water on the slope.

In the Floodgate in Operation scenario the assumed hydrograph was used for the seepage analysis. Since daily flow velocities and shear stresses during the flood were unknown the maximum calculated, by KGS Group's Flow3D model was used through the whole duration of the flood. This is a conservative assumed amount of erosion. The global factor of safety obtained is 1.141.

CHAPTER 6: DISCUSSION AND RECOMMENDATIONS

6.1 Laboratory Results

The following observations can be drawn from the tests completed.

6.1.1 Erosion Results

Throughout the testing it was clear that roots and vegetation bind the soil material and reduce the erosion rate. Once enough of the material was eroded and/or the vegetation had been eroded large chunks were taken off the sample which created gaps that may have also caused increased scouring. Bubbles and fractures in the samples created weaker regions of the samples that also showed accelerated erosion. The soils flaked off during the tests in areas with inclusions present. These are most likely the causes that created fluctuations in the erosion rate graphs in addition to the sections where the material was less cohesive soil as indicated in the observation tables.

The erosion rates of the second phase of testing are generally comparable to the first phase when compared to the same range of shear stress.

More testing is required for completeness. When the erosion rate results were grouped by their classifications it is evident that the inside bend samples had higher erosion rates than the rest, likely due to lower cohesion due to a reduced clay fraction.

6.1.2 Grain Size Analyses

The grain size analyses indicated all specimens were high plastic clayey silt materials of limited varying plasticity.

6.1.3 Atterberg Limits and Unified Soil Classification System

The ranges in moisture content of the samples tested were between 19.2% and 50.6%; liquid limits of 56.4% to 72.9%; plastic limit of 20.2% and 28.0%; and plasticity index of 32.9% to 45.8%. The USCS classifications were generally CI (intermediate plastic clay).

6.1.4 Comparison of Erosion Rates with Moisture Content, Atterberg Limits, and SAR

There was no relationship observed between erosion rates and moisture content, plasticity index, nor SAR values. This could perhaps be due to the samples not being the same in terms of grain size and also differences in roots and other content and perhaps other unknown differences.

6.1.5 Additional Analyses of Phase II

6.1.5.1 Grain Size Analyses of Sump Material

Since the tests were conducted at relatively lower velocities than the range in the first phase the larger and heavier material that were eroded were caught in the junction connection that was placed right after the rectangular flume for the purpose of emptying the flume prior to opening the lid. As a result there were no significant differences between the grain size analyses of the return and intake halves of the sump except for the most granular sample, ST8 St. Adolphe, where 70% of the material in the left side (return side) of the sump were fine sands or larger.

6.1.5.2 Grain Size Analyses of Flume Water

As it can be expected after seeing the effect of the weir and filter in the sump, the hydrometer results show that most of the sediment in the eroding water was clay and some silt.

6.2 Model Results

The model results of Red River Drive are discussed below.

6.2.1 Calibration Model

The boundary conditions and the hydraulic conductivity of each zone were adjusted to achieve a less than 1 meter tolerance range for the baseline and transient simulation to the measured data for the flood event.

6.2.2 Flood Models

The parameters obtained from the calibration stage of the modelling were used in simulating the effect of erosion and seepage of a flood event as it would occur naturally compared to the same flood with the use of the floodway. Since the starting elevation of the flood was used for both simulations the baseline analysis is the same for both models. The factory of safety calculated in the baseline is 1.256.

6.2.2.1 Natural Condition

The seepage analysis was calculated on a daily basis for the second peak of the 2009 flood with the natural hydrograph obtained. The stability of the river bank cross section was also analysed at the 16th day of flood after the peak elevation and at the end of the flood. The cross section of the two slope analyses where changed to take into account the calculated amount of erosion. As could be expected the stabilizing hydraulic load on the river bank at high water elevations can be seen in the higher global factor of safety of 1.587 located at mid-bank. The stability of the slope was also calculated for the end of the flood at the 31st day with a global factor of safety of 1.097 located at lower toe. This is approximately a 13% reduction in global factor of safety compared to the baseline.

6.2.2.2 Floodgate in Operation

The analysis settings were the same for the simulation with the Floodway in operation as the one with natural conditions with the difference of using the assumed higher elevation hydrograph and different resulting eroded cross section using the calculated amount of erosion. The seepage analysis was coupled with slope stability analysis to get a global factor of safety of 1.141 at the end of the 31 day flood located at the lower toe. Compared to the initial factor of safety the reduction is approximately 9% in this scenario.

6.3 Recommendations

There are many factors governing stability of river bank slopes. Some of which were not included in this study are deposition and ice scouring. These are some of the factors that need further studying. To understand these factors better it is recommended to conduct long term study, say five years, with a survey of the riverbank cross section twice a year: once after ice breakup in the spring and one at the end of fall. This would provide more information about ice scouring and sediment deposition and also the actual erosion due to the flow of the river. It goes without saying that well placed and monitored instrumentation is key to this study.

There are also many factors that govern erosion rates such as: the chemistry, temperature, and suspended load of the eroding water; the soil particles and their pore water's chemistry and presence and formation of roots and organics in the soils being tested. Also to get better long term erosion rates it is recommended that the erosion tests conducted in the lab be performed on longer durations to get a more accurate critical shear stress and shape of the erosion function obtained.

CHAPTER 7: CONCLUSIONS

7.1 Laboratory Testing

The results and observations indicate that, as expected, the erosion curves show a similar shape where erosion is limited until a threshold value after which the erosion increases at an increased rate. The threshold erosion level is less in specimens that are less cohesive and the rate of erosion is higher in the less cohesive materials. This can be broadly linked to the typical riverbank profiles where alluvial deposits exist more predominantly on inside bends and more cohesive materials on outside bends. However, the character of the riverbank sediments at shallow depths that comprised the tube samples show less distinction in index properties.

The results show that, regardless of the material, the erosion rate increased with increasing flow velocity and therefore increasing shear stresses. If operation of a floodway increases the velocity in the backwater region then erosion will be accelerated over natural conditions. If operation of a floodway decreases flow velocity in the backwater region then erosion will be reduced from natural conditions. The degree to which the increase or decrease of erosion occurs over natural conditions in the backwater region will depend on the difference in velocity from the controlled to natural conditions.

The erosion rates obtained in the common range of shear stresses tested for in both phases of testing were relatively consistent reinforcing validity of the conclusion made in the first phase of testing that the inside bends material samples have higher erosion rates than the materials sampled from the outside bends.

Even though there were some outliers in the erosion rate graphs due to the non-homogeneity of the samples, the general trend observed throughout the second phase of testing was that both increase in velocity/shear stress and increase in sediment load in the eroding fluid increased the erosion rate of the sample.

The results presented for the nine sites in this study provided a basis for estimating the magnitude of this impact on riverbanks by developing the transient backwater conditions and then integrating the erosion rate curves over the difference in velocity at any given position along the river and through the cross section at that position with respect to time. This is the first measured data of this nature that has allowed, to some degree of certainty, erosion impacts to be examined in a quantitative manner.

As observed in the two phases of testing the presence of roots has the greatest impact on the erosion rate of the samples tested.

Some new modes of erosion were observed including fracturing and flaking of the soils when there was brown marbling visible, perhaps due to decayed organic matter and/or surrounding larger twigs; and erosion of finer and cohesive soils surrounding larger pebbles till a threshold amount of exposure of the pebble was reach for it to be dislodged.

7.2 Finite Element Analysis

As expected the hydraulic conductivity of the soil regions close to the toe of the bank had to be assigned higher values than further back from the toe toward the crest and beyond to be able to calibrate the model to the piezometer data. This may be due to the many factors including previous failures of the slope which would disturb the material.

As observed from the calculated global factors of safety obtained from the simulation of the two scenarios of without and with the use of the Floodway it is evident that the scenario simulated with the Floodway in operation has a higher global factor of safety. This is because the backwater curve fundamentally changes by the operation of the hydraulic structure. This results in the reduced backwater velocity due to the forced increase in elevation of the water such that it can pass over the Floodgate. This reduced velocity results in a shear stress profile that is less than what the river bank experiences during a natural flood. Even though the water reaches further up on the river bank because of its slower flow velocity and lower shear stress the amount that is eroded is less than the amount of erosion during a natural flood.

REFERENCES

Alizadeh, A., 1974. "Amount and Type of Clay and Pore Fluid Influences on the Critical Shear Stress and Swelling of Cohesive Soils", Ph.D. Dissertation, University of California, Davis.

Anderson, D.E.S., Kenyon, R.M., Blatz, J.A., Smith, J.B. 2004. "Numerical Modelling of the 1962 Red River Floodway Test Pit Excavation". Proceedings of the 57TH Canadian Geotechnical Conference, Quebec City, Quebec.

Arulanandan, K., Lganathan, P., and Krone, R.B., 1975. "Pore and Eroding Fluid Influences on Surface Erosoin of Soil." Proceedings of the American Society of Civil Engineering - Journal of the Geotechnical Engineering Division, January, pp.51-66.

Arulanandan, K., Gillogley, E., and Tully, R., (1980). "Development of a Quantitative Method to Predict Critical Shear Stress and Rate of Erosion of Natural Undisturbed Cohesive Soils." Report GL-80-5, U.S. Army Corps of Engineers, Waterways Experiment Station, Vicksburg, MS.

ASCE (1998). "River Width Adjustment. I: Processes and Mechanisms." Journal of Hydraulic Engineering, 124(9), 881-902

Baracos, A., 1960: "The Stability of Riverbanks in the Metropolitan Winnipeg Area". Preceedings of the 14th Canadian Soil Mechanics Conference, Niagara Falls, Ontario.

Baracos, A., 1971. "River Bank Investigation Tache Avenue St.Boniface, Manitoba". Letter report to Mr. R.Todd, Distric Director, Canada Public Works, Winnipeg, Manitoba, December 21, 1971. University of Manitoba, Department ofCivil Engineering, Winnipeg, Canada.

Baracos, A., 1977. "Compositional and Structural Anisotropy of Winnipeg Soils - A Study Based on Scanning Electron Microscopy and X-Ray Diffraction Analysis." Canadian Geotechnical Journal, 14, 125-137.

Baracos, A., 1978: "The Effects of River Levels, Ground Water and Other Seasonal Changes on Riverbanks in Winnipeg". 31st Canadian Geotechnical Conference, Proceedings, p.7.2.2 - 7.2.19.

Baracos, A., and Graham, J., 1981: "Landslide problems in Winnipeg". Canadian Geotechnical Journal, vol.18, p.390-401.

Baracos, A., Graham, J., Kjartanson, B.H., and Shields, D.H. 1983. "Geology and soil properties of Winnipeg." Geological Environment and Soil Properties. ASCE Convention, Houston, TX, October 1983, 39-56.

Baracos, A., Kingerski, D. and Leung, K., 1988: "Riverbank Stability Analyses with Uncertain Soil Properties". 41st Canadian Geotechnical Conference, Proceedings, Winnipeg, Manitoba.

Baracos, A., and Kingerski, D., 1998. "Geological and Geotechnical Engineering for Urban Development of Winnipeg, Manitoba in Urban Geology of Canadian Cities". Edited by P.F. Karrow and O.L. White, GAC Special Paper 42, p. 171-190.

Baracos, A., Lew, K.V., 2003. "Riverbank Slides, Erosion and Deposition at 758 Crescent Drive, Winnipeg, Manitoba - Volume 1 Report", prepared for Department of Justice Canada, Winnipeg, Manitoba.

Barbour, S.L., Fredlund, D.G. 1989. "Physico-Chemical State Variable of Clay Soils", In Proceedings, 12th International Conference of Soil Mechanics and Foundation Engineering, Rio de Janeiro, Brazil, vol.3, pp.1839-1843.

Barbour, L.S., Krahn, J., 2004. "Numerical Modelling – Prediction or Process?", Geotechnical News.

Bloom, A.L. 2004. "Geomorphology A Systematic Analysis of Late Cenozoic Landforms" 3rd Ed., Waveland Press Inc., USA.

Briaud, J.L., Chen, H.C., and KWAK K. 2000. "The EFA, Erosion Function Apparatus: An Overview", presented at the international Symposium on Scour of Foundations held in Melbourne Australia on November 19, 2000.

Briaud, J.L., Ting, F.C.K., Chen, H.C., Cao, Y., Han, S.W., Kwak, K.W., 2001. "Erosion Function Apparatus for Scour Rate Predictions". ASCE Journal of Geotechnical and Geoenvironmental Engineering, Vol. 127, No. 2, February.

Brooks, G.R., and Nielsen, E., 2000. "Red River, Red River Valley, Manitoba". The Canadian Geographer, 44, no.3, pp.304-309.

Brooks, G.R., 2002. "Floodplain Chronology and Vertical Sedimentation Rates Along the Red River, Southern Manitoba". Geographie Physique et Quaternaire, vol. 56, no. 2-3, p.171-180.

Brooks, G. R., 2003. "Holocene Lateral Channel Migration and Incision of the Red River, Manitoba, Canada". Geomorphology, 54, pp.197-215.

Brooks, G.R., 2003. "Alluvial Deposits of a Mud-Dominated Stream; the Red River, Manitoba, Canada". Sedimentology, 50: 441-458.

Brooks, G.R., St.George, S., Lewis, C.F.M., Medioli, B.E., Nielsen, E, Simpson, S. and Thorliefson, L.H., 2003. "Geoscientific Insights Into Red River Flood Hazards In Manitoba". Geological Survey of Canada Open File Report 4473, 35 p.

Chang, H., 1988. "Fluvial Processes in River Engineering", John Wiley & Sons, Inc., New York.

Darby, S.E., 1998. "Modeling Width Adjustment in Straight Alluvial Channels". Hydrological Processes, 12, pp.1299-1321.

Department of Resources and Development - Water Resources Division, 1953. "Red River Basin Investigation - Report on Investigations into Measures for the Reduction of the Flood Hazard in the Greater Winnipeg Area", Manitoba.

Duncan, J.M., 1996. "State-of-the-Art: Limit Equilibrium and Finite-Element Analysis of Slopes", ASCE Journal of Geotechnical Engineering, Vol. 122, No. 7, July, pp.577-596.

Fredlund, D.G., Scoular, R.E.G and Zakerzadeh, N., 2004. "Using A Finite Element Stress Analysis to Compute the Factor of Safety", 52nd Canadian Geotechnical Conference, pp.73-78.

Graham, J. and Shields, D.H., 1985. "Influence of Geology and Geologic Processes on the Geotechnical Properties of a Plastic Clay." Engineering Geology, 22, 109-126.

Griffiths, D.V. and Lane, P.A., 1999. "Slope Stability Analysis by Finite Elements", Géotechnique, 49, No.3, pp.387-403.

Hanson, G.J. and Simon, A., 2001. "Erodibility of Cohesive Streambeds in the Loess Area of the Midwestern USA". Hydrological Processes 15(1): 23-38.

Heinzen, R.T., 1976. "Erodibility Criteria for Soils", MS Thesis, University of California, Davis.

Julien, P.Y., (1998), "Erosion and Sedimentation", Cambridge University Press, NY, USA

Knighton, D., (1998), "Fluvial Forms and Processes: A New Perspective", Oxford University Press, USA.

Lane, E.W., 1953. "Progress Report on Studies on the Design of Stable Channels by the Bureau of Reclamation", American Society of Civil Engineers - Proceedings, v79, separate n 280, Sept., 31p.

Langendoen, E.J., 2000. "CONCEPTS - Conservational Channel Evolution and Pollutant Transport System", USDA-ARS National Sedimentation Laboratory, Oxford, MS.

Macdonald, A.E., Report of the Winnipeg Branch of the Engineering Institute of Canada Committee on Foundations, The Engineering Journal, November 1937.

Manitoba Geological Survey, 2002. "Environmental Geoscience in the Red River Valley", 2002 Energy and Mines Ministers' Conference, Winnipeg, Manitoba, CPG/NGSC Field Trip Guide Book.

Merten, G.H., Nearing, M.A., and Borges, A.L.O. 2001. "Effect of Sediment Load on Soil Detachment and Deposition in Rills", Soil Science Society of America Journal, 65: 861-868

Mishtak, J., 1964. "Soil Mechanics Aspects of the Red River Floodway". Canadian Geotechnical Journal.

Mitchell, J.K. and Soga, K., 2005. "Fundamentals of Soil Behavior 3rd Edition", John Wiley and Sons Inc., New Jersey.

Morisawa, M., 1968. "Streams: Their Dynamics and Morphology", McGraw-Hill Book Company, New York.

Morisawa, M.,1985. "Rivers", Longman Group Limited, New York.

Nielsen, Eric, Brian, W., McKillop, B. and Conley, G.G., 1993. "Fluvial Sedimentology and Peleocology of Holocene Alluvial Deposits, Red River, Manitoba". Geographie physique et Quaternaie, 1993, Vol. 47 no. 2, p.193-210, 17 fig., 3 tabl.

Olsen, O. J., Florey, Q.L., 1952. "Sedimentation Studies in Open Channels Boundary Shear and Velocity Distribution by Membrane Analogy, Analytical and Finite-Difference Methods," U.S. Bureau of Reclamation, Laboratory Report N. SP-34, August 5.

Osman, A. M., and Thorne, C.R., 1988. "Riverbank Stability Analysis. I: Theory." Journal of Hydraulic Engineering., 114(2), 134-150.

Partheniades, E., 1965. "Erosion and Deposition of Cohesive Soils". Journal of Hydraulics Division of the American Society of Agricultural Engineers, 91: 105-139.

Preston, J.H., 1954. "Determination of Turbulent Skin Friction by Means of Pitot Tubes", Jour. Royal Aeronautical Society, Vol. 8.

Quigley, R.M., 1980. "Geology, Minerology and Geochemistry of Canadian Soft Soils: A Geotechnical Perspective." Canadian Geotechnical Journal, 17, 261-285.

Render, F.W., 1970. "Geohydrology of the Metropolitan Winnipeg Area as Related to Ground Water Supply and Construction." Canadian Geotechnical Journal, 7(3), 243-274.

Richards, K., 1985. "Rivers: Form and Process in Alluvial Channels", Methuen & Co. Ltd, New York.

Rutherford, D.H., and Baracos, A., 1953. "Damage to Houses - Red River Valley Flood 1950". Technical Report No.9 of the Division of Building Research, Ottawa, NRC No. 2976, DBR No. 23.

Schumm, S.A., 1960. "The shape of alluvial channels in relation to sediment type", U.S. Geol. Surv. Prof. Paper 352B.

Shulits, S., 1941. "Rational equation of riverbed profiles", Trans. Am. Geophys. Union, Vol. 22, pp.622-629.

Simon, A., Curini, A., Darby, S.E., and Langendoen, E.J., 1999. "Streambank Mechanics and the Role of Bank and Near-Bank Processes in Incised Channels." Incised River Channels, S.E. Darby and A. Simon, eds., John Wiley and Sons, New York, NY, 123-152.

Simon, A., Langendoen, E.J., Collison, A., Layzell, A., 2003. "Incorporating Bank-Toe Erosion by Hydraulic Shear into a Bank Stability Model: Missouri River, Eastern Montana", American Society of Civil Engineers Water Resources Conference Proceedings, World Water and Environmental Resources Congress.

Simons, D.B., Senturk, F., 1992. "Sediment Transport Technology – Water Sediment Dynamics", Water Resources Publications, Colorado.

Sutherland, H.B., 1966. "The Stability of the River Banks in the Winnipeg Area." Unpublished report to the Rivers and Streams Authority, No.1, Winnipeg, MB.

Teller, J.T. and Fenton, M.M., 1980. "Late Wisconsinan Glacial Stratigraphy and History of Southeastern Manitoba." Canadian Journal of Earth Sciences, 17, 19-35.

Teller, J.T. and Clayton, L., 1983. "Glacial Lake Agassize" Special Paper 26, Geological Association of Canada, 3-5.

Thorleifson, H., Brooks, G., Hanuta, I., Kroker, S., Matile, G., Nielson, E., Prevost, C., and Rannie, W. 1998. "Red River Flooding: Evolutionary Geomorphic Trends and Evidence for Major Floods in Recent Centuries (NTS 62H/W)". In Manitoba Energy and Mines, Geological Services, report of Activities, 1998, p.186-195.

Thorne, C.R., 1982. "Processes and Mechanisms of River Bank Erosion", Gravel-Bed Rivers, edited by R.D. Hey, J.C. Bathurst and C.R. Thorne. John Wiley and Sons Ltd.

Tutkaluk, J., 2000. "The Effect of Seasonal Variations in the Red River and Upper Carbonate Aquifer on Riverbank Stability in Winnipeg", M.Sc. Thesis, University of Manitoba.

Tutkaluk, J., Blatz, J., Graham, J., and Wingrove, T., 2002. "A Generic Study of the Influence of a Confined Aquifer on Slope Stability in Lacustrine Clay Slopes". Proceedings from the 2002 Canadian Geotechnical Conference.

APPENDICES

Appendix A: Cross Sections of Selected Sites
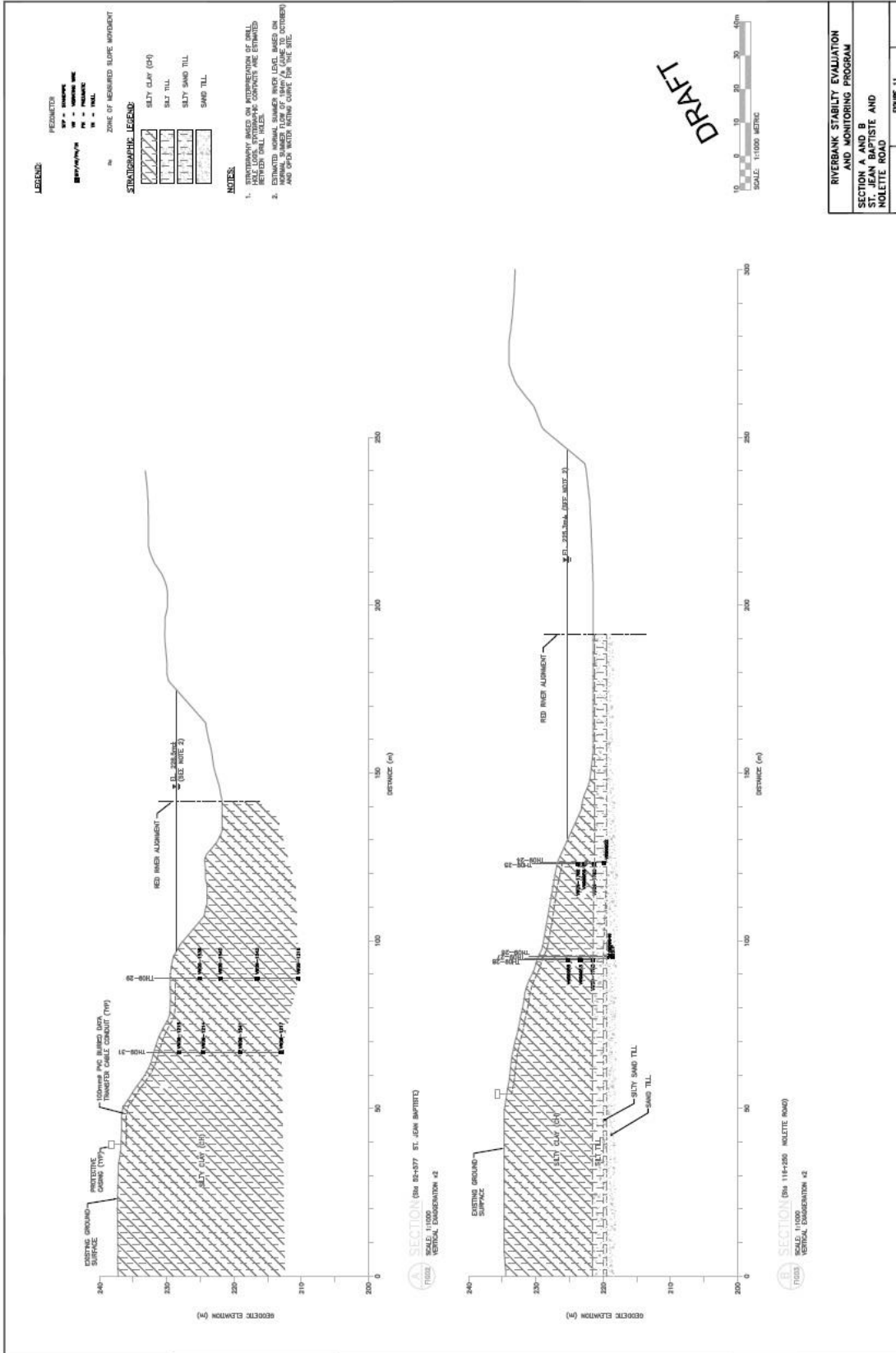
Figure A.1: Cross Section of St Jean Baptiste and Nolette Road (used with permission from KGS Group April 8th 2013)
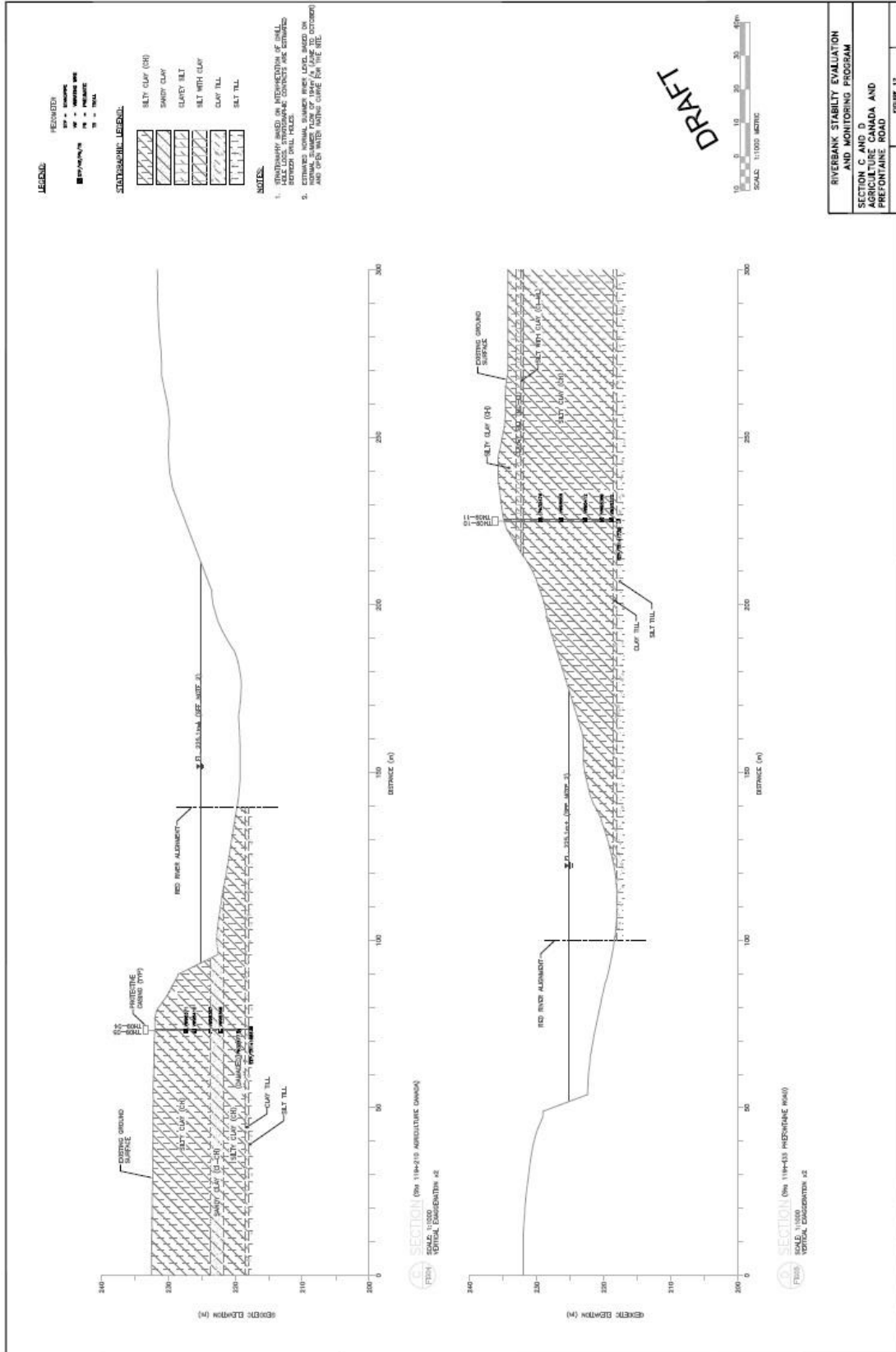
Figure A.2: Cross Section of Agriculture Canada and Prefontaine Road (used with permission from KGS Group April 8th 2013)

106
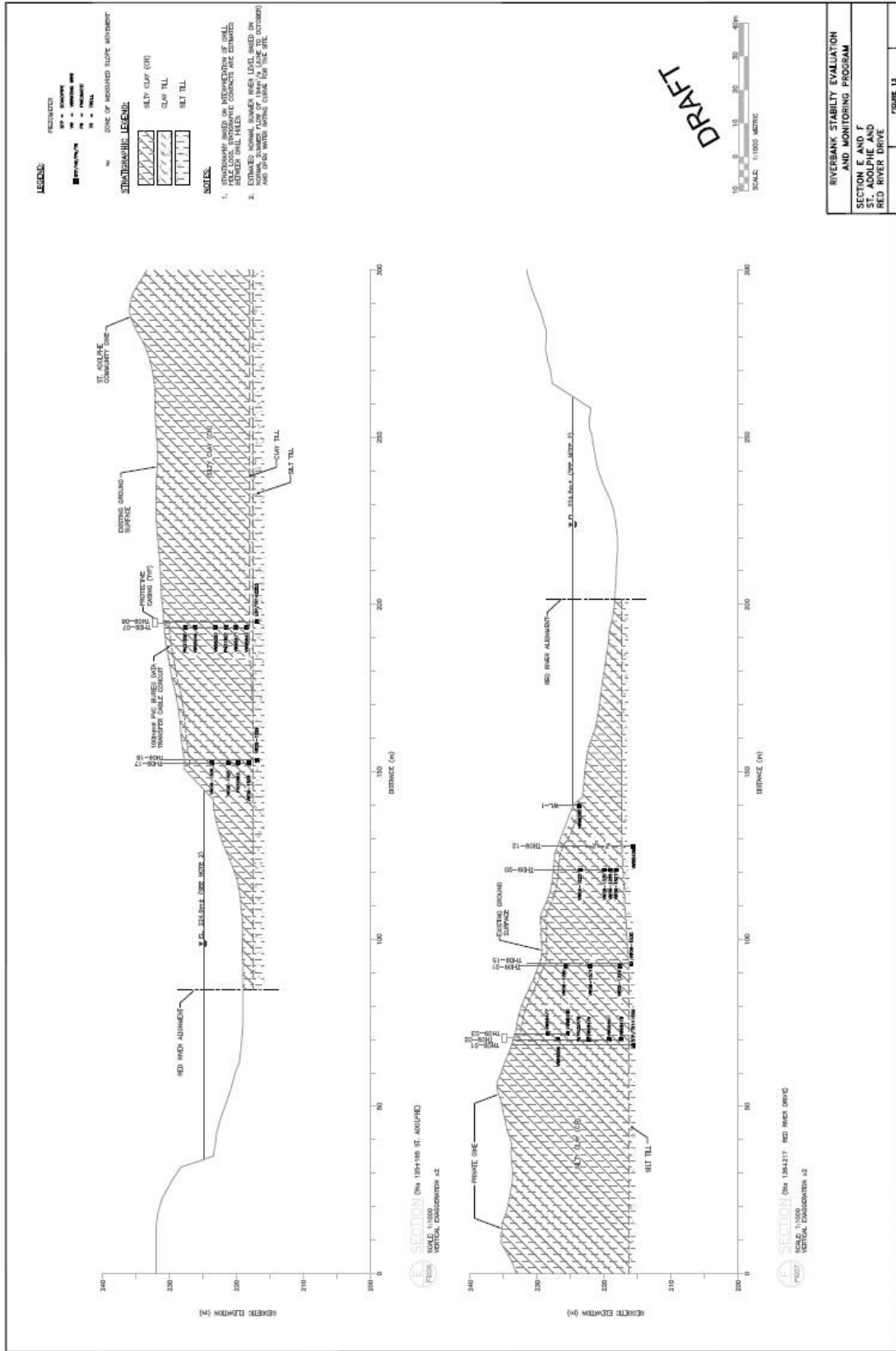
Figure A.3: Cross Section of St. Adolphe and Red River Drive (used with permission from KGS Group April 8th 2013)
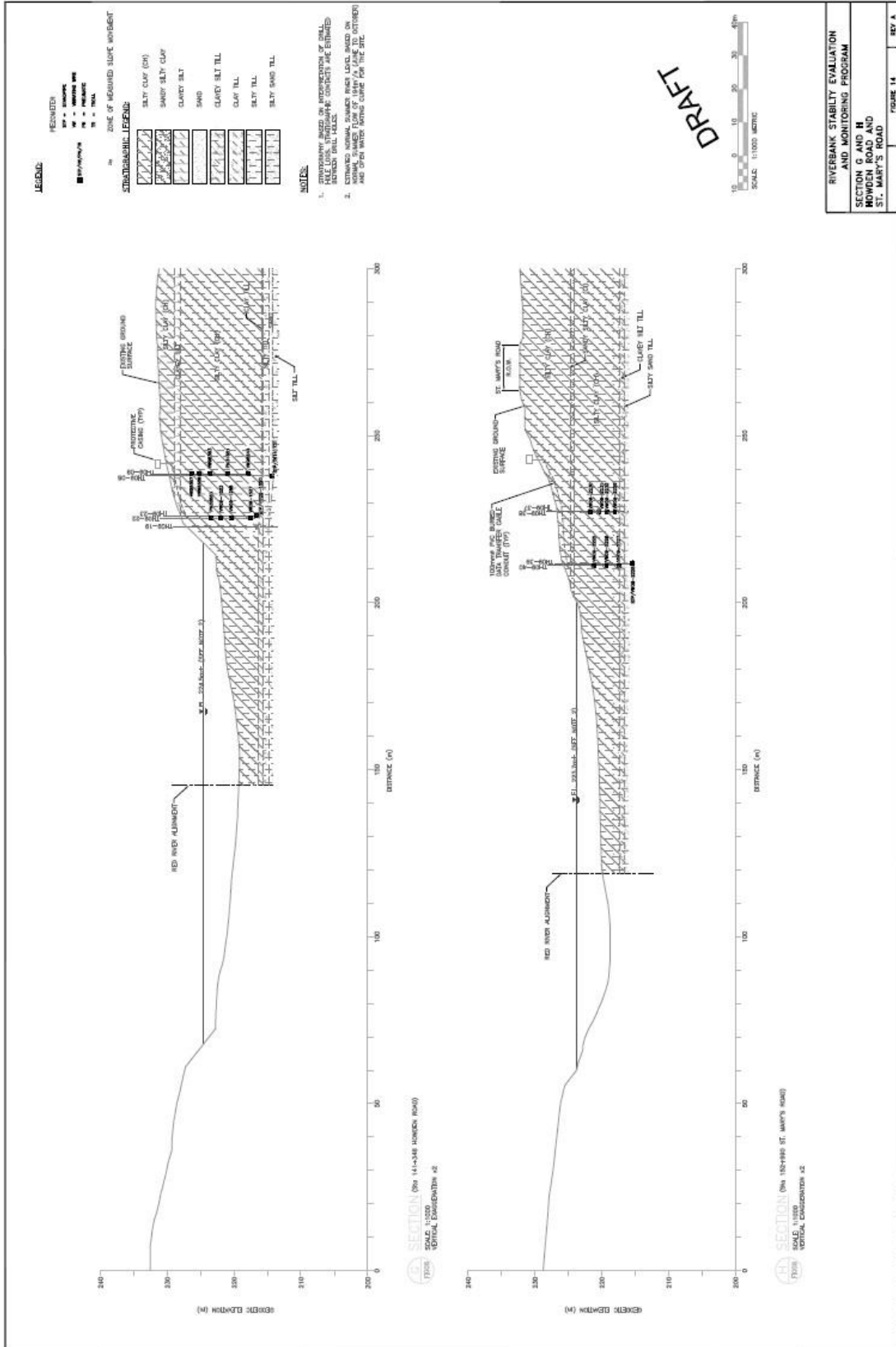
Figure A.4: Cross Section of Howden Road and St. Mary's Road (used with permission from KGS Group April 8th 2013)
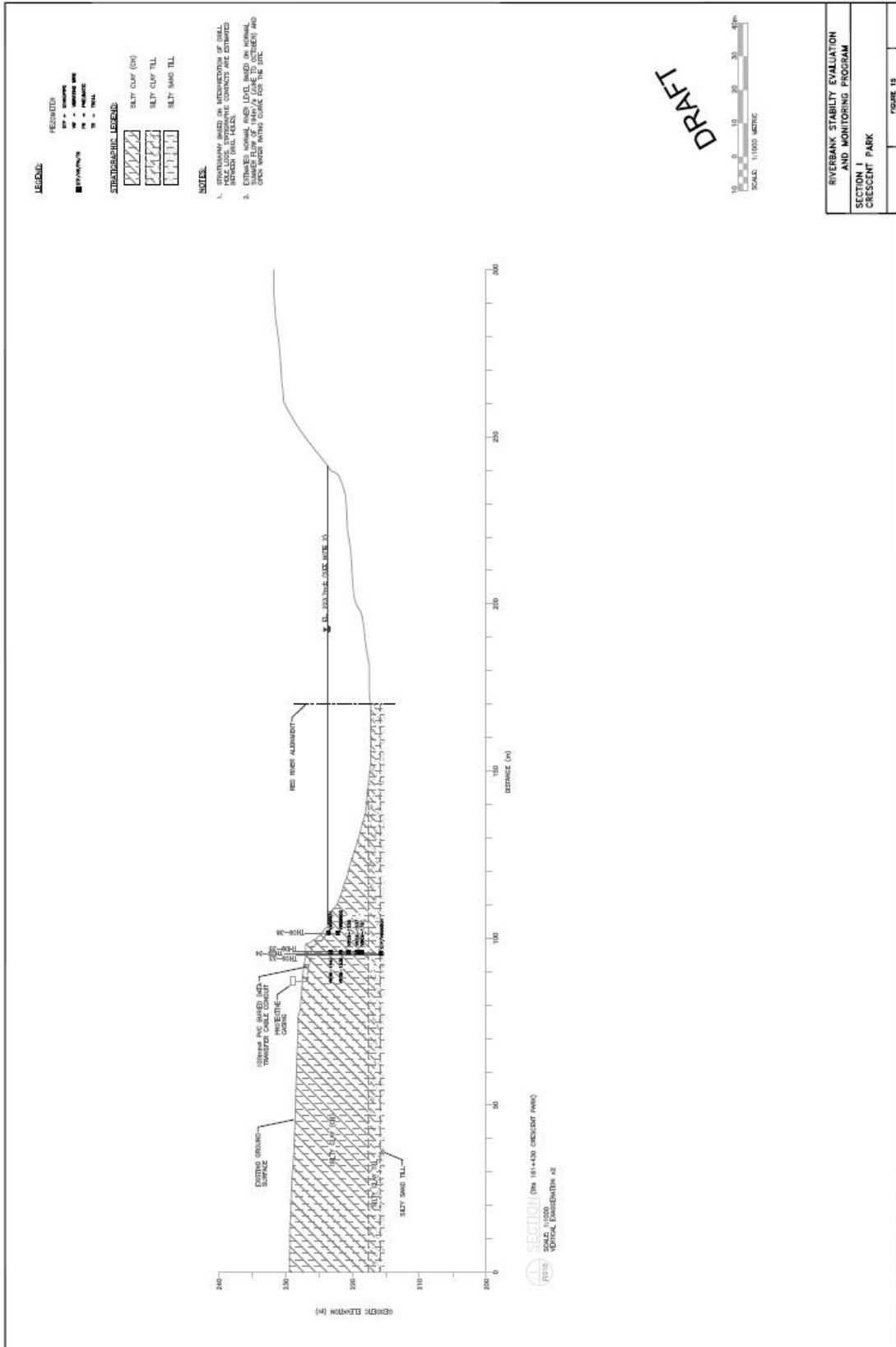
Figure A.5: Cross Section of Crescent Park (used with permission from KGS Group April 8th 2013)

Appendix B: Phase I Grain Size Distribution

| CLAY | SILT | FINE SAND | COARSE - MED. SAND | GRAVEL |
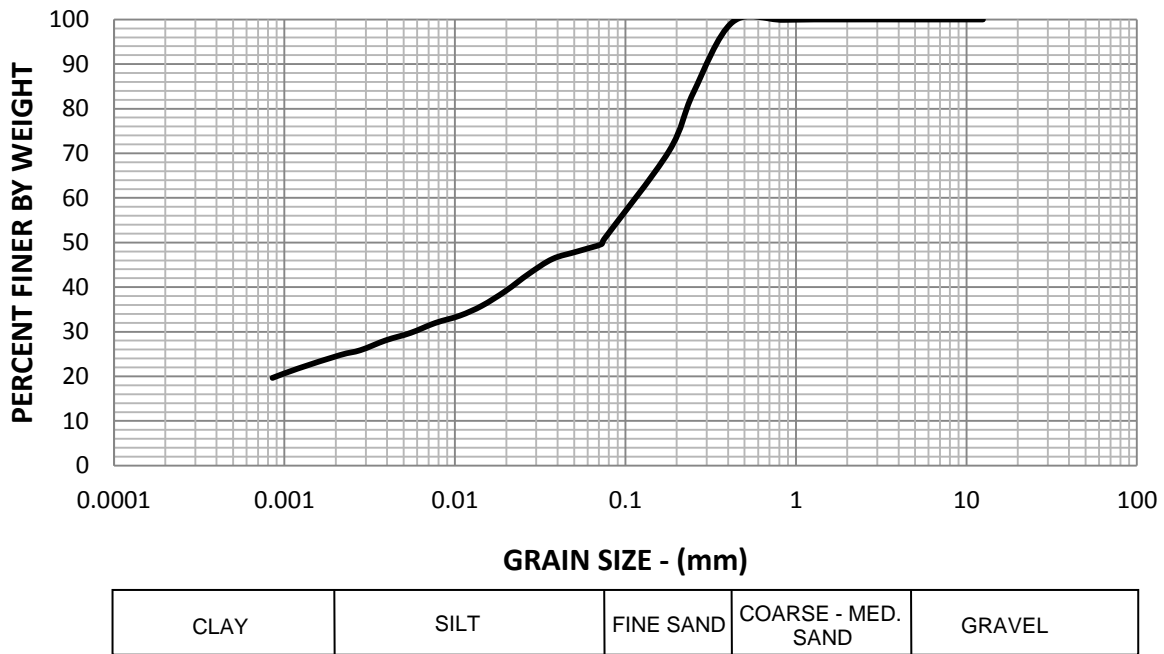
Figure B.1: Grain Size Analysis of Crescent Park

| CLAY | SILT | FINE SAND | COARSE - MED. SAND | GRAVEL |
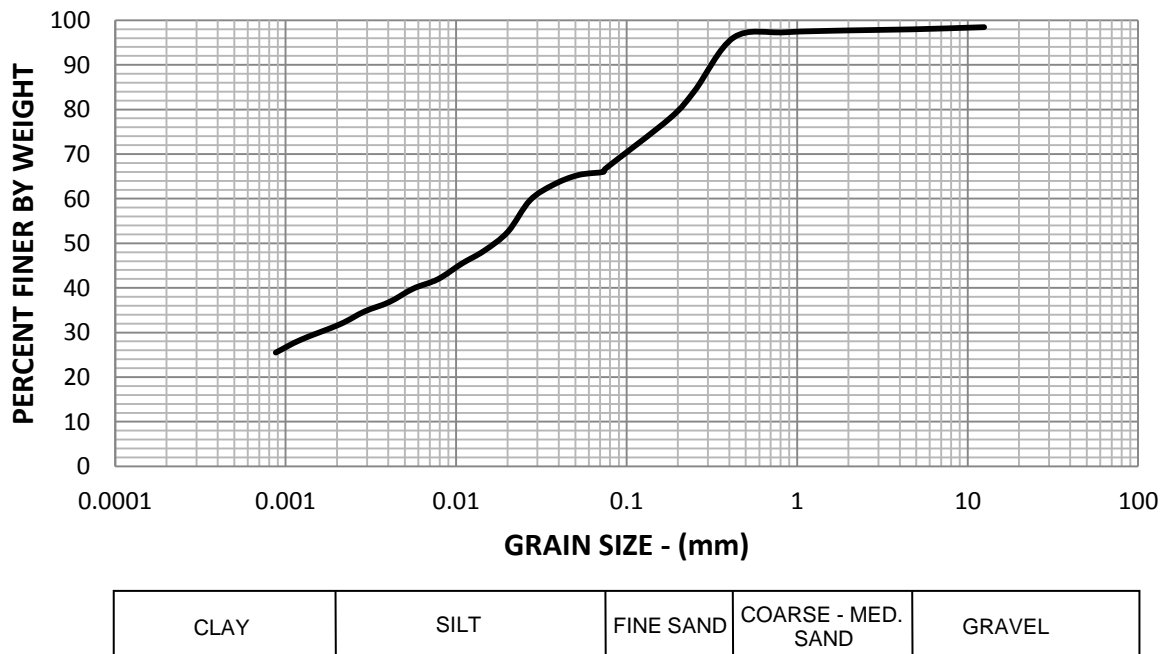
Figure B.2: Grain Size Analysis of St. Mary`s Road

111
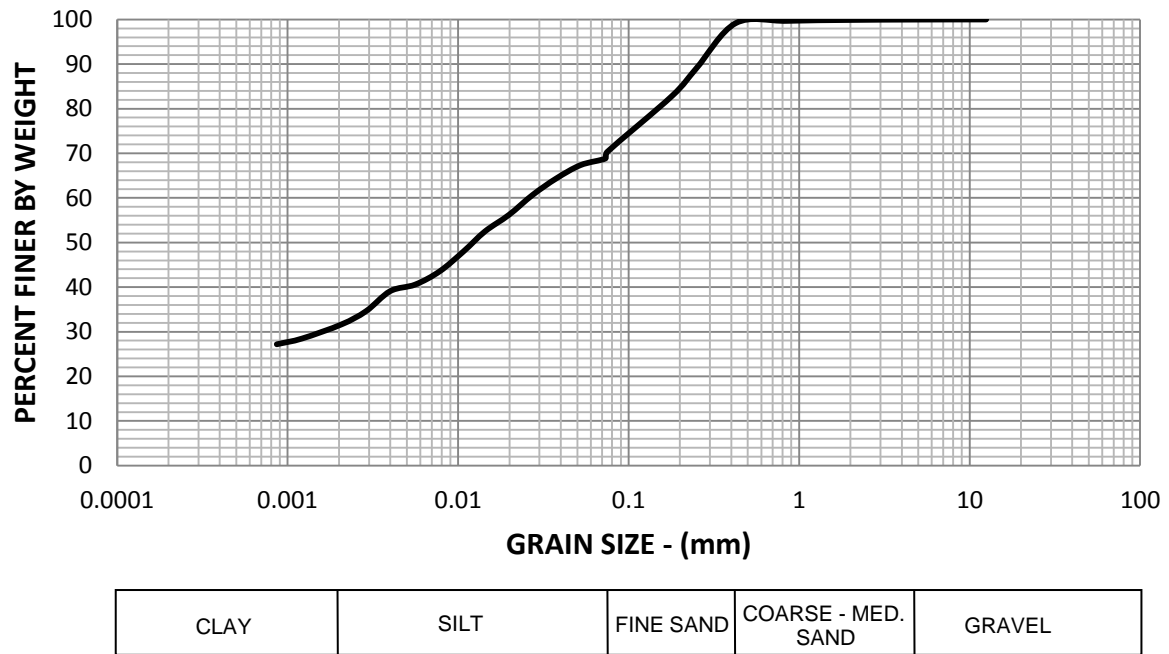
Figure B.3: Grain Size Analysis of Howden Road
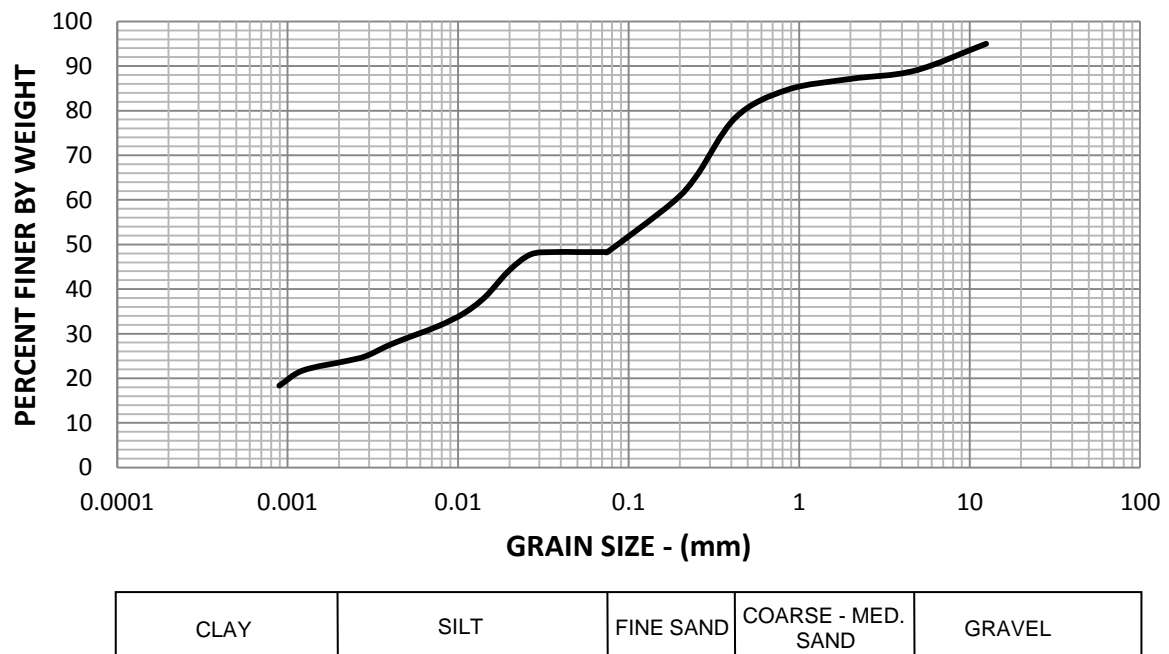
Figure B.4: Grain Size Analysis of Red River Drive

112
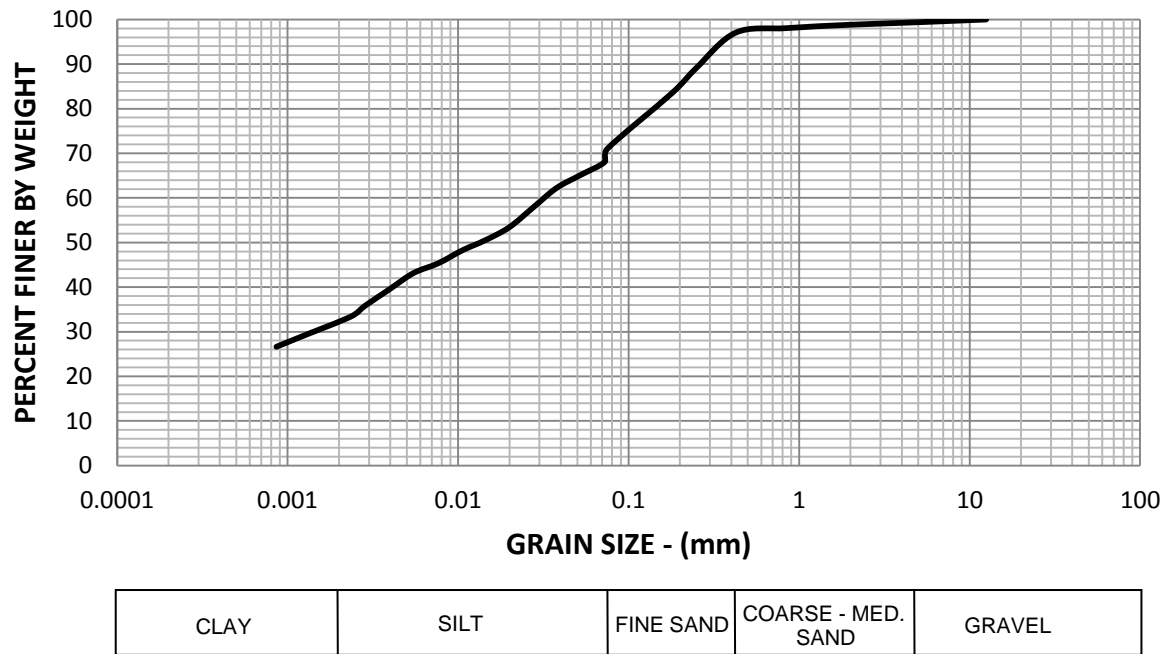
Figure B.5: Grain Size Analysis of St. Adolphe
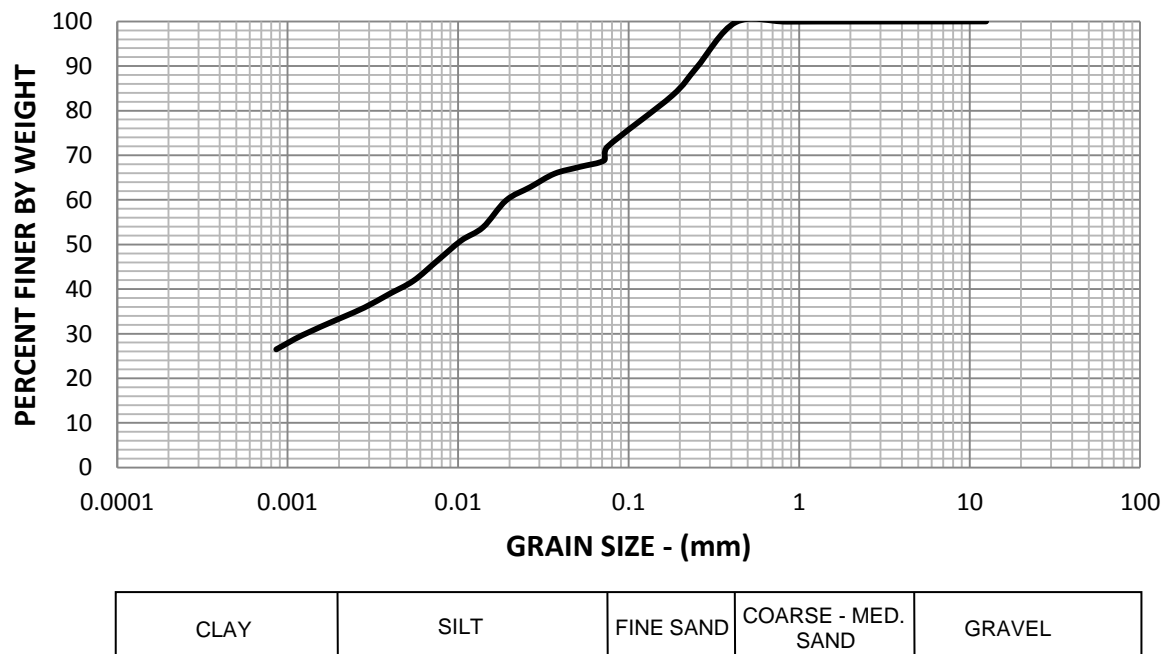
Figure B.6: Grain Size Analysis of Prefontaine Road

113
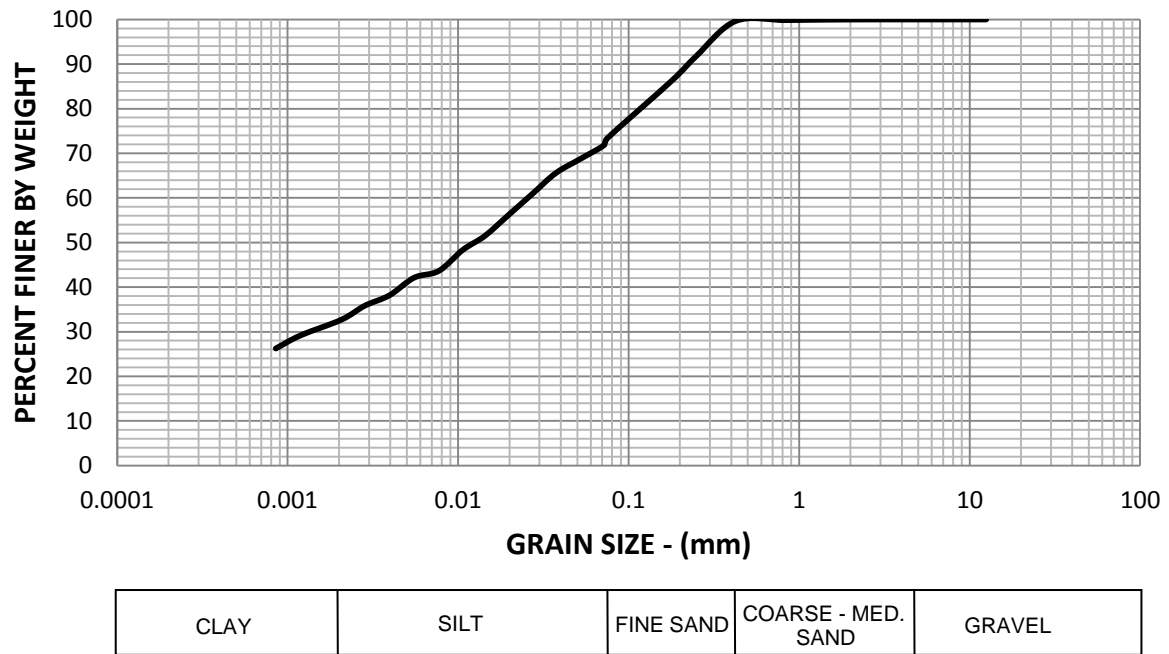
Figure B.7: Grain Size Analysis of Agriculture Canada
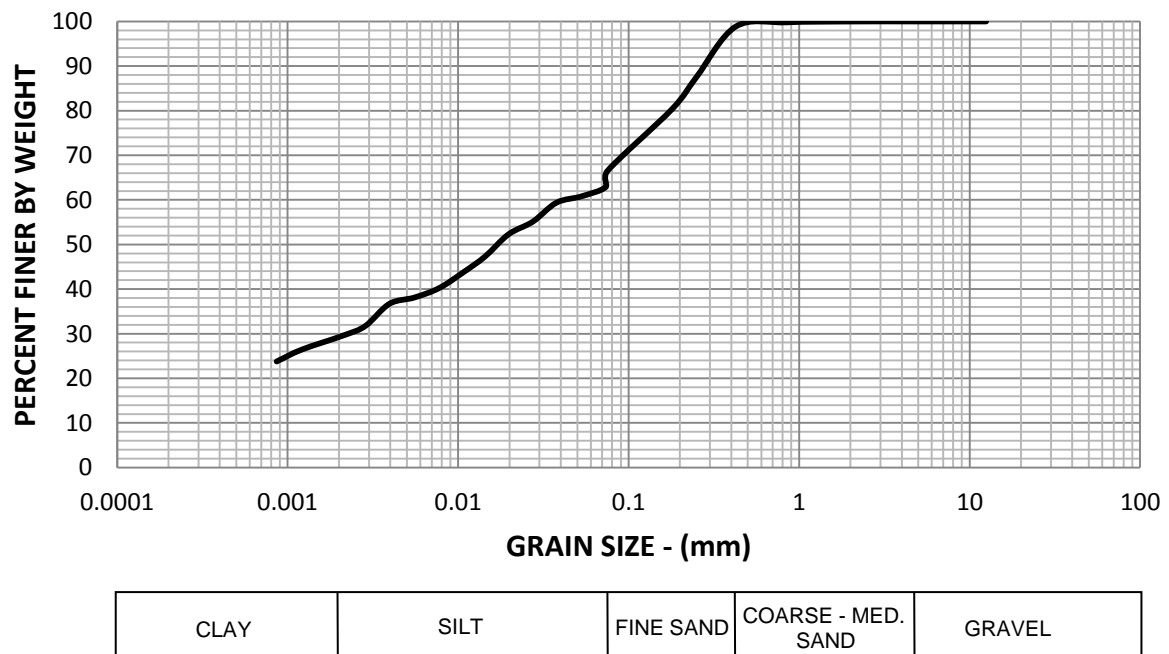
Figure B.8: Grain Size Analysis of Nolette Road

114
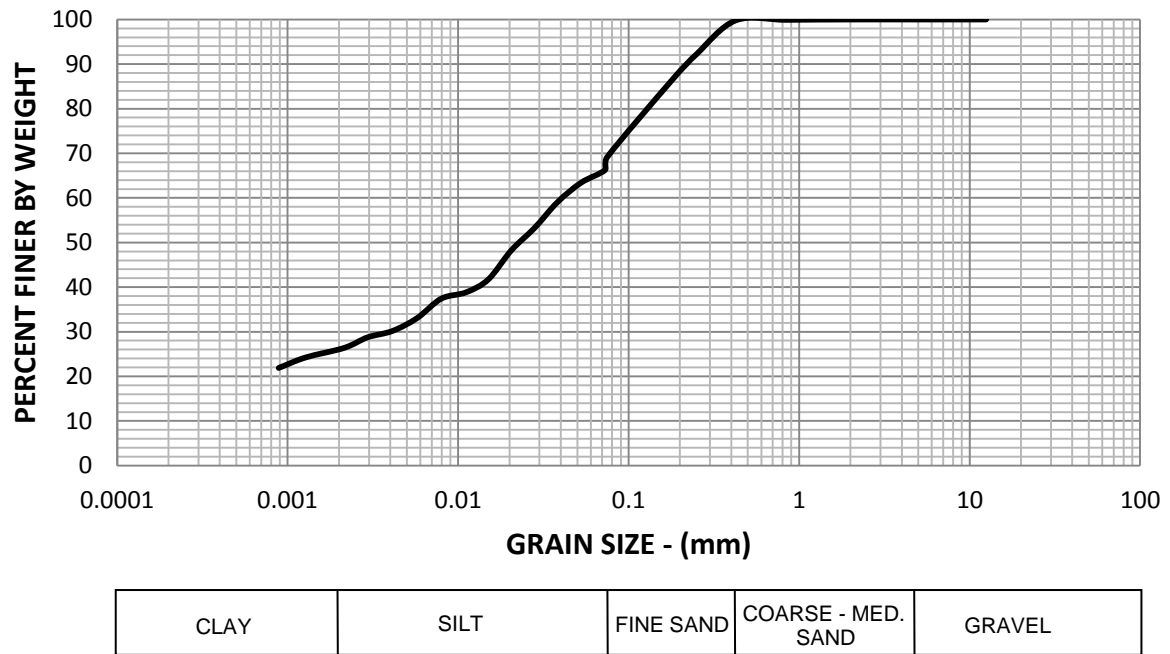
Figure B.9: Grain Size Analysis of St. Jean Baptiste

Appendix C: Phase II Grain Size Distribution

Figure C.1: Grain Size Analysis of Crescent Park

Figure C.2: Grain Size Analysis of St. Mary`s Road
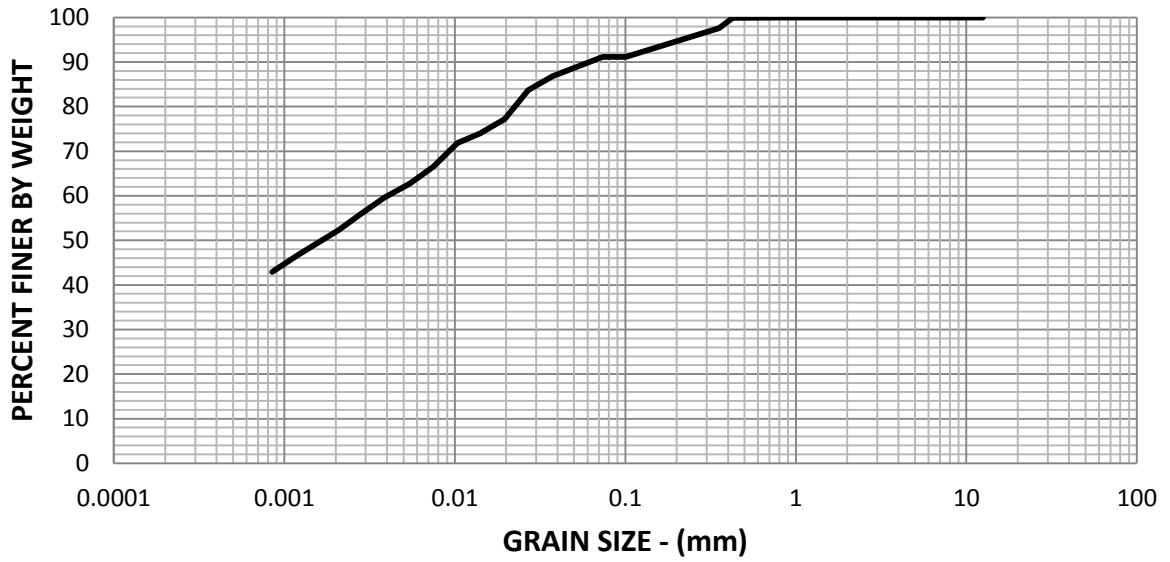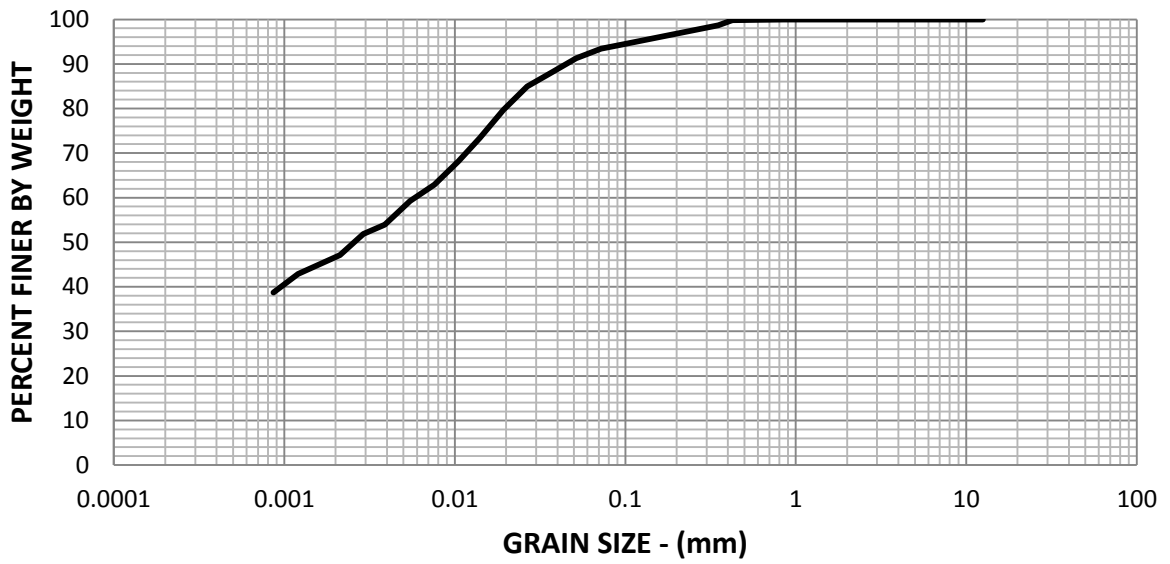
CLAY	SILT	FINE SAND	COARSE - MED. SAND	GRAVEL

Figure C.3: Grain Size Analysis of Howden Road
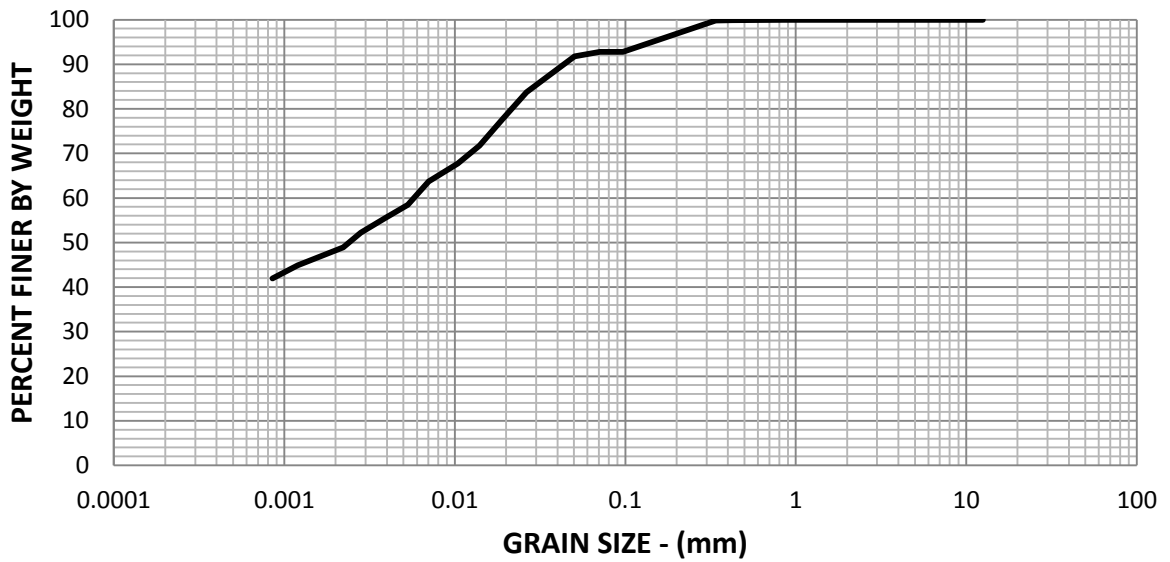
CLAY	SILT	FINE SAND	COARSE - MED. SAND	GRAVEL

Figure C.4: Grain Size Analysis of Red River Drive

118
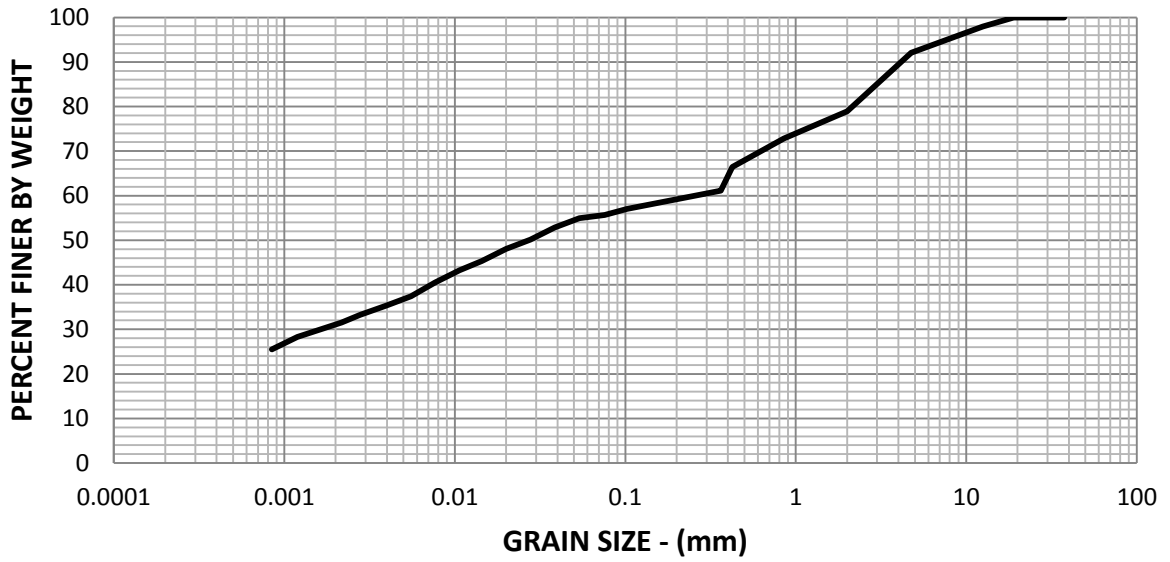
Figure C.5: Grain Size Analysis of St. Adolphe
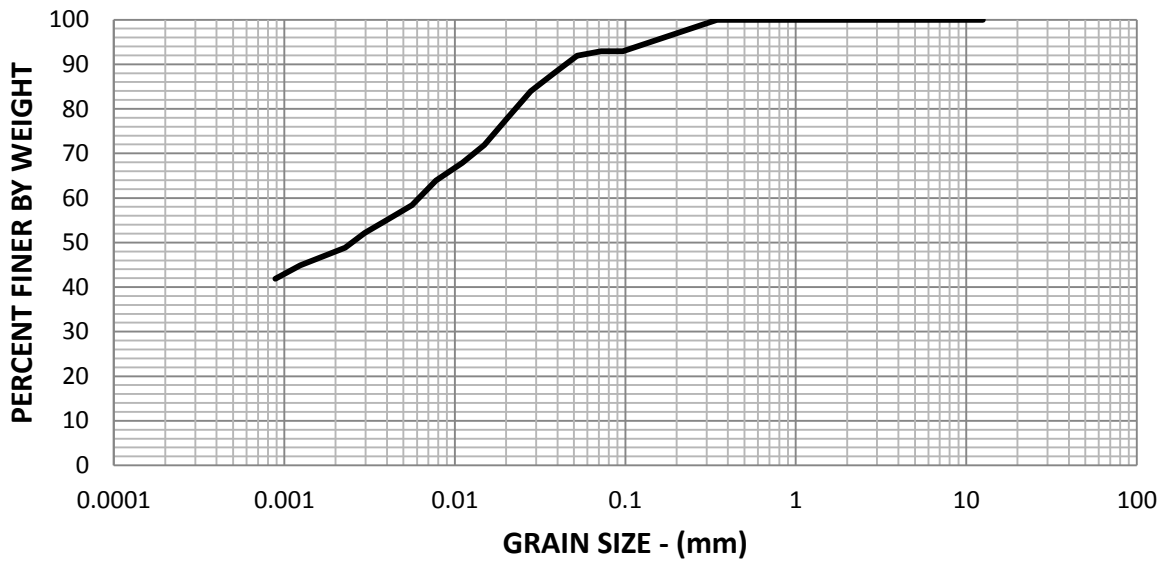
Figure C.6: Grain Size Analysis of Prefontaine Road

119
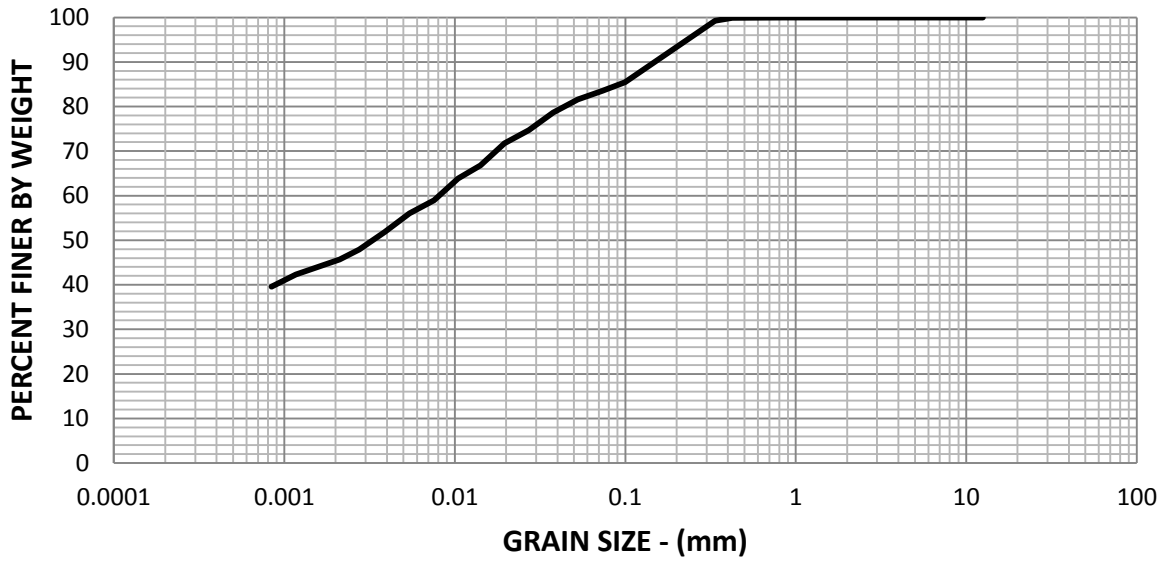
Figure C.7: Grain Size Analysis of Agriculture Canada
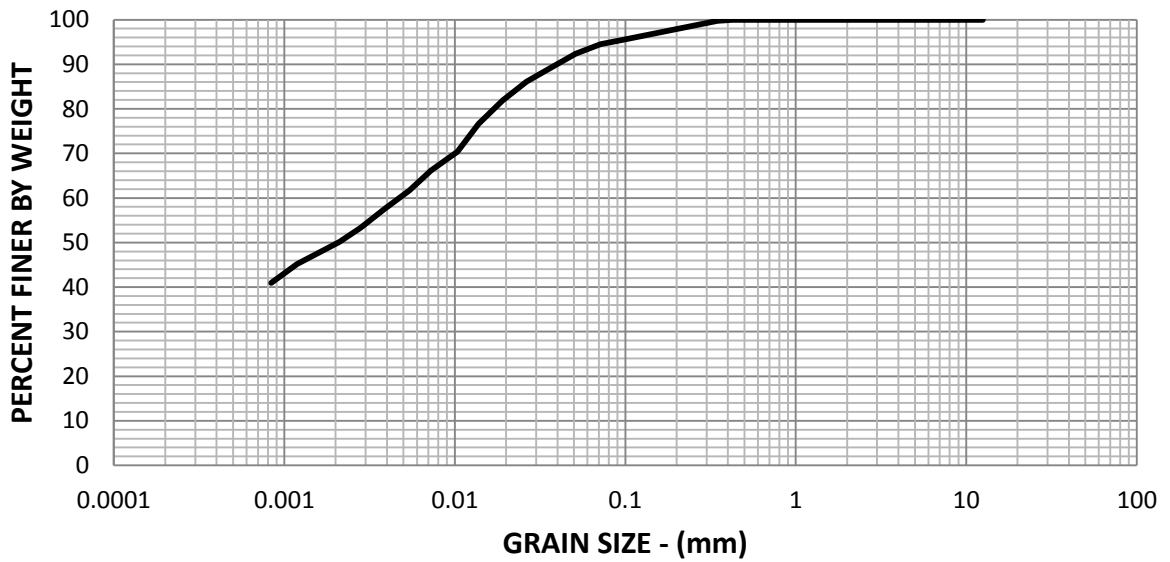
Figure C.8: Grain Size Analysis of Nolette Road

120
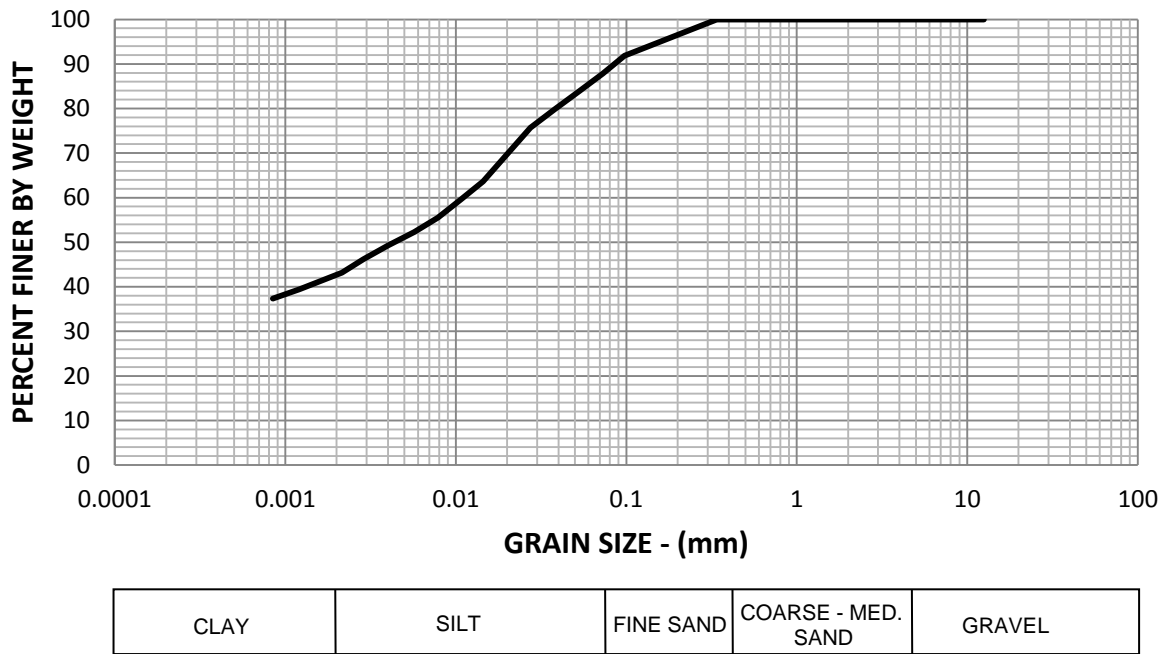
Figure C.9: Grain Size Analysis of St. Jean Baptiste

Appendix D: Grain Size Distribution of Sump Sediment
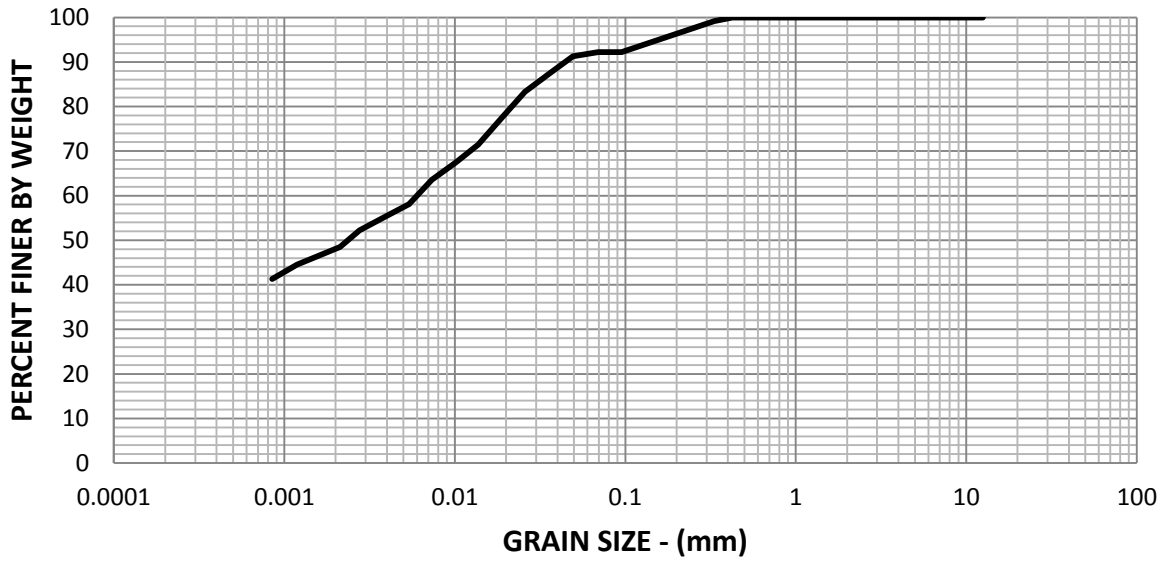
| CLAY | SILT | FINE SAND | COARSE - MED. SAND | GRAVEL |

Figure D.1: Grain Size Analysis of Return Sump after ST1
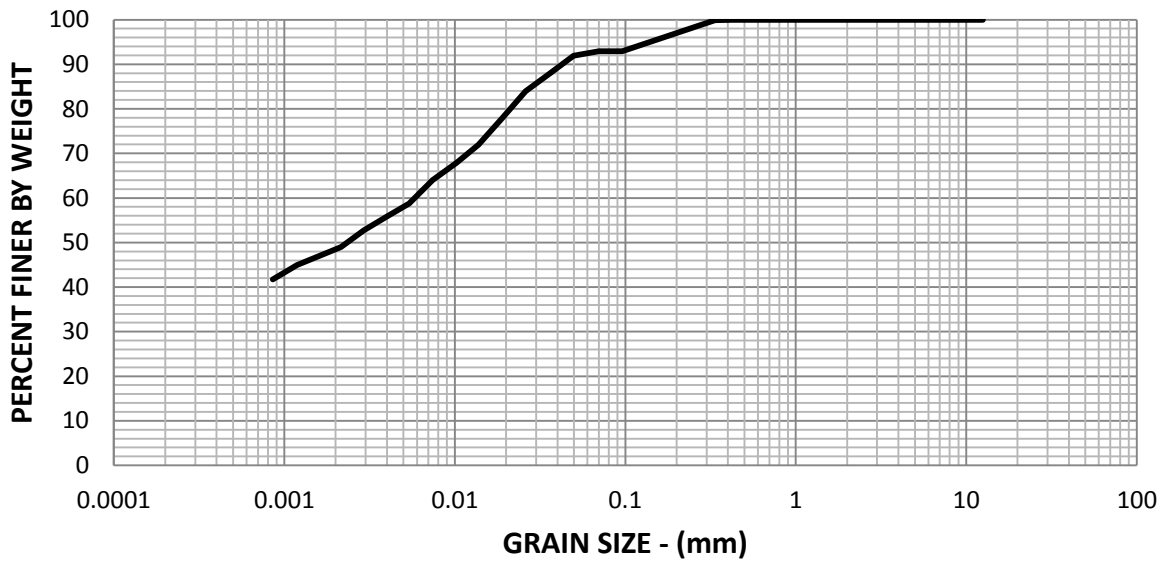
| CLAY | SILT | FINE SAND | COARSE - MED. SAND | GRAVEL |

Figure D.2: Grain Size Analysis of Intake Sump after ST1
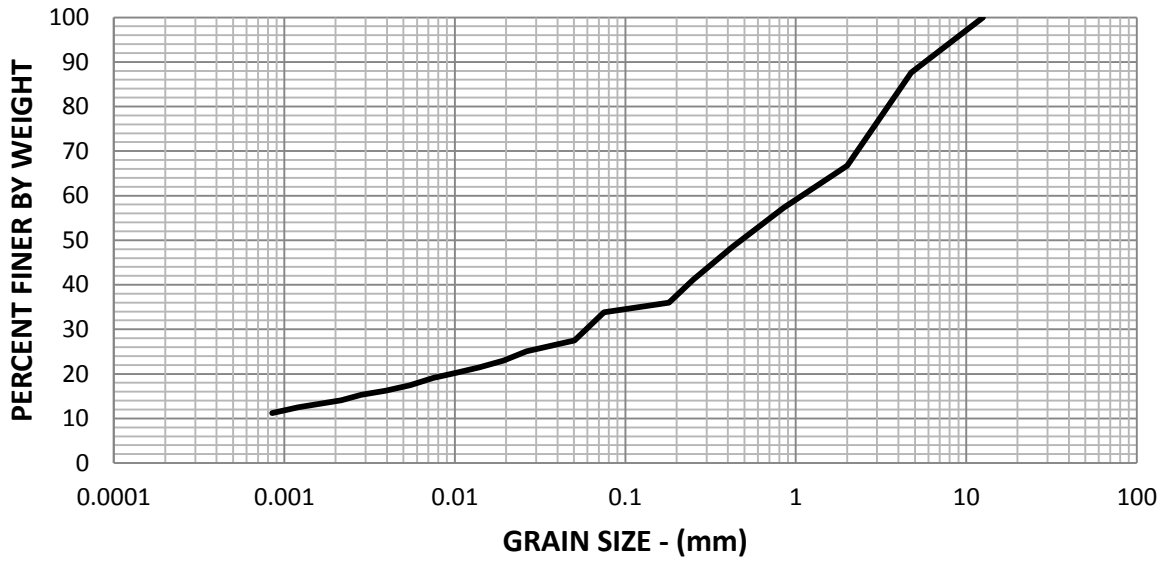
| CLAY | SILT | FINE SAND | COARSE - MED. SAND | GRAVEL |

Figure D.3: Grain Size Analysis of Return Sump after ST8
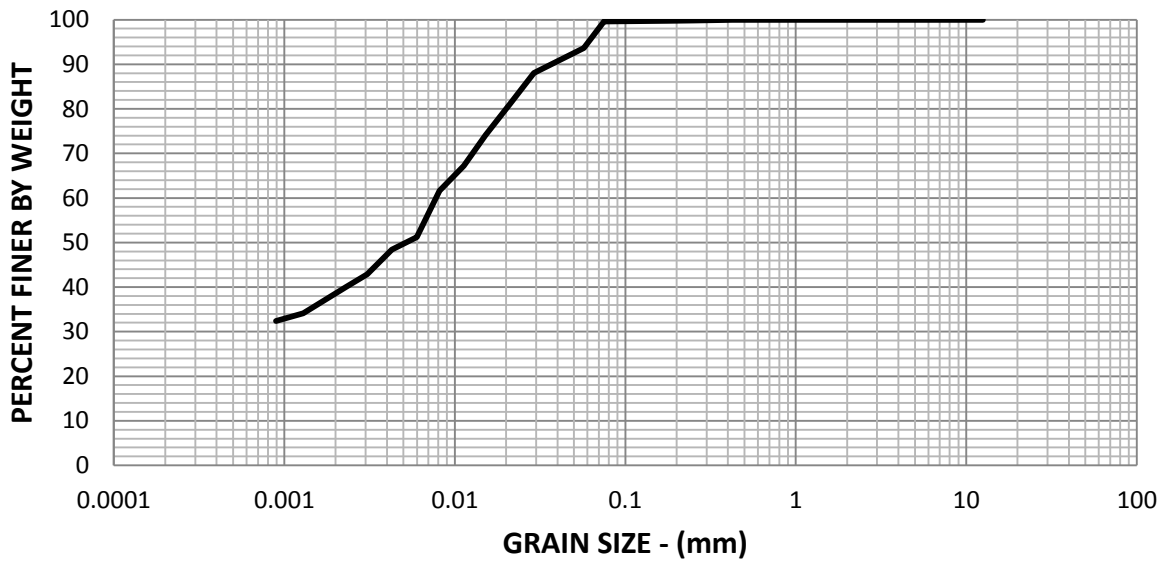
| CLAY | SILT | FINE SAND | COARSE - MED. SAND | GRAVEL |

Figure D.4: Grain Size Analysis of Intake Sump after ST8
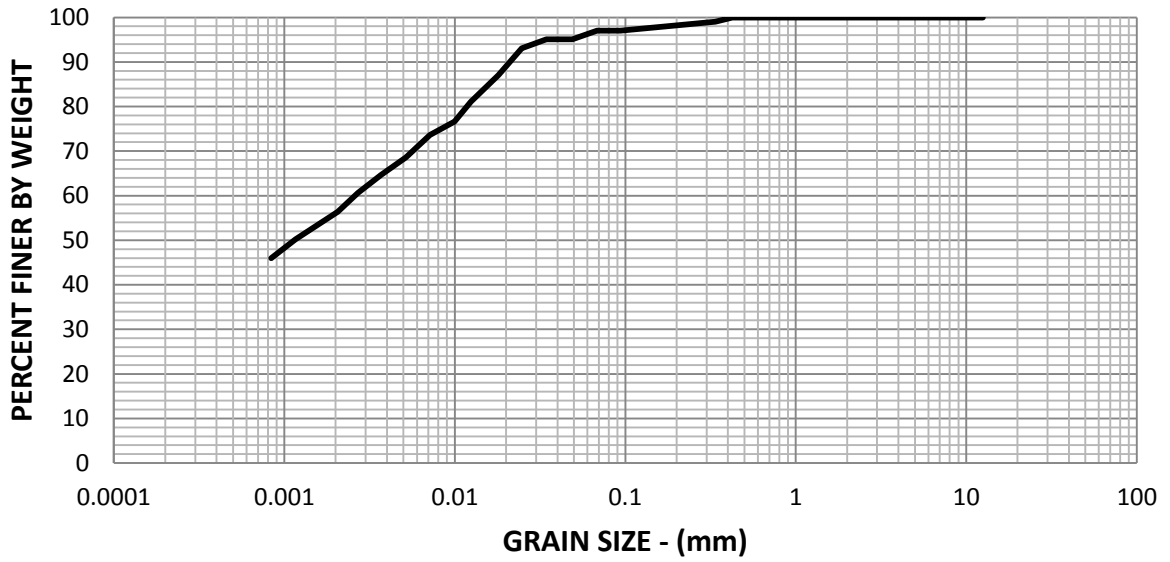
| CLAY | SILT | FINE SAND | COARSE - MED. SAND | GRAVEL |

Figure D.5: Grain Size Analysis of Return Sump after ST14
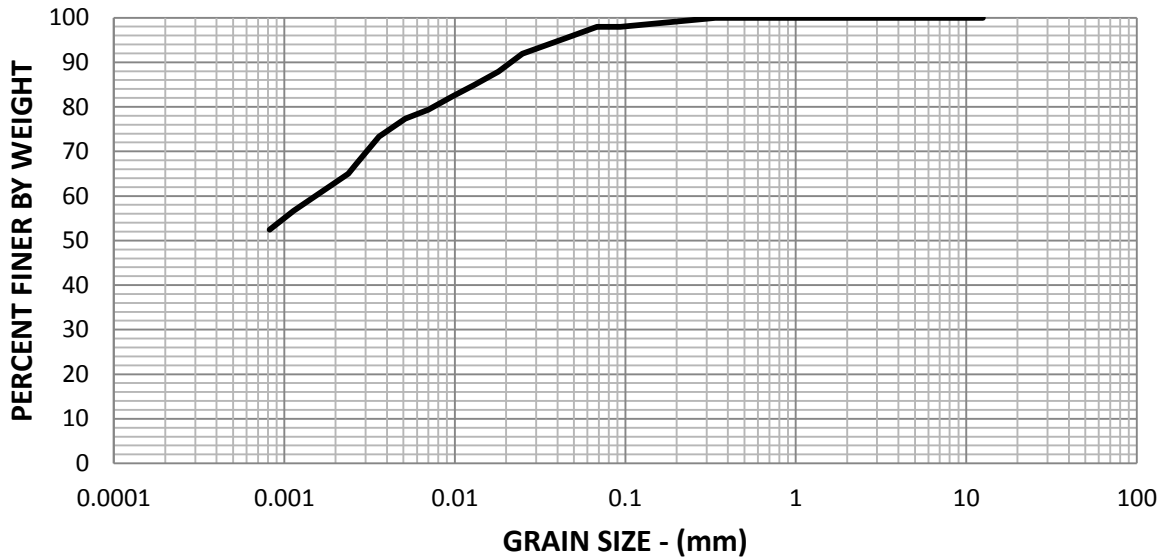
| CLAY | SILT | FINE SAND | COARSE - MED. SAND | GRAVEL |

Figure D.6: Grain Size Analysis of Intake Sump after ST14

Appendix E: Phase I Erosion Rates and Observations

Crescent Park Erosion Rate
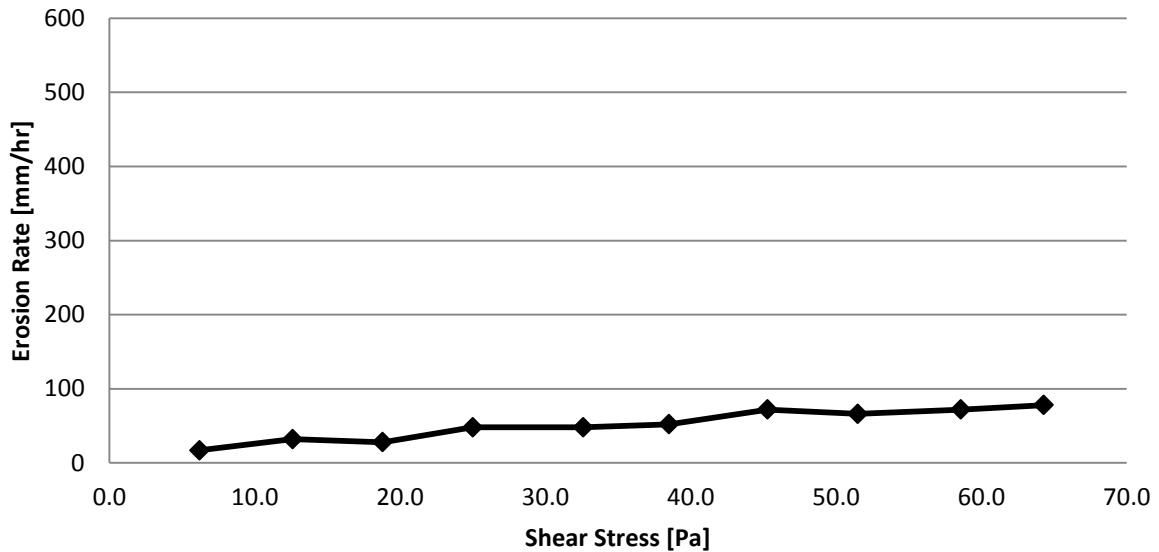
Figure E.1: Crescent Park Erosion Rate

Shear [Pa]	Erosion [mm/hr]	Observations
6.2	16.8	twig and some small roots
12.6	32	little chunks (~2mm) flying off where the twig was
18.8	28	twig still holding on barely
25.0	48	twig washed off at beginning
32.6	48	a little bit larger chunks (~4mm) being taken off
38.5	52	some roots visible
45.3	72	chucks (<5mm) eroded faster
51.5	66	chucks (<5mm) eroded faster
58.6	72	chucks (<5mm) eroded faster
64.3	78	chucks (~5mm) eroded very fast

Table E.1: Crescent Park Erosion Observation Logs

St. Mary's Road Erosion Rate
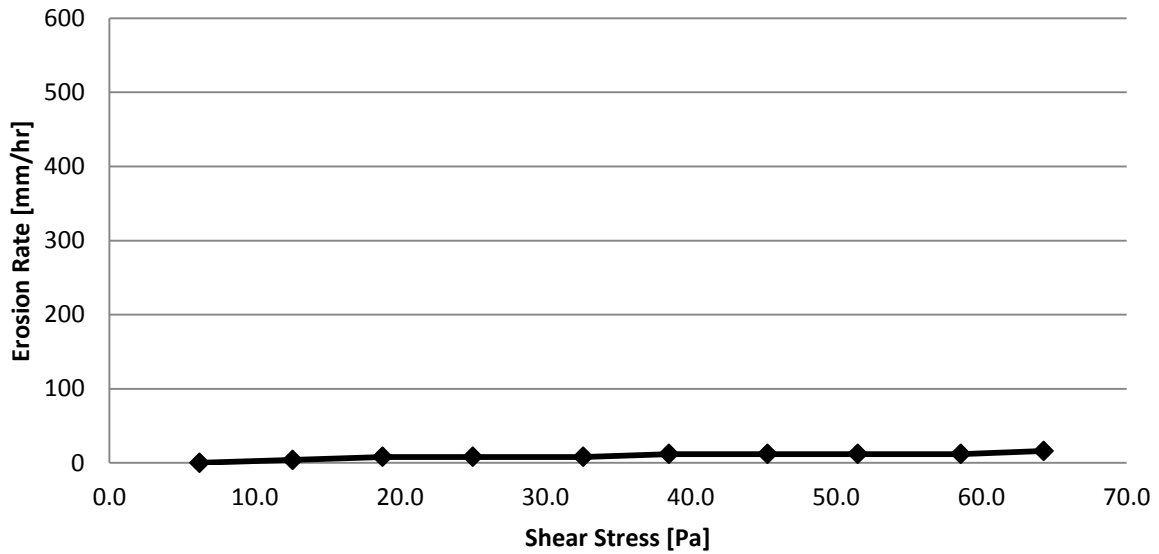
Figure E.2: St. Mary`s Road Erosion Rate

Shear [Pa]	Erosion [mm/hr]	Observations
6.2	0	lots of little roots
12.6	4	lots of little roots
18.8	8	lots of little roots
25.0	8	lots of little roots
32.6	8	lots of little roots
38.5	12	lots of little roots
45.3	12	lots of little roots
51.5	12	lots of little roots
58.6	12	lots of little roots
64.3	16	lots of little roots

Table E.2 St. Mary`s Road Erosion Observation Logs

Howden Road Erosion Rate
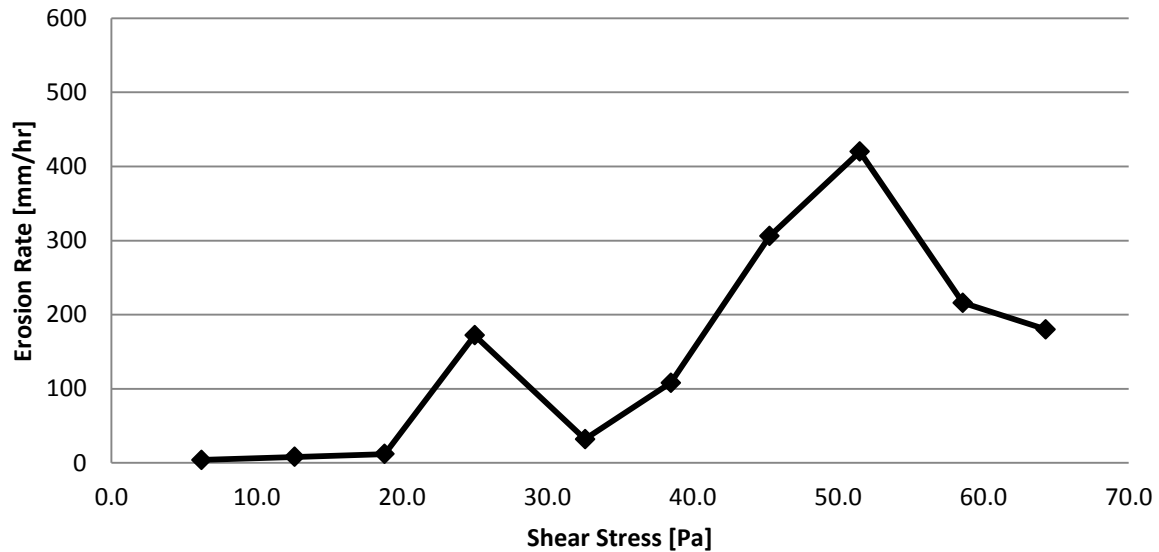
Figure E.3: Howden Road Erosion Rate

Shear [Pa]	Erosion [mm/hr]	Observations
6.2	4	few roots present
12.6	8	few roots present
18.8	12	few roots present
25.0	172	few roots present, small chunks (<2mm) eroded sometimes then big chunk (~5mm) that were held together with roots
32.6	32	not much roots
38.5	108	not much roots, chucks (<5mm) eroded
45.3	306	larger chucks (~5mm) eroded, cracks forming and taking big pieces, not much roots seen
51.5	420	large chucks (<10mm) eroded
58.6	216	large chucks (<10mm) eroded, some roots present
64.3	180	some roots present

Table E.3: Howden Road Erosion Observation Logs

Red River Drive Erosion Rate
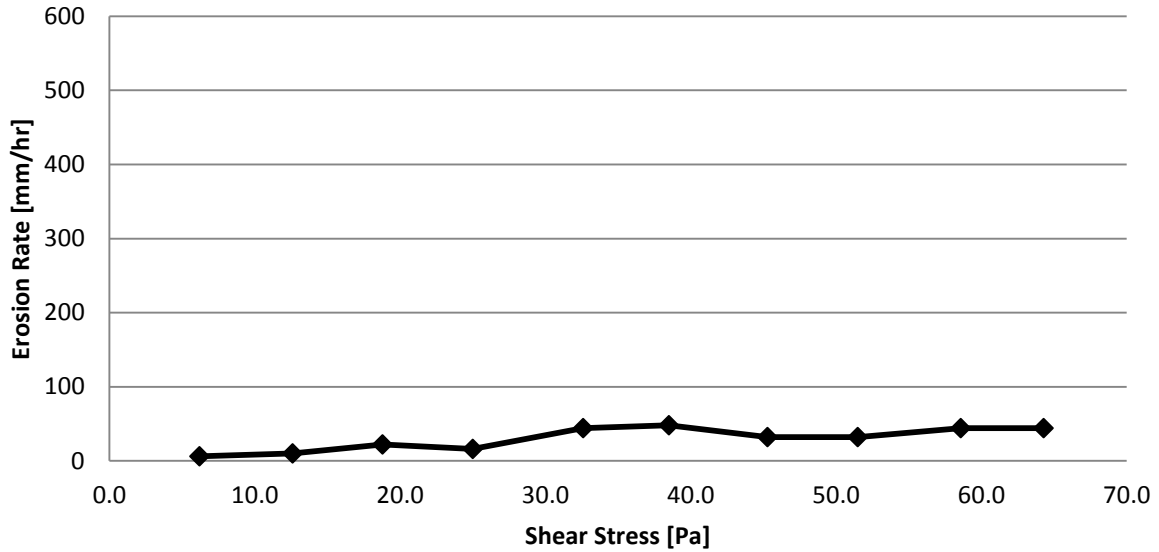
Figure E.4: Red River Drive Erosion Rate

Shear [Pa]	Erosion [mm/hr]	Observations
6.2	6	the little bit of rotten wood worn off, then scouring occurred
12.6	10	few small chunks (~2mm) eroded, bubbles were seen in sample
18.8	22	same as above
25.0	16	
32.6	44	some roots visible, chunks (<5mm) eroded
38.5	48	some roots visible, chunks (<5mm) eroded
45.3	32	small chunks (<5mm) eroded
51.5	32	bubbles visible in sample
58.6	44	very smooth texture visible through acrylic
64.3	44	smooth through acrylic with a few bubbles, medium sized twig and some roots were visible

Table E.4: Red River Drive Erosion Observation Logs

St. Adolphe Erosion Rate
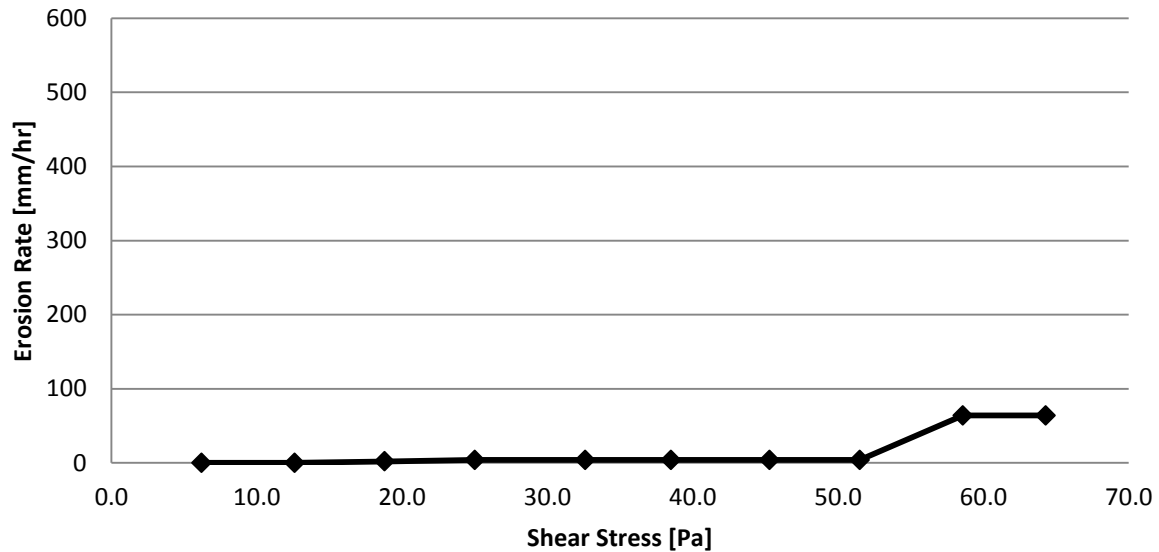
Figure E.5: St. Adolphe Erosion Rate

Shear [Pa]	Erosion [mm/hr]	Observations
6.2	0	small pebbles present (<3mm)
12.6	0	small pebbles present (<3mm)
18.8	2	pebbles present (<3mm)
25.0	4	small pebbles (<3mm) and one slightly larger (about 1cm) visible on top of sample
32.6	4	same as above, little bit of erosion from the front of specimen
38.5	4	same as above
45.3	4	same as above
51.5	4	same as above
58.6	64	larger chunks (<5mm) eroded
64.3	64	chunks and pebbles (<5mm) eroded

Table E.5: St. Adolphe Erosion Observation Logs

Prefontaine Road Erosion Rate
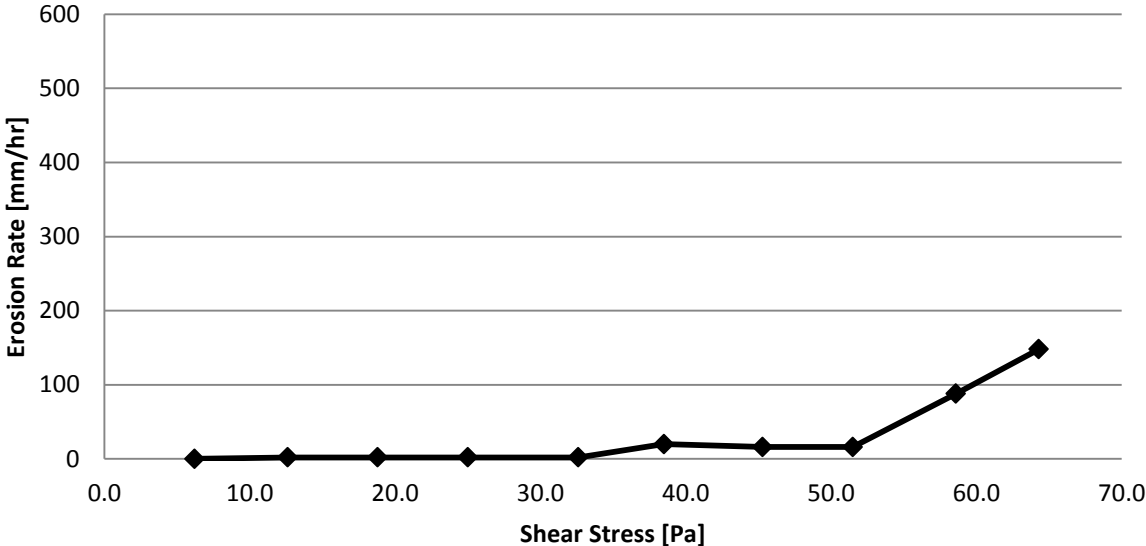
Figure E.6: Prefontaine Road Erosion Rate

Shear [Pa]	Erosion [mm/hr]	Observations
6.2	0	a couple of tiny roots visible
12.6	2	same as above
18.8	2	same as above
25.0	2	same as above
32.6	2	same as above
38.5	20	little chunks (<2mm) eroded
45.3	16	the sample seems uniform/no bubbles or cracks
51.5	16	same as above
58.6	88	little chucks (<5mm) eroded
64.3	148	chunks (<5mm) eroded

Table E.6: Prefontaine Road Erosion Observation Logs

Agriculture Canada Erosion Rate
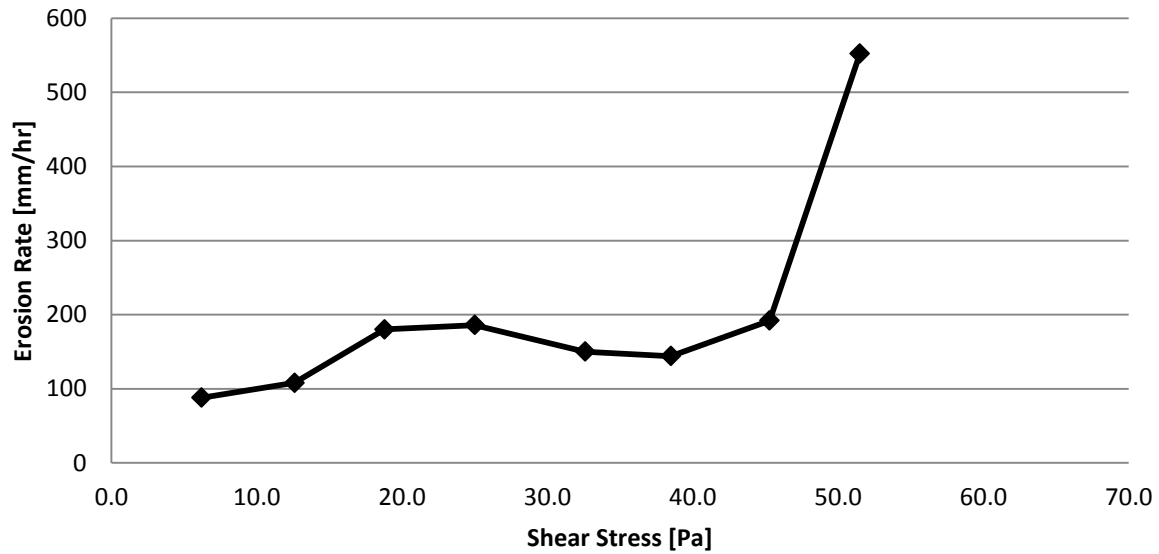
Figure E.7: Agriculture Canada Erosion Rate

Shear [Pa]	Erosion [mm/hr]	Observations
6.2	88	roots and twigs, chunks (<3mm) eroded
12.6	108	same as above
18.8	180	same as above, bigger chunks (<5mm) eroded, scouring
25.0	186	same as above
32.6	150	same as above
38.5	144	sample more uniform and solid through acrylic, no scouring
45.3	192	same as above
51.5	552	same as above with scouring, large pieces (5-7mm), bubble and roots visible

Table E.7: Agriculture Canada Erosion Observation Logs

Nolette Road Erosion Rate
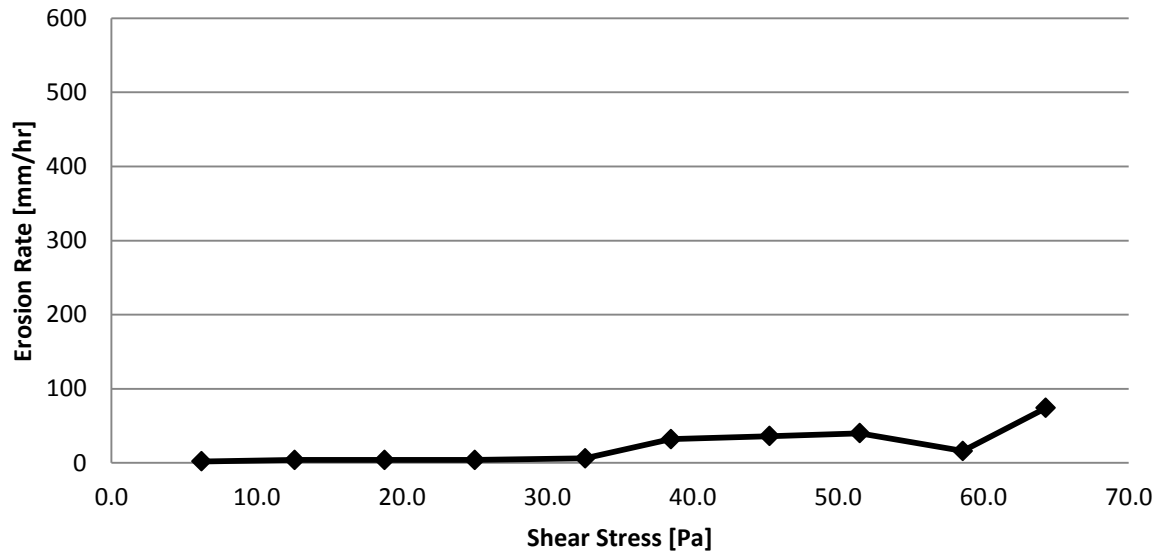
Figure E.8: Nolette road Erosion Rate

Shear [Pa]	Erosion [mm/hr]	Observations
6.2	2	
12.6	4	
18.8	4	
25.0	4	
32.6	6	
38.5	32	little chucks (<3mm) eroded, bubbles and/or cracks in the sample
45.3	36	looked smooth and uniform under the flume
51.5	40	same as above
58.6	16	same as above, larger roots visible
64.3	74	same as above

Table E.8: Nolette Road Erosion Observation Logs

St. Jean Baptiste Erosion Rate
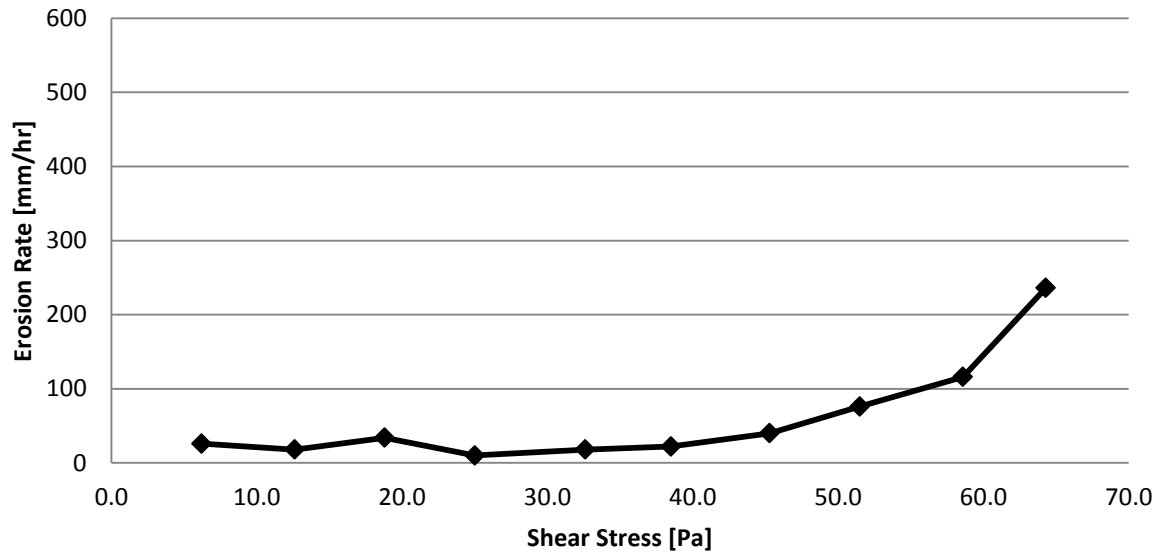
Figure E.9: St. Jean Baptiste Erosion Rate

Shear [Pa]	Erosion [mm/hr]	Observations
6.2	26	big chunk (<5mm) eroded (may have had a crack there or bubble)
12.6	18	same as above
18.8	34	some small chunks (<3mm) eroded
25.0	10	looks smooth and uniform through acrylic, with little to no organics and bubbles
32.6	18	same as above, some roots visible
38.5	22	same as above, some roots visible
45.3	40	same as above, some roots visible
51.5	76	same as above, scouring (front)
58.6	116	same as above
64.3	236	looks smooth through acrylic, big chunks (~5mm) and scouring

Table E.9: St. Jean Baptiste Erosion Observation Logs

Appendix F: Phase II Erosion Rates and Observations
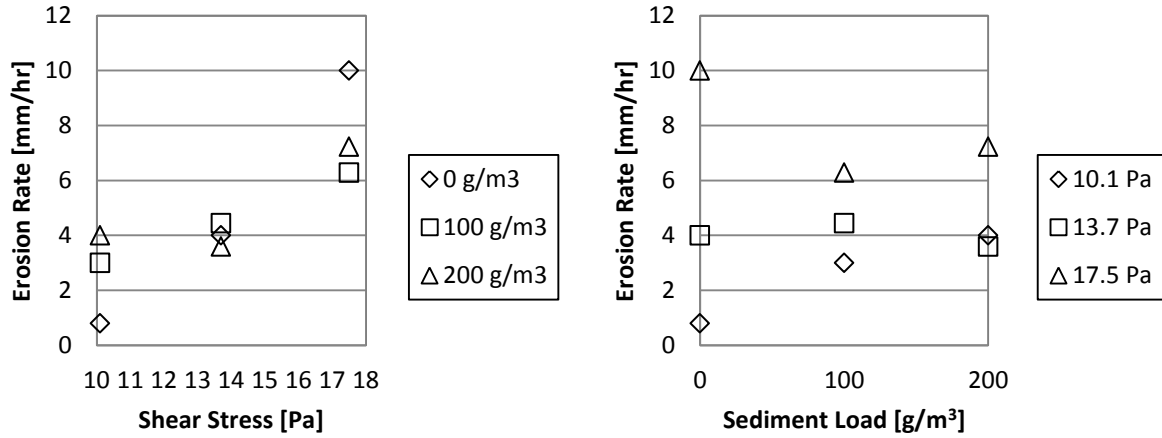
Figure F.1: ST1 Crescent Park Erosion Rates

Shear Stress	Sediment Load [g/m^3]		
[Pa]	0	100	200
10.1	Some roots, eroding very slowly, fine particles eroded (<<1mm).	Some roots, eroding very slowly, fine particles eroded (<<1mm).	Some roots, eroding very slowly, fine particles eroded (<<1mm), larger roots visible (~1mm).
13.7	Couple of big roots (<0.5mm) and some fine roots.	Some small roots, erosion occurring mostly in the center of sample, particles eroded (~1mm). Erosion was slower on the second half, mostly on front and center of sample, the sides eroded slower, maybe due to some roots being present in those sections.	Some roots. Some bubbles seen through acrylic which may cause big pieces to be eroded once the sample is pushed up further.
17.5	A big root (~0.5mm) and some fine roots. Larger particles getting eroded (1 to 2 mm).	Some small roots. A big piece eroded off the center 30 minutes into testing (~3cm in width, <1cm thickness). Bubbles visible through acrylic which may cause big pieces to be eroded as soon as the sample is pushed further up.	Bubbles visible through acrylic. 15 minutes in bubbles gave way and a large piece was eroded (<1cm). Roots visible. Not many large pieces were visible to be eroding, most likely it was particle by particle.

Table F.1: ST1 Crescent Park Erosion Observations

Figure F.2: ST4 St. Mary's Road Erosion Rates

Shear Stress	Sediment Load [g/m³]		
[Pa]	0	100	200
10.1	Very fractured. Lots of roots. Very fast erosion.	Large particles getting eroded. Less fractured material. Still full of roots.	Sample is looking more uniform and less fractured, and erosion rate seems to be decreasing because of it.
13.7	SKIPPING THIS SHEAR DUE TO NOT HAVING ENOUGH SAMPLE, THEREFORE COVERING THE TWO HIGH AND LOWER SHEARS.	SKIPPING THIS SHEAR DUE TO NOT HAVING ENOUGH SAMPLE, THEREFORE COVERING THE TWO HIGH AND LOWER SHEARS.	SKIPPING THIS SHEAR DUE TO NOT HAVING ENOUGH SAMPLE, THEREFORE COVERING THE TWO HIGH AND LOWER SHEARS.
17.5	Sample doesn't look as fractured. Still full of roots.	Sample is looking more uniform and less fractured, and erosion rate seems to be decreasing because of it.	Sample is looking more uniform and less fractured.

Table F.2: ST4 St. Mary's Road Erosion Observations

Figure F.3: ST6 Howden Road Erosion Rates

Shear Stress	Sediment Load [g/m³]		
[Pa]	0	100	200
10.1	Some fine roots visible. Virtually no erosion.	Some fine roots visible.	Some fine roots visible.
13.7	Some fine roots visible. Some small particle getting eroded slowly (<1mm).	Some fine roots visible. Some small particles being eroded (<1mm).	Some fine roots visible. Some larger particles (<1mm thick and <5mm wide).
17.5	Some fine roots visible. Very little erosion in front side of sample.	Some fine roots visible. Some small particles being eroded (<<1mm).	Some fine roots visible.

Table F.3: ST6 Howden Road Erosion Observations
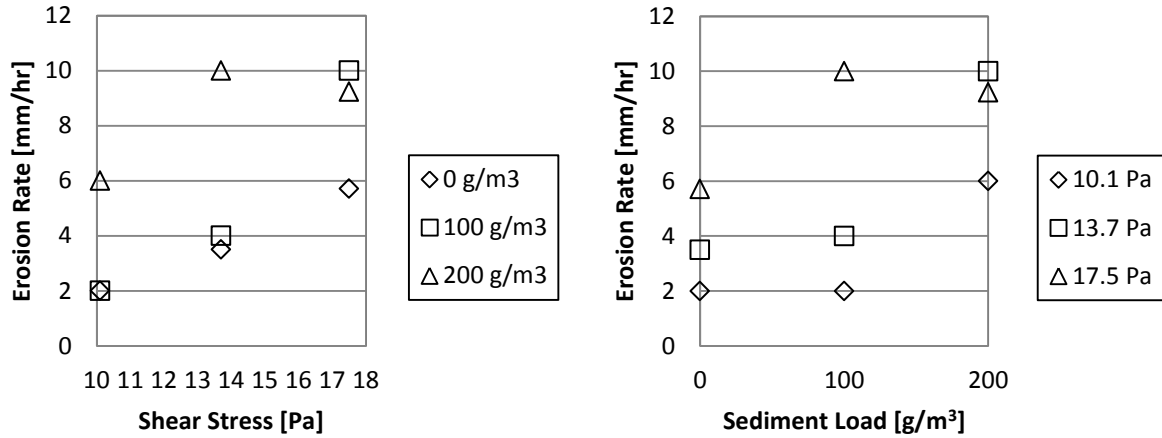
Figure F.4: ST14 Red River Drive Erosion Rates

Shear Stress	Sediment Load [g/m³]		
[Pa]	0	100	200
10.1	Fine sands present with some roots, rotten twigs and organics. Most of erosion occurring in front of sample. Small particles eroding (~1mm), sometimes up to 1cm. Sample has fractures that become visible as it is eroding and the particles taken off are mostly at these fracture points.	Fine sands present with some roots, rotten twigs and organics. Small particles eroding (~1mm). Sample has fractures that become visible as it is eroding and the particles taken off are mostly at these fracture points. Twig about 3 or 4 mm thick.	Fine sands present with some roots, rotten twigs and organics. Small particles eroding (~1mm), sometimes up to 1cm. Sample has fractures that become visible as it is eroding and the particles taken off are mostly at these fracture points. Some scouring in the front of sample.
13.7	Fine sands present with some roots, rotten twigs and organics. Small particles eroding (~1mm), sometimes up to 1cm. Sample has fractures that become visible as it is eroding and the particles taken off are mostly at these fracture points.	Fine sands present with some roots, rotten twigs and organics. Small particles eroding (~1mm). Sample has fractures that become visible as it is eroding and the particles taken off are mostly at these fracture points. Twig about 3 or 4 mm thick.	Fine sands present with some roots, rotten twigs and organics. Small particles eroding (~1mm), sometimes up to 1cm. Sample has fractures that become visible as it is eroding and the particles taken off are mostly at these fracture points. Some scouring in the front of sample.
17.5	Fine sands present with some roots, rotten twigs and organics. Small particles eroding (~1mm), sometimes up to 1cm. Sample has fractures that become visible as it is eroding and the particles taken off are mostly at these fracture points. More large particles (~1cm) eroding. 30minutes in some large particles eroded (2 to 3cm).	Fine sands present with some roots, rotten twigs and organics. Small particles eroding (~1mm). Sample has fractures that become visible as it is eroding and the particles taken off are mostly at these fracture points. The eroded particles are larger (~5mm in width). At around 45 minutes a large particle off the back of sample was eroded (~5mm deep, 1 to 2 cm wide) there was a twig there (~7mm, sitting sideways under the particle that was eroded). More and more particles came off the same spot along the twig that was under laying that side of the sample.	Fine sands present with some roots, rotten twigs and organics. Small particles eroding (~1mm), sometimes up to 1cm. Sample has fractures that become visible as it is eroding and the particles taken off are mostly at these fracture points. Not as many roots visible. The sample doesn't look as silty/sandy. Less fractured and flaking of the sample observed. May reduce erosion rate.

Table F.4: ST14 Red River Drive Erosion Observations

140
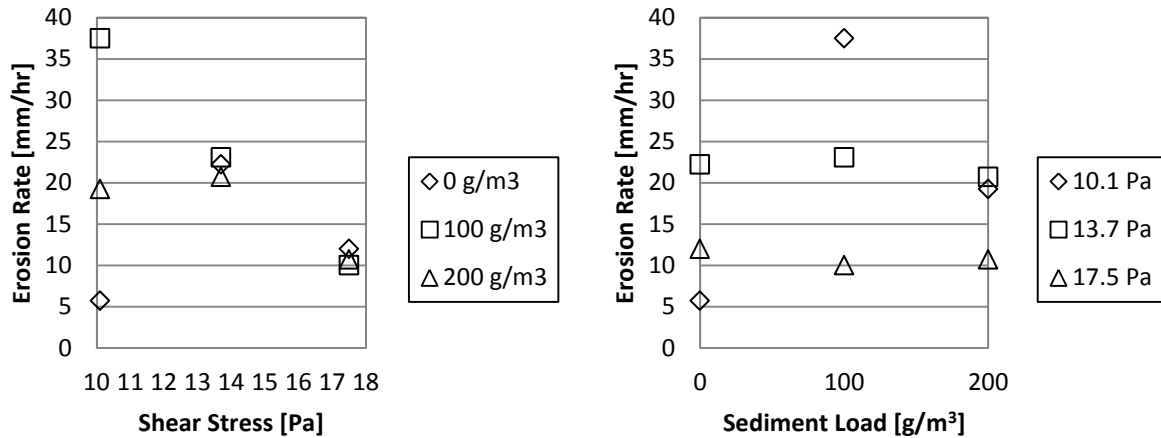
Figure F.5: ST8 St. Adolphe Erosion Rates

Shear Stress	Sediment Load [g/m³]		
[Pa]	0	100	200
10.1	Lots of sands and small pebbles (3 to 4 mm), some larger rocks visible through sample (>1.5cm), mostly fine and small particles (<1mm) eroding, sometimes larger pieces are eroded (2 to 3mm). As fine material is eroded the larger pebbles are exposed allowing them to be eroded afterwards. Erosion was slower at first while removing fine sediments (cohesive soils) to expose rocks, and then it was faster as the larger rocks/pebbles were eroded.	Larger pebbles visible. As they were eroded bigger gaps appeared which also caused more turbulence and more scouring.	Some large rocks present (<2cm), erosion of the large rocks leave big gaps that cause scouring.
13.7	Lots of pebbles (1mm to 1cm). Cohesive soils being eroded quick around the rocks and then the rocks get eroded. Some larger rocks visible (>1cm). 1 or 2 tiny roots visible.	More cohesive soils visible, which would make erosion slower. One big rock (~1.5 cm) that was eroded and caused a big hole in the sample surface.	More cohesive soil visible. A big rock (<2.5 cm) present throughout testing. Big rock washed away @ 16.5 minutes into testing.
17.5	Many little pebbles (1 to 3mm) and some larger ones (1 to 2cm). The cohesive soils are also being eroded more in larger pieces (1 to 2 mm). Occasional roots visible (very thin) (~0.5mm).	Some small pebbles (1 to 2mm) and some larger ones visible (1 to 1.5cm). More cohesive soils visible.	Some small (1 to 2mm) and medium (~0.5 cm) pebbles. The larger pebbles (~5mm) getting eroded faster. Cohesive soils are also being eroded more in blocks.

Table F.5: ST8 St. Adolphe Erosion Observations

Figure F.6: ST10 Prefontaine Road Erosion Rates

Shear Stress	Sediment Load [g/m^3]		
[Pa]	0	100	200
10.1	Fine roots present, some organics and rotten twigs (~3mm).	Fine roots present. Once in a while small particles are eroded (<0.5mm). Most of erosion occurring in front of the sample.	Fine roots present. Small particles eroded (<1mm).
13.7	Fine roots present. Not much erosion, mostly in front of the sample. Around the 50 minute mark some particles were eroded (<0.5mm thick and 3 to 5 mm wide), some of these were taken from the center of the sample surface where the brown colouring of a rotten twig was visible.	Fine roots present. Most of erosion occurring in front of the sample. Some small particles eroding (<1mm).	Roots present. Small particles eroded (<1mm). Most of erosion occurring at center of sample surface.
17.5	Fine roots present. Particles are eroding faster (mostly <0.5mm), scouring occurring. Most of erosion on the front of sample surface.	Fine roots present. Some larger particles eroding (<0.5mm thickness, <5mm width).	Roots present. Small particles eroded (~1mm). Twigs visible (~5mm).

Table F.6: ST10 Prefontaine Road Erosion Observations
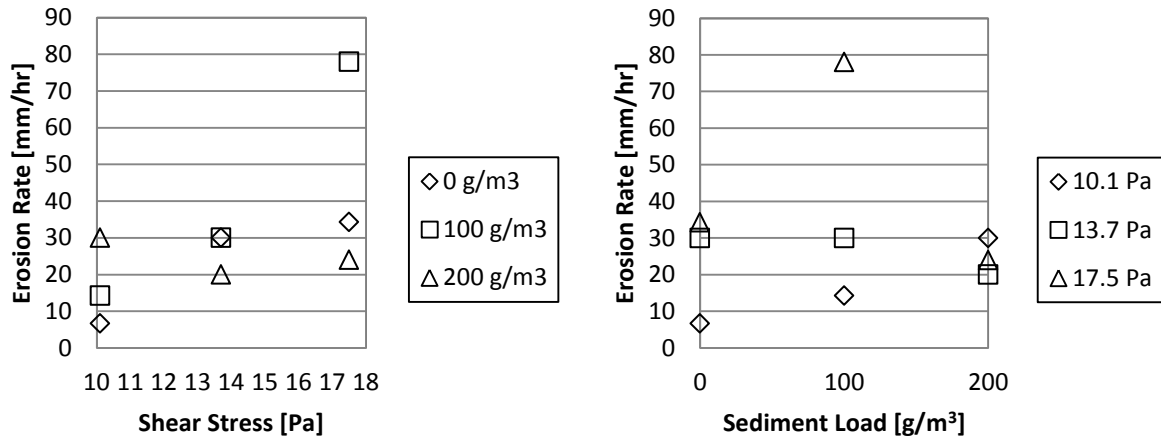
Figure F.7: ST16 Agriculture Canada Erosion Rates

Shear Stress	Sediment Load [g/m³]		
[Pa]	0	100	200
10.1	Lots of fine roots and some organics (twigs). Particles being eroded (1 to 2 mm). Back end of sample seems to have more sandy soil which was eroded initially (it had lots of roots in it, which made it not erode as fast as if it didn't). Sometimes the particles that were eroded were up to 1cm.	Lots of fine roots and some organics (twigs). Small particles eroding (<1mm).	Lots of fine roots and some organics (twigs).
13.7	Lots of fine roots and some organics (twigs). Multiple scouring occurring along surface.	Lots of fine roots and some organics (twigs). Less sand than previous increment.	Lots of fine roots and some organics (twigs). Some clayey soil visible on one side of the sample surface causing bulging. Lots of roots of all sizes as thick as 3mm.
17.5	Lots of fine roots and some organics (twigs). Lots of roots that are holding on to the soil.	Lots of fine roots and some organics (twigs). Larger particles eroding. May have encountered a sand seem, which made the erosion faster.	Lots of fine roots and some organics (twigs). Clayey soil on one side causing another bulge to remain as the sample is extruded. Lots of roots of all sizes as thick as 3mm.

Table F.7: ST16 Agriculture Canada Erosion Observations

Figure F.8: ST11 Nolette Road Erosion Rates

Shear Stress	Sediment Load [g/m³]		
[Pa]	0	100	200
10.1	Some fine roots present along with very few twigs/rotten organics. Initially some particles (flakes) (~5mm wide and <1mm thick) were eroded from the front edges of the sample. Not much erosion after the initial particles was eroded.	Some fine roots present along with very few twigs/rotten organics. Particles eroding on the back/side of the sample surface.	Looks more uniform clay, some fine roots. Not much erosion.
13.7	Some fine roots present along with very few twigs/rotten organics.	Some fine roots present along with very few twigs/rotten organics. Some particles eroding on the side. Looks siltier. Some gravel (~1mm) visible through acrylic. About 80 minutes in test a big particle from back side was eroded, most likely due to the little gravels/pebbles/sand. Also gaps visible in sample through acrylic.	Looks more uniform clay, some fine roots. Most of erosion along central track of sample. No fractures or bubbles visible through acrylic, which could mean that the sample is strong and may not erode as much.
17.5	Some fine roots present along with very few twigs/rotten organics. Sometimes small particles seen to be eroding (1 or 2mm).	Sample looks more clayey than silty and eroding slower. Particles are sometimes seen to be eroded (1 to 2mm).	Looks more uniform clay, some fine roots. No fractures or bubbles visible through acrylic, which could mean that the sample is strong and may not erode as much.

Table F.8: ST11 Nolette Road Erosion Observations
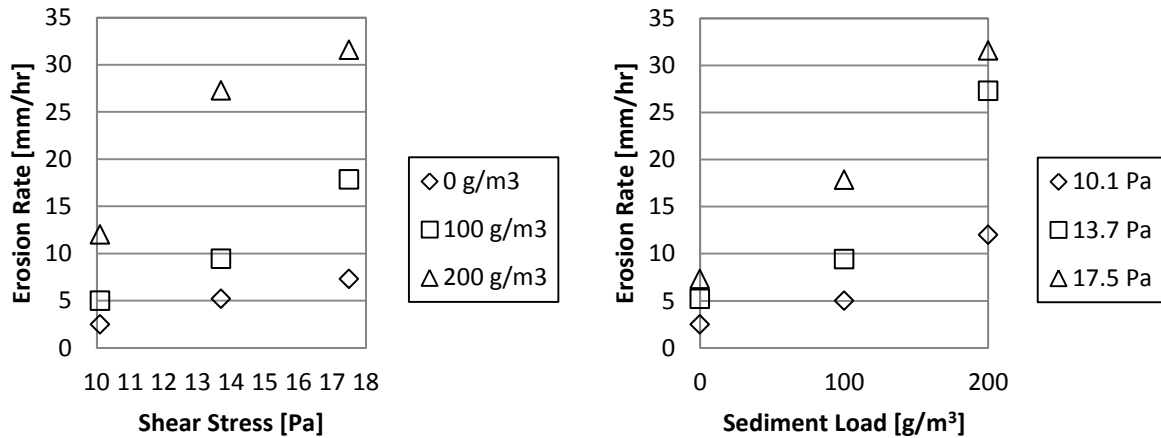
Figure F.9: ST17 St. Jean Baptiste Erosion Rates

Shear Stress	Sediment Load [g/m^3]		
[Pa]	0	100	200
10.1	Looks silty, some organics (rotten twigs) fine roots visible. Particles eroding (1 to 2mm) in flakes. Fine material also being eroded (<<1mm).	Looks silty, some organics (rotten twigs) fine roots visible. Particles eroding (1 to 2mm) in flakes. Fine material also being eroded (<<1mm). Most of erosion is on the back end of the sample surface, leaving a little mount in the front. This was due to a twig that was holding on. It was eroded at the end of the testing.	Looks silty, some organics (rotten twigs) fine roots visible. Particles eroding (1 to 2mm) in flakes. Fine material also being eroded (<<1mm).
13.7	Looks silty, some organics (rotten twigs) fine roots visible. Particles eroding (1 to 2mm) in flakes. Fine material also being eroded (<<1mm).	Looks silty, some organics (rotten twigs) fine roots visible. Particles eroding (1 to 2mm) in flakes. Fine material also being eroded (<<1mm).	Looks silty, some organics (rotten twigs) fine roots visible. Particles eroding (1 to 2mm) in flakes. Fine material also being eroded (<<1mm). More twigs visible, which is increasing erosion rate due to the soil slipping off the twigs surroundings.
17.5	Looks silty, some organics, fine roots visible. Particles eroding (1 to 2mm) in flakes. Fine material also being eroded (<<1mm). Erosion seems faster (both small and large particles). At this level there doesn't seem to be any rotten twigs visible, which was causing some of the flaking previously.	Looks silty, some organics (rotten twigs) fine roots visible. Particles eroding (1 to 2mm) in flakes. Fine material also being eroded (<<1mm).	Looks silty, some organics (rotten twigs) fine roots visible. Particles eroding (1 to 2mm) in flakes. Fine material also being eroded (<<1mm). More twigs visible, which is increasing erosion rate due to the soil slipping off the twigs surroundings. One side with some roots is not eroding as much as the rest resulting in a little bulge.

Table F.9: ST17 St. Jean Baptiste Erosion Observations

145

Appendix G: Hydrograph and Sensor Data for Red River Drive

Figure G.1: Red River Drive Upper Bank Piezometer Data (used with permission from KGS Group April 8th 2013)

Figure G.2: Red River Drive MidBank Piezometer Data (used with permission from KGS Group April 8th 2013)

Figure G.3: Red River Drive Lower Bank Piezometer Data (used with permission from KGS Group April 8th 2013)

Appendix H: Shear Stress and Erosion Calculations of Natural Condition Flood

day	spring flood1	h	area	wet perm	R	τ_{max2}	erosion at toe ė (mm/hr)	0 / 223.2	0.5 / 223.7	1 / 224.2	1.5 / 224.7	2 / 225.2	2.5 / 225.7	3 / 226.2	3.5 / 226.7	4 / 227.2	4.5 / 227.7	5 / 228.2	5.5 / 228.7
1	225.34	2.141	289.035	150.281	1.923	3.50	1.2	0.029	0.023	0.016	0.009	0.002							
2	225.35	2.150	290.422	150.412	1.931	3.51	1.2	0.030	0.023	0.016	0.009	0.002							
3	225.38	2.183	295.303	150.871	1.957	3.56	1.3	0.031	0.024	0.017	0.010	0.003							
4	225.43	2.232	302.671	151.561	1.997	3.63	1.4	0.034	0.026	0.019	0.011	0.003							
5	225.51	2.312	314.817	152.693	2.062	3.75	1.5	0.037	0.029	0.021	0.013	0.005							
6	225.65	2.450	335.981	154.645	2.173	3.95	1.8	0.043	0.034	0.026	0.017	0.008							
7	225.84	2.642	365.831	157.357	2.325	4.23	2.2	0.052	0.042	0.032	0.022	0.013	0.003						
8	226.02	2.820	393.992	159.874	2.464	4.49	2.5	0.059	0.049	0.038	0.028	0.017	0.007						
9	227.00	3.798	556.683	173.708	3.205	5.83	4.2	0.100	0.087	0.074	0.061	0.048	0.034	0.021	0.008				
10	227.76	4.559	692.622	184.478	3.754	6.83	5.4	0.131	0.116	0.102	0.088	0.073	0.059	0.045	0.030	0.016			
11	228.33	5.134	800.519	192.601	4.156	7.56	6.4	0.153	0.138	0.123	0.108	0.093	0.078	0.064	0.049	0.034	0.019	0.004	
12	228.66	5.457	863.200	197.167	4.378	7.97	6.9	0.165	0.150	0.135	0.120	0.105	0.090	0.074	0.059	0.044	0.029	0.014	
13	228.80	5.603	892.037	199.233	4.477	8.15	7.1	0.171	0.156	0.140	0.125	0.110	0.095	0.079	0.064	0.049	0.034	0.018	0.003
14	228.86	5.656	902.564	199.982	4.513	8.21	7.2	0.173	0.157	0.142	0.127	0.112	0.096	0.081	0.066	0.051	0.035	0.020	0.005
15	228.85	5.646	900.577	199.841	4.506	8.20	7.2	0.172	0.157	0.142	0.127	0.111	0.096	0.081	0.066	0.050	0.035	0.020	0.004
16	228.80	5.601	891.624	199.203	4.476	8.15	7.1	0.171	0.155	0.140	0.125	0.110	0.094	0.079	0.064	0.049	0.034	0.018	0.003
17	228.70	5.505	872.706	197.850	4.411	8.03	7.0	0.167	0.152	0.137	0.122	0.106	0.091	0.076	0.061	0.046	0.030	0.015	
18	228.54	5.343	841.060	195.566	4.301	7.83	6.7	0.161	0.146	0.131	0.116	0.101	0.086	0.071	0.056	0.040	0.025	0.010	
19	228.27	5.068	787.964	191.673	4.111	7.48	6.3	0.150	0.136	0.121	0.106	0.091	0.076	0.061	0.047	0.032	0.017	0.002	
20	227.91	4.715	721.338	186.674	3.864	7.03	5.7	0.137	0.122	0.108	0.093	0.079	0.064	0.050	0.035	0.021	0.006		
21	227.49	4.295	644.499	180.738	3.566	6.49	5.0	0.120	0.106	0.092	0.078	0.064	0.050	0.036	0.022	0.008			
22	226.91	3.708	541.274	172.445	3.139	5.71	4.0	0.097	0.084	0.071	0.058	0.045	0.032	0.018	0.005				
23	226.28	3.076	435.366	163.502	2.663	4.85	2.9	0.070	0.059	0.047	0.036	0.025	0.013	0.002					
24	225.71	2.506	344.607	155.434	2.217	4.04	1.9	0.046	0.037	0.027	0.018	0.009							
25	225.31	2.109	284.157	149.820	1.897	3.45	1.2	0.028	0.021	0.015	0.008	0.001							
26	225.03	1.826	242.516	145.829	1.663	3.03	0.6	0.015	0.011	0.007	0.003								
27	224.83	1.627	213.815	143.014	1.495	2.72	0.2	0.006	0.004	0.002									
28	224.72	1.518	198.300	141.469	1.402	2.55	0.0												
29	224.61	1.415	183.805	140.010	1.313	2.39	0.0												
30	224.52	1.323	170.993	138.708	1.233	2.24	0.0												
31	224.46	1.261	162.396	137.828	1.178	2.14	0.0												
								1.552	1.367	1.183	0.999	0.814	0.652	0.524	0.406	0.292	0.187	0.094	0.015
								2.549	2.245	1.941	1.636	1.335	1.065	0.838	0.632	0.439	0.266	0.122	0.015

Figure H.1: Calculations of Shear Stress and Erosion During Natural Flood

151